University of Alberta

Contribution of FOXC1 to the development of Axenfeld-Rieger Syndrome and glaucoma

by

Yoko Anne Ito

A thesis submitted to the Faculty of Graduate Studies and Research
in partial fulfillment of the requirements for the degree of

Doctor of Philosophy

in

Medical Sciences – Medical Genetics

Fall 2013
Edmonton, Alberta

To ルパン.

Abstract

Axenfeld-Rieger syndrome (ARS) is a rare developmental disease that affects structures in the anterior segment of the eye. Approximately 50% of ARS patients develop glaucoma, a progressively blinding condition. Although glaucoma is an aging-related disease, ARS patients usually have earlier-onset of the disease. Mutations in Forkhead box C1 (FOXC1) are associated with ARS. FOXC1 is a member of the Forkhead box family of transcription factors that share a highly conserved DNA binding domain known as the Forkhead domain (FHD).

Two missense mutations, L130F and W152G, which are both located within the FOXC1 FHD were molecularly characterized. Overexpression experiments in cell culture showed that both mutations resulted in compromised ability of the mutant proteins to localize to the nucleus, bind DNA, and transactivate a reporter gene. Immunofluorescence experiments showed that the L130F mutant proteins are able to form potentially protective aggresomes.

In addition, the role of FOXC1 in the stress response pathway was examined. Using human trabecular meshwork (HTM) cells, HSPA6, a member of the HSP70 family of proteins, was validated to be a direct target gene of FOXC1. HSPA6 protein appears to be an anti-apoptotic protein that is only detected under severe oxidative stress conditions. Interestingly, the FOXC1 transcription factor appears to be stress-

responsive itself since exposure to H_2O_2 resulted in decreased FOXC1 RNA and protein levels. Decreased FOXC1 levels increased apoptotic cell death. Thus, FOXC1 may continue to play a role in the adult eye by maintaining homeostasis.

Mutations in FOXC1 may compromise the ability of TM cells to respond to oxidative stress due to dysregulation of anti-apoptotic genes such as HSPA6. The TM cells of ARS patients with FOXC1 mutations may be more vulnerable to environmental stresses including mechanical and oxidative stresses. As a result, increased TM cell death may occur, resulting in the dysregulation of aqueous humor drainage and elevation of IOP, which is a major risk factor for developing glaucoma. TM cell death may occur earlier in ARS patients with FOXC1 mutations, resulting in the earlier onset of glaucoma in this subset of ARS patients.

Acknowledgements

Thank-you to my supervisor, Dr. Michael Walter. I have gained invaluable experience and memories (some that I would like to forget, but probably never will) during my time in your lab. Thank-you for your guidance and patience.

Thank-you to my committee members Dr. Heather McDermid, Dr. Alan Underhill, Dr. Ordan Lehmann, and Dr. Brian Link. Thank-you for your time and tough questions over the years.

Thank-you to all past and present members of the Walter lab.

> Thank-you to Tim Footz for your help, friendship, and humour. Thank-you to Dr. Lijia Huang, Dr. Christina Fetterman, Dr. Moulinath Acharya, and Megan Chi for dealing with various states of me. Thank-you to May Yu for always cheering me up with kind words and dumplings. Thank-you to Freda Mirzayans for making me feel welcome in the lab.

Thank-you to Dr. Fred Berry for getting me hooked on research. I think it's a good thing, but I'll let you know later.

Thank-you to Dr. Ing Swie Goping for helpful advice on the FOXC1 stress response/HSPA6 project.

Thank-you to Dr. Mika Asai-Coakwell for being my role model both inside and outside of the lab. I'm so thankful that I met you. Thank-you to your family for keeping me happy.

Thank-you to Dr. Sarah Hughes for being a great graduate co-ordinator and more.

Thank-you to Dr. Gina Macintyre. I can't possibly remember all of the things we talked about, but I know they were all useful. Thank-you for supporting my "habit."

Thank-you to Lindsey Brown and Shari Barham for helping me with administrative duties and for helping me decorate Mike's office with mermen and gnomes.

Thank-you to everybody on the 8th floor that I've crossed paths with. Whether it was through ball hockey, hockey, beer, coffee, or just roaming around, (most) everyday at the lab was a good day because of you guys.

Thank-you to Dr. Jessica Boyd. We've come a long way and now we are both doctors! I was able to have fun during my graduate studies because of you.

Thank-you to my friends for your kindness and well, I guess it would be love. Sophie, Nancy, and Saba: there's nothing like childhood friends eh?

Finally, thank-you to my family in Canada and Japan. Mom and Dad, I hope you can worry about me less now.

Table of Contents

List of Tables

Chapter 3

Chapter 4

List of Figures

Chapter 1

Chapter 2

Chapter 3

Chapter 4

Chapter 5

Appendix

List of Symbols and Abbreviations

°C	degrees Celsius
^{32}P-dCTP	^{32} phosphorus deoxycytidine triphosphate
8-OHdG	8-hydroxy-2`-deoxyguanosine
AD	transactivation domain
AIF	apoptosis inducing factor
ANOLEA	atomic nonlocal environment assessment
Apaf-1	apoptotic protease activating factor 1
ARS	Axenfeld-Rieger Syndrome
ATP	adenosine triphosphate
BS	binding site
C	cytosine
C-terminal	carboxyl terminal
cDNA	complementary DNA
ch	congenital hydrocephalus
ChIP	chromatin immunoprecipitation
CIP	calf intestinal alkaline phosphatase
CO_2	carbon dioxide
CXCL6	Chemokine, CXC motif, ligand 6
Cy3	cyanine 3
CYP1B1	Cytochrome P450, Family 1, Subfamily B, Polypeptide 1
DAPI	4′,6-diamidine-2-phenylindole
DMEM	Dulbecco’s modified Eagle’s medium
dMO	double morpholino
E	embryonic day
ECM	extracellular matrix

E. coli	*Escherichia coli*
EDTA	ethylenediaminetetraacetic acid
EMSA	electrophoretic mobility shift assay
ERK	extracellular signal-regulated kinase
EV	empty vector
FBS	fetal bovine serum
FHD	Forkhead Domain
FOX	Forkhead Box
FOXC1	Forkhead Box C1
FOXC2	Forkhead Box C2
FOXL2	Forkhead Box L2
FOXO1	Forkhead Box O1
G	guanine
GAG	glycosaminoglycan
GFP	green fluorescent protein
GPx	glutathione peroxidase
h	hour
H_2O	water
H_2O_2	hydrogen peroxide
H1	α-helix 1
H2	α-helix 2
H3	α-helix 3 or histone 3
H4	α-helix 4
HCl	hydrochloric acid
HPRT1	Hypoxanthine Phosphoribosyltransferase 1
HSE	heat shock element
HSF	heat shock transcription factor

HSP70	Heat Shock Protein 70
HSP70B’	Heat Shock Protein 70B’
HSPA6	Heat Shock Protein A6
HTM	human trabecular meshwork
ID	inhibitory domain
IL8	Interleukin 8
IOP	intraocular pressure
KCl	potassium chloride
LacZ	β-galactosidase
MAPK	mitogen-activated protein kinase
MCP1	monocyte chemotactic protein 1
MMP	matrix metalloproteinase
N-terminal	aminoterminal
NaCl	sodium chloride
NAD	nicotinamide adenine dinucleotide
NLAS	nuclear localization accessory signal
NLS	nuclear localization signal
NPCE	non-pigmented ciliary epithelial
O_2	oxygen
$O_2^{-}\cdot$	superoxide free radical anion
OH·	hydroxyl radical
PARP	poly (ADP-ribose) polymerase
PAX6	Paired Box 6
PBS	phosphate buffered saline
PCR	polymerase chain reaction
PIPES	piperazine-N,N′-bis(2-ethanesulfonic acid
PITX2	Pituitary Homeobox 2

PMSF	phenylmethanesulfonyl fluoride
PTM	post-translational modification
POAG	primary open-angle glaucoma
qPCR	quantitative polymerase chain reaction
RGC	retinal ganglion cell
ROS	reactive oxygen species
S1	β-strand 1
S2	β-strand 2
S3	β-strand 3
SBD	substrate binding domain
SDS-PAGE	sodium dodecyl sulfate polyacrylamide gel electrophoresis
siRNA	small interfering RNA
SOD	superoxide dismutase
T	thymine
TGF-β	transforming growth factor β
TIMP	tissue inhibitors of metalloproteinase
TM	trabecular meshwork
W1	wing 1
W2	wing 2
WT	wild type
ZO-1	zonula occludens 1

Chapter 1. General Introduction

This chapter contains work published in:

Ito YA and Walter MA. (2013). Genetics and Environmental Stress Factor Contributions to Anterior Segment Malformations and Glaucoma. Shimon Rumelt (Ed.). *Glaucoma - Basic and Clinical Aspects* (pp.27-56). InTech. (1)

Glaucoma

Glaucoma is one of the leading causes of irreversible blindness worldwide (2). A gradual loss of retinal ganglion cells (RGCs) result in degeneration of the optic nerve head and visual field loss. Glaucoma is an age-related disease with a strong genetic basis. The risk of developing glaucoma significantly increases after age 40 (3,4). An estimated 79.6 million people worldwide will have glaucoma by 2020 (2). Patients with mutations in glaucoma-associated genes are more likely to develop juvenile-onset and early adult-onset glaucoma. In any case, early detection of glaucoma is essential to effectively manage the progression of the disease by preventing further loss of RGCs. The pathophysiology of glaucoma is complicated as environmental, genetic, and even stochastic factors all contribute to the pathology of glaucoma. Also, both the posterior segment, where the RGCs are located, and the anterior segment of the eye play a role in the development of the disease (Figure 1A). The death of RGCs is hypothesized to partially be due to the deprivation of neurotrophins (reviewed by (5,6)). Neurotrophins are small secreted peptides that promote RGC survival. Events such as ischemia and increased intraocular pressure (IOP) are suggested to disrupt the transport of neurotrophins along the RGC axon, resulting in axonal injury (5).

Glaucoma can be classified as being primary, secondary, or congenital. Primary glaucoma is non-syndromic and is not associated with any underlying condition. Primary congenital glaucoma is a rare form of

glaucoma present at birth or within the first two years after birth. Glaucoma that develops as a result of an underlying ocular or systemic condition or eye injury is categorized as secondary glaucoma. Pseudoexfoliative glaucoma is an example of secondary glaucoma whereby fibrillar extracellular material deposits and accumulates in various ocular tissues, predisposing the patient to developing glaucoma. Glaucoma can also be categorized to be open-angle or closed-angle, depending on the anterior chamber angle. In closed-angle glaucoma, the angle between the iris and the cornea is narrowed resulting in obstruction of aqueous humour flow.

Open angle glaucoma is a common type of glaucoma where the iridocorneal angle is unobstructed. Although open angle glaucoma can occur in patients with normal IOP, sometimes referred to as normal-tension glaucoma, elevated IOP is a major risk factor of developing open angle glaucoma.

Regulation of intraocular pressure

IOP is dependent on proper flow of aqueous humour from the site of production in the posterior chamber to the site of drainage in the anterior chamber of the eye (Figure 1B). Aqueous humour is a colourless and transparent fluid that makes contact with various structures in both the anterior and posterior chambers of the eye including the lens, iris, and cornea. The lens and the cornea are clear and avascular, which enables light to be effectively transmitted to the photoreceptors in the back of the

eye. Aqueous humour provides nutrients to the avascular lens and cornea and also removes metabolic waste products. The composition of aqueous humour has been of great interest due to the potential regulatory effects on all the structures to which it makes contact. For example, the presence of antioxidants such as glutathione and ascorbic acid (7,8) in the aqueous humour suggest that this fluid affects the ability of cells to respond and adapt to stress.

Aqueous humour flows from the site of production, which is the non-pigmented ciliary epithelial cells (9,10) in the posterior chamber, to the site of drainage, which is the trabecular meshwork (TM) and Schlemm's canal in the anterior chamber (Figure 1B). Production and drainage of aqueous humour is a continuous and dynamic process. Diurnal variations in aqueous humour turnover rates occur ranging from 3.0µL/min in the morning to 1.5µL/min at night (11). The balance between aqueous humour production and drainage is essential for maintaining a healthy IOP of approximately 15mmHg within the eye (12). Abnormalities in aqueous humour drainage due to increased resistance at the TM are thought to result in elevated IOP, which is a major risk factor for developing glaucoma (13).

Aqueous humour is drained from the eye by two distinct outflow pathways: the trabecular pathway and the uveoscleral pathway. The uveoscleral pathway is an IOP-independent pathway in which the aqueous humour leaves the anterior chamber by passing through the ciliary muscle

bundles into the supraciliary and suprachoroidal spaces and eventually diffuses through the sclera (14-16). In humans, the majority of aqueous humour is transported through the TM via the trabecular pathway. Disruption of aqueous humour drainage through the trabecular pathway is thought to be the major contributing factor to alteration of IOP.

The TM is a multi-layered tissue located in the anterior chamber angle. From the anterior chamber the aqueous humour passes through the multiple layers of the TM: the uveal meshwork, the corneoscleral meshwork, and the juxtacanalicular meshwork (also known as the cribriform plexus) (Figure 2). Each layer consists of a central connective tissue (aka beam) surrounded by an outer endothelial layer. Connecting fibrils tightly connect the network of elastic fibres in the juxtacanalicular meshwork to the inner endothelial wall of Schlemm's canal (17-20). As the aqueous humour passes through each layer of the TM, the intercellular space narrows resulting in increased resistance. Then, aqueous humour progresses through the inner endothelial cell layer of Schlemm's canal. The endothelial cells of Schlemm's canal express the tight junction protein zonula occludens 1 (ZO-1), which allows aqueous humour to be transported via the intercellular route (21). The aqueous humour is also transported via the transcellular route through giant vacuoles (22-24). Aqueous humour passes through Schlemm's canal and returns to the general circulation via the aqueous and episcleral veins (23,25). IOP is affected by the episcleral venous pressure and the resistance to aqueous

humour flow within the TM. Episcleral venous pressure directly affects IOP because aqueous humour must flow out of the eye against the pressure in the episcleral veins. The main source of resistance to aqueous humour flow is thought to be located in the intercellular (aka subendothelial) region of the juxtacanalicular network (26-29).

Extracellular matrix (ECM) occupies the intercellular space between the beams of TM cells. The ECM consists of glycosaminoglycans (GAGs), proteoglycans, laminin, various collagens, fibronectin, and vitronectin (reviewed in (30)). The constant turnover of this ECM has been proposed to play a role in maintaining proper aqueous humour resistance (reviewed in (31)). The family of matrix metalloproteinases (MMPs) are secreted zinc proteinases that initiate ECM turnover (32,33). MMP activity is inhibited by the family of tissue inhibitors of metalloproteinases (TIMPs). MMP activity is suggested to be important in regulating aqueous humour outflow facility by proteolytic alterations. Using perfused human anterior segments, Bradley *et al*. observed that increasing MMP activity increased the outflow rate while inhibiting MMP activity by the addition of TIMP decreased outflow rate (33). MMP activity is suggested to have various functional consequences including degradation of ECM components, cleavage and modification of signaling molecules, and cleavage of intercellular junctions and basement membrane (reviewed in (34)).

Another factor that affects resistance is the ciliary muscle. The elastic anterior tendons of the ciliary muscle insert into the network of

elastic fibres in the juxtacanalicular meshwork and corneoscleral meshwork (19,20,35). The elastic fibres are surrounded by a collagen-based sheath (20). Ciliary muscle contractions result in increased aqueous humour outflow facility (36). Upon ciliary muscle contraction, the connecting fibres straighten. Since the ciliary muscle is connected to the TM and the inner wall of Schlemm's canal by the connecting fibrils, ciliary muscle contraction widens the intercellular space in the juxtacanalicular meshwork allowing aqueous humour to flow against less resistance (36). In contrast, relaxation of the ciliary muscles results in the opposite effect where there is increased resistance to aqueous flow (37).

As outlined above, the aqueous humour flow pathway is a complex process regulated by structures in both the posterior and anterior chambers of the eye. Factors such as aging and developmental structural anomalies of tissues such as the TM are predicted to compromise the efficiency of the aqueous humour flow pathway. Disruptions of the aqueous humour flow pathway are predicted to result in elevated IOP, which is a major risk factor of glaucoma.

Change in trabecular meshwork during the normal aging process

Aging is a major risk factor for developing glaucoma. However, at the physiological level, minimal changes in aqueous humour flow dynamics occur in normal healthy subjects as aging progresses (reviewed in reference (38)). The outflow facility measured by fluorophotometry was

0.23±0.10µL/min/mmHg in 20-30 year old subjects (n=51) and 0.27±0.13µL/min/mmHg in subjects 60 years and older (n=53) (39). Thus, fluorophotometric measurements indicate that there is in fact no difference in outflow facility as aging progresses (39). Many studies using tonographic and fluorophotometric measurements have consistently shown that with age, aqueous humour production decreases (39-44). Since outflow facility remains stable, it is not surprising that IOP remains stable in normal healthy subjects as aging progresses. Although outflow facility remains stable and aqueous humor production decreases, IOP remains stable in normal healthy subjects as aging progresses. Toris *et al.* have recently measured IOP to be 14.7±2.5mmHg in 20-30 year old subjects (n=51) and 14.3±2.6mmHg in subjects 60 years and older (n=53) (39). A decrease in anterior chamber depth (39,45,46) with aging may account for the lack of change in IOP.

Interestingly, prominent changes at the structural and cellular levels occur with age. Connecting fibrils ensure that contact is maintained between the juxtacanalicular meshwork and the inner endothelial wall of Schlemm's canal (19,20). The sheath surrounding these elastic fibres thickens with age (47). The intercellular space narrows due to an increase in the amount of extracellular material from the thickened sheath, resulting in increased resistance (48,49). Also, as aging progresses, the number of TM cells decrease (50,51). Grierson and Howes estimate that at age 20, there are approximately 763 000 cells in the TM. By age 80, approximately

403 000 cells remain (51). The outer TM layers lose more TM cells while the least number of TM cells are lost from the inner juxtacanalicular layer (51,52). This decline in TM cells appears to be a continuous and linear process with an estimated 0.58% loss of cells annually (50,52). The linear decrease in TM cellularity is intriguing because the mechanism of cell loss may be different between the ages (52). Age-related mechanisms such as accumulation of reactive oxygen species (ROS) and misfolded proteins are likely to contribute to cell loss in older subjects. However, other non-age-related mechanisms such as exposure to mechanical stress are likely responsible for cell death in the TM in younger subjects. Interestingly, Alvarado *et al.* observed that TM cells may have a reduced reparative capacity, which would further contribute to the decrease in cellularity with age (52). The loss of TM cells with age could have a more severe consequence in some individuals because there appears to be great variation in the absolute number of TM cells between individuals (53). Therefore, individuals with less TM cells would be predicted to be less efficient in fulfilling the function of TM cells.

Regardless of the individual variation in TM cell number, the consequence of losing TM cells in all aging individuals can be predicted. As avid phagocytes, TM cells are thought to clear debris from the aqueous humour outflow pathway (54-58). Although TM cells have the ability to ingest particulate matters rapidly, the phagocytic process may have detrimental effects on the overall health of the cell, even leading to

necrosis (59). Zhou *et al.* also showed that after phagocytosis, temporary alteration of TM cells occurred including rearrangement of the cytoskeleton and increased migratory activity (60). These alterations, although temporary, have been speculated to be linked to the age-related loss of TM cells (60). TM cells also maintain aqueous humour outflow by releasing factors that regulate permeability of the endothelial cells of Schlemm's canal (61). TM cells release various enzymes and cytokines both in the presence and absence of stimulation such as mechanical stretching and exposure to pro-inflammatory cytokines (61,62). TM endothelial cells constitutively secrete cytokines such as interleukin 8 (IL8), chemokine, CXC motif, ligand 6 (CXCL6), and monocyte chemotactic protein 1 (MCP1), strengthening the notion that the release of cytokines is important in maintaining aqueous humour outflow (62).

The risk of developing primary open-angle glaucoma (POAG) significantly increases after age 40. Despite the fact that glaucoma is an age-related disease, aging in most people does not result in this disease. Although the changes that occur in the TM during the normal aging process may make the tissue more susceptible to malfunction, the TM is still able to effectively drain aqueous humour. However, other unknown factors and even stochastic factors must be present for the TM to fail to a point that the glaucoma phenotype develops.

Change in trabecular meshwork in glaucoma disease phenotype

In patients with glaucoma, the structural and cellular changes in the TM are more pronounced than those seen in the aging TM and as a result, TM function is disrupted. In glaucomataous eyes, there is more prominent and irregular thickening of the sheaths of the elastic fibers. Also, there is increased deposition of sheath-derived plaques compared to normal eyes (47,63). This increase in extracellular material in the TM is predicted to block aqueous humour outflow (20) contributing to the development of disease. As in normal aging, there is a linear decrease in cellularity as aging progresses in the TM of POAG patients. Moreover, Alvarado *et al.* observed fewer cells in the glaucomatous TM compared to the non-glaucomatous TM over a wide range of ages (50).

Preventing and delaying TM cell death is postulated to be an effective means of preventing IOP-related glaucoma. However, the molecular mechanisms underlying TM cell death are not fully understood. Rare diseases such as Axenfeld-Rieger Syndrome (ARS), where glaucoma develops secondarily, may provide valuable insight into the molecular mechanisms underlying TM cell death. Analysis of ARS-associated genes may highlight specific pathways that play key roles in mediating TM cell death and/or survival.

Axenfeld-Rieger Syndrome

ARS is a rare autosomal dominant disorder that is part of the anterior segment dysgenesis group of developmental disorders. ARS is a phenotypically heterogeneous disorder that is characterized by ocular and systemic abnormalities. ARS patients exhibit a spectrum of anterior segment abnormalities that are highly penetrant, including iris hypoplasia, corectopia, polycoria, posterior embryotoxon (ie. anteriorly displaced Schwalbe's line), and iris strands that extend from the iridocorneal angle to the TM (Figures 3A to 3D). In addition, ARS patients may present with systemic abnormalities including facial dysmorphisms (eg. hypertelorism, prominent forehead, telecanthus), dental anomalies (eg. hypodontia, microdontia), and a redundant preumbilical skin (Figures 3E and 3F).

Approximately 50% of ARS patients secondarily develop open angle glaucoma (64-66). In non-ARS patients, glaucoma usually develops after age 40. However, ARS patients tend to develop glaucoma in adolescence or in early adulthood (<30 years) (67). In cases where the patient has a heterozygous mutation in ARS-associated genes such as *Forkhead Box C1 (FOXC1)* and *Pituitary Homeobox 2 (PITX2)*, the incidence of glaucoma increases to 75% (67). Mutations in these two transcription factor genes account for ~40% of ARS cases (68). Although the gene has yet to be identified, a third chromosomal locus at 13q14 is associated with ARS (69). *In this thesis, I examine the contribution of the FOXC1 transcription factor to the development of ARS and glaucoma.* To

date, at least 28 FOXC1 missense mutations have been identified in ARS patients. All but one of these missense mutations occurs within the FOXC1 DNA-binding Forkhead Domain (FHD). Also, segmental duplications and deletions of the 6p chromosomal region that include the FOXC1 gene cause ARS phenotypes (70-74). Thus, FOXC1 levels need to be strictly regulated for normal development of ocular tissues to occur.

Forkhead Box C1

FOXC1 is a single exon gene located on chromosome 6p25. FOXC1 belongs to the Forkhead Box (FOX) family of transcription factors. The FOX proteins are evolutionarily conserved and play essential roles in many biological processes during and after development, including cell differentiation, cell proliferation, and apoptosis. Since many FOX proteins regulate major signalling pathways, such as the transforming growth factor β (TGF-β) and mitogen-activated protein kinase (MAPK) pathways, FOX proteins are thought to be molecular integrators of extracellular signals (75). Members in this family share a highly conserved 110-amino acid DNA-binding sequence known as the FHD. The FHD consists of three N-terminal α-helices (H1, H2, H3) and three β-strands (S1, S2, S3) (Figures 4 and 5) (76). Some FOX transcription factors, including FOXC1, have a smaller fourth helix (H4) that is located between H2 and H3 (77). The antiparallel β-strands interact with each other to form a β-sheet, which results in a tight hydrophobic core (76-78). Two wings (W1 and W2) emerge between S2 and S3 (W1) and between S3 and the C-terminal

(W2). These two loop-like wings give the FHD a characteristic “winged-helix” motif. The two wings have been suggested to be involved in bending the DNA double helix at an angle of 80° to 90° (79). H3 and W2 are predicted to be the subdomains within the FHD that make contact with DNA. The recognition helix H3 makes contact with the major groove of DNA. H3 recognizes the FHD core target sequence RTAAAYAAA (76,79). The W2 loop is predicted to contact the minor groove of DNA.

The FOXC1 FHD is located between amino acid residues 69 and 178. The FHD is essential for FOXC1 to function as a transcription factor. FOXC1 regulates the expression of downstream target genes after binding via the FHD to specific binding sites. A hormone-inducible FOXC1 construct was used to identify potential target genes of FOXC1 (80). FOXC1 was transfected into non-pigmented ciliary epithelial (NPCE) cells and then induced. The protein synthesis inhibitor, cyclohexamide, was added to enrich for mRNA from *direct* target genes of FOXC1. Microarray analysis identified hundreds of genes that were potentially upregulated or downregulated by FOXC1. Identifying direct target genes of FOXC1 is essential in determining the specific pathways that FOXC1 may be involved in. Also, since ~60% of ARS patients do not have mutations in either FOXC1 or PITX2, FOXC1 target genes are potential ARS candidate genes.

Identification of several additional FOXC1 functional domains other than the DNA-binding FHD has given insight into how the FOXC1 protein

behaves at the molecular level (Figure 5). Two nuclear localization signals (NLS) present within the FHD enable the FOXC1 transcription factor to localize to the nucleus so that DNA binding can occur. The N-terminally located NLS (residues 77 to 93) is suggested to be an accessory domain because it is necessary, but not sufficient on its own to promote nuclear localization (81). Fusion of green fluorescent protein (GFP) to the C-terminally located NLS (residues 168 to 176) resulted in the accumulation of the chimeric protein exclusively to the nucleus, indicating that this NLS is sufficient on its own to promote nuclear localization. FOXC1 contains two transactivation domains (AD), which are both located outside of the FHD (81). AD-1 is located between residues 1 and 51 while AD-2 is located between residues 466 and 553. Amino acid residues 367 to 553, which include AD-2, are essential for the FOXC1 protein to be targeted to the ubiquitin 26S proteasomal pathway (82). A phosphorylated inhibitory domain (ID) is located within residues 215 and 366 (81). The molecular characteristics of a specific FOXC1 mutant protein are dependent on location of the missense mutation within the gene. For example, the P297S mutation, located in the ID, is the only known FOXC1 mutation that occurs outside of the FHD (83). The P297S mutant does not have any nuclear localization or DNA binding defects, characteristics that are normally regulated by the FHD. However, the P297S mutant has altered transactivation ability and half-life, which are both characteristics that have been suggested to be mediated by the ID. Thus, characterization of

FOXC1 functional domains provides a useful means of predicting the molecular consequences of a particular FOXC1 mutation.

Role of FOXC1 during ocular development

Analysis of FoxC1 mouse models have revealed that the proper expression of FoxC1 is critical for the normal development of the cardiac, skeletal, and urogenital systems, as well as structures in the anterior segment of the eye. At E11.5, FoxC1 is expressed in the neural crest-derived periocular mesenchyme cells in the anterior segment and the surrounding the optic cup and stalk (84). Many structures in the anterior segment of the eye are derived (mostly) from the periocular mesenchyme, including the corneal endothelium, corneal stroma, TM, iris stroma, and ciliary stroma. The congenital hydrocephalus (*ch*) mouse ($Mf1^{ch}$) has a point mutation in FoxC1, which results in a truncated protein lacking the DNA-binding FHD (85). Homozygous *ch* mice die at birth due to a defective respiratory system and enlarged hemorrhagic cerebral hemispheres (86,87). A range of ocular phenotypes that resemble human ARS are present in heterozygous *ch* mice, including corectopia, posterior embryotoxon, and iridocorneal adhesions (86). In the homozygous $Mf1^{lacZ}$ mouse, where the FoxC1 protein coding sequence is replaced with the β–galactosidase gene, severe abnormalities in the development of the anterior segment of the eye are observed. Since the cornea does not separate from the lens, the anterior chamber does not form in these FoxC1 null mice (Figure 6). Kidson *et al.* suggest that FoxC1 mediates

signalling from the lens epithelium that is necessary for differentiation of the corneal endothelium to occur (88). Proper differentiation of the corneal endothelium appears to be a necessary event preceding anterior chamber formation.

Anterior segment abnormalities are also observed in another animal model, zebrafish (80,89,90). Double knockdown of foxC1a and foxC1b, foxC1dMO, results in smaller eyes, as well as disruptions to the corneal endothelium and corneal stroma (89). At 48hpf, undifferentiated and unorganized periocular cells are observed in the iridocorneal angle of foxC1dMO zebrafish (89). Also, the basement membrane of these double morphants is compromised, potentially contributing to disruptions to the hyaloid vasculature (89). Thus, studies using various animal models support the important role FOXC1 plays during ocular development.

Developmental model of ocular structural defects in Axenfeld-Rieger patients

Shields proposed that the structural abnormalities observed in the anterior segment of ARS patients may be caused by an arrest late in development (91). Both the arrest in posterior recession of the iris and the retention of the primordial endothelial layer, which initially covers the developing TM, have been suggested to result in abnormalities of the anterior surface of the iris, development of iridocorneal tissue strands, and an anteriorly displaced prominent Schwalbe's line. The precise

involvement of FOXC1 in these processes needs to be further examined. Interestingly, the iridocorneal tissue strands do not appear to disrupt the aqueous humour flow as there is no correlation between the presence of iridocorneal tissue strands and the severity of glaucoma (91,92). Instead, structural abnormalities in the aqueous humour drainage structures, specifically the TM and Schlemm's canal, are hypothesized to be the contributing factors of ARS-associated glaucoma (91). Histopathological examination of multiple ARS specimen (ten eyes from eight patients) suggests that the intertrabecular space fails to properly develop as the trabecular endothelial cells are not separated from the adjacent connective tissue (91). In addition, the examined ARS specimen displayed a rudimentary or absent Schlemm's canal (91). Inefficient drainage of the aqueous humour from the anterior chamber would result in elevated IOP which is a major risk factor for the development of glaucoma. Thus, improper development of the TM and Schlemm's canal appears to be a major contributing factor to the development of ARS-associated glaucoma. Although the ARS phenotype is fully penetrant in individuals with FOXC1 mutations, there is great variability in the phenotypes of affected individuals (variable expressivity). Also, not all ARS patients develop glaucoma. About 25% of individuals with FOXC1 mutations and 50% of ARS patients without FOXC1 mutations do not develop glaucoma. In some ARS patients, the TM and Schlemm's canal may be sufficiently developed for aqueous humour to be drained from the eye. Moreover,

factors other than developmental abnormalities of the anterior segment structures likely contribute to the development of glaucoma in ARS patients.

Potential role of FOXC1 in the adult eye

In recent years, there has been great interest in the contribution of environmental stress factors such as mechanical and oxidative stresses in the development of POAG (93-97). Although FOXC1 plays a critical role in the development of ocular tissues, FOXC1 may also function in the adult eye. FOXC1 is expressed in the adult anterior segment structures including the TM, ciliary body, cornea, and iris (98). In addition, FOXC1 is expressed in the adult posterior chamber structures including the optic nerve head and choroid/retinal pigment epithelium (98). Berry *et al.* observed that human trabecular meshwork (HTM) cells are more sensitive to oxidative stress when FOXC1 is knocked down (80). FOXC1 appears to mediate the stress response through the regulation of Forkhead Box O1 (FOXO1). Interestingly, oxidative stress has recently been implicated as a contributing factor to the development of POAG. Specifically, the death of TM cells due to chronic exposure to oxidative stress has been proposed to contribute to TM tissue malfunction and subsequent elevation in IOP (99), which is a major risk factor of glaucoma. Thus, FOXC1 expression may be important for maintaining homeostasis in the fully developed TM.

Exposure of the trabecular meshwork to oxidative stress

The TM is a highly specialized tissue that is able to adapt to the dynamic nature of aqueous humour outflow. Similar to any other cell in the body, TM cells are exposed to a variety of environmental stresses. Due to the location of cells of the TM, one of the major types of stress these cells are exposed to is oxidative stress. Cells are constantly exposed to free radicals that are the by-products of normal cellular metabolism. In addition, the aqueous humour is itself a source of free radicals. Hydrogen peroxide (H_2O_2) is normally present in the aqueous humour and is suggested to be the key source of oxidative stress for the TM (100). An accurate concentration of H_2O_2 is difficult to obtain and may vary greatly between individuals (101,102). Nevertheless, long-term exposure to free radicals such as H_2O_2 (ie. chronic oxidative stress) is suggested to have detrimental effects on TM cells (50,52,99). Long-term exposure to free radicals can damage proteins and DNA, promote lipid peroxidation, disrupt mitochondrial function, and ultimately trigger cell death (reviewed in (103)).

Cellular defence mechanisms

The presence of cellular defence mechanisms enables TM cells to quickly and effectively respond and adapt to their environment. Two cellular defence mechanisms present in TM cells are the antioxidant system, which defends against ROS, and the proteolytic system, which removes unwanted biomaterials from the cell, many of which are products

of oxidative stress-related damage. Cells have an antioxidant defence mechanism to counter the deleterious effects of ROS. For example, superoxide dismutase (SOD) is an antioxidant enzyme that converts superoxide free radical anion ($O_2^{-}\cdot$) into H_2O_2 and molecular oxygen (O_2) (104). H_2O_2 must then be converted into water (H_2O) by two other antioxidant enzymes: peroxisomal catalases and the family of glutathione peroxidases (GPx). In the event that H_2O_2 is not converted, it then may split into the hydroxyl radical ($OH\cdot$), which can be dangerous because it can react with almost any macromolecule within a short diffusion distance.

Although aqueous humour is a source of free radicals, aqueous humour appears to also protect TM cells because it is a source of antioxidants. Since low concentrations of free radicals are necessary for normal cellular function, TM cells rely on the very high content of antioxidant in the aqueous humour to achieve a balance that maximizes cell survival. High aqueous humour concentration of the antioxidant ascorbic acid (aka Vitamin C), which is about 20 times higher than in plasma (101), suggests that this antioxidant may be a major protector against free radicals in the eye (105-107). Ascorbic acid has also been suggested to protect cells against ultraviolet light (107,108). In addition to being an antioxidant, ascorbic acid is suggested to also have a role regulating the ECM of the TM. TM cells synthesize many types of GAGs into the ECM including hyaluronic acid (109). Ascorbic acid can increase hyaluronic acid synthesis (109). Since hyaluronic acid has been shown to

increase the expression of several MMPs (110), altered levels of this GAG would affect ECM turnover. Interestingly, Knepper *et al.* has shown that there is significantly less hyaluronic acid in the TM of POAG patients compared to the TM of normal subjects (111,112). Thus, ascorbic acid is predicted to affect the aqueous outflow pathway by acting as an antioxidant and by regulating the ECM components that are important in maintaining the aqueous humour outflow pathway. Although some groups observed no difference in aqueous ascorbic acid levels between POAG patients and senile cataract patients (113,114), Lee *et al.* observed greater levels of ascorbic acid in the aqueous humour of POAG patients (115). The difference in observation may be due to the great individual variation in ascorbic acid levels (114). Nevertheless, ascorbic acid appears to play a protective role for TM cells.

In addition to the antioxidant system, the proteolytic system is another cellular defence mechanism present in TM cells. The proteolytic system is essential for the removal of oxidatively damaged proteins and organelles. The 20S proteasome, 26S proteasome, and immunoproteasome are the main cellular systems in eukaryotic cells that eliminate damaged proteins. The 20S proteasome tends to degrade oxidized proteins while the 26S proteasome degrade ubiquitynated proteins.

Global gene expression profile is another major part of a cell's adaptive response to stress (reviewed in (116)). The change in gene

expression profile in response to stress has revealed that signal transduction pathways are a necessary means of integrating complex signals and propagating these signals to effectors. For example, Porter *et al.* examined the global gene expression profile of phagocytically challenged TM cells under normal and acute oxidative stress conditions (117). As avid phagocytes, TM cells are predicted to keep the aqueous humour outflow pathway clear of debris (55). When TM cells were phagocytically challenged with *E. coli* under normal conditions, 1190 genes were upregulated and 728 genes were downregulated (117). When TM cells were phagocytically challenged with *E. coli* under oxidatively stressed conditions at 40% O_2, 976 genes were upregulated and 383 genes were downregulated. Although many of the altered genes were involved in immune response, cell adhesion, and regulation of ECM, there were only 6 genes that were altered in both the normal and oxidatively stressed conditions. FOXC1 levels were not detected to change by Porter *et al*.. Nevertheless, FOXC1 may function under a different condition as TM cells appear to have a distinct gene expression profile depending on the nature of the stress.

Consequences of chronic oxidative stress on the aging trabecular meshwork

However, as aging progresses, the normal cellular defence mechanisms become less effective and the cell is less able to remove potential toxic materials such as ROS and misfolded proteins (Figure 7).

This gradual accumulation of toxic materials will lead to an environment where the cells are exposed to chronic oxidative stress. The cellular defence mechanisms, already compromised due to the aging process, may become completely overwhelmed under such chronic oxidative stress conditions. Chronic oxidative stress is recognized to be a major contributor to the aging process and various diseases including neurodegenerative diseases such as Parkinson's (118,119) and Alzheimer's (120-122), cancer (123,124), and cardiovascular diseases (125). Since POAG is an age-related disease, chronic oxidative stress is also suggested to have a role in the pathophysiology of this disease (reviewed in (96)). Cell death will occur when the cells are no longer able to adapt to the environment. Since accumulation of ROS occurs with age, the loss of TM cells during the aging process may also be in part due to exposure of TM cells to chronic oxidative stress conditions. The presence of fewer TM cells as aging progresses could also be detrimental to the TM tissue as there are fewer cells to protect against ROS in the aqueous humour.

TM cells of glaucoma patients appear to have more oxidative stress-related damages than non-glaucomatous individuals. Oxidative stress can damage DNA, resulting in the formation of 8-hydroxy-2`-deoxyguanosine (8-OHdG). The levels of 8-OHdG were found to be increased in DNA extracts from glaucomatous TM cells compared to healthy controls (126,127). Also, aqueous humour and serum levels of 8-

OHdG were significantly higher in glaucoma patients (n=28) compared to the age-matched control group of senile cataract patients (n=27) (128).

In addition, there is a decline in proteasomal activity with age in many tissues including the TM. Caballero *et al.* reported that primary cultures of HTM cells from healthy older donors (ages 66, 70, and 73) had decreased proteasomal activity compared to healthy young donors (ages 9, 14, and 25) (129). Since the overall proteasomal content did not change between the older and younger donors, the decrease in proteasomal activity is most likely due to oxidation of the proteasomal subunits and the overload of the proteasomal machinery with damaged proteins. Caballero *et al*. observed an increase in oxidized proteins in the older donors (129). Accumulation of oxidized protein is not the only biomolecule detrimental to proteasomal function. The accumulation of lipid peroxidation products in the TM is suggested to also contribute to proteasomal dysfunction (130). The calpains are a family of calcium-activated non-lysosomal cysteine proteases. In glaucomatous TM tissue, aggregated and degraded calpain-1 is present, but calpain-1 activity is lower compared to normal TM tissue (130). In glaucomatous TM, the lipid peroxidation products isolevuglandins, specifically iso[4]levuglandin E2, modifies calpain-1, thereby inhibiting calpain-1 activity. Calpain-1 modified by isolevuglandins is more prone to form larger aggregates. One of the major consequences of this modification is a disruption in the proteasomal machinery. This type of malfunction of the proteasomal machinery appears to be specific to the

TM and does not occur in the posterior segment of the eye. Thus, accumulation of oxidative stress-related biomolecules along with a decrease in proteasomal activity with age perpetuates a vicious cycle that is postulated to greatly hinder cell survival.

Despite having more oxidative stress-related damages, TM cells of glaucoma patients appear to have increased activity of some components of the antioxidant defence mechanism. Increased levels of GPx and SOD activities were measured in aqueous humour of glaucomatous patients compared to the control group of senile cataract patients (97,131). However, no apparent change in catalase activity levels was detected (97,131). Thus, at least some components of the antioxidant defence mechanism are functioning to prevent TM cell death under glaucomatous conditions.

Hypothesis and Rationale

In chapters 2 and 3, the molecular consequences of two novel FOXC1 missense mutations, L130F and W152G, will be examined. I hypothesize that both the L130F and W152G mutations alter the normal molecular characteristics of the FOXC1 protein. Since both the L130 and W152 residues lie within the FHD, characteristics regulated by the FHD including DNA binding and nuclear localization are hypothesized to be altered by the mutations. Disruptions to the molecular abilities of the FOXC1 due to these two mutations are suggested to contribute to the

malfunctioning of FOXC1 protein during development, resulting in the ARS phenotype.

As mentioned previously, about 75% of ARS patients with FOXC1 mutations develop earlier-onset glaucoma. In addition to developmental structural defects of anterior segment structures, I hypothesize that individuals with FOXC1 mutations have a compromised ability to respond and adapt to environmental stresses. In adult eye, FOXC1 may be part of the mechanism that enables TM cells to adapt and survive to ongoing environment stresses. Impaired regulation of FOXC1 direct target genes involved in cellular stress response, due to FOXC1 mutations may underlie part of the pathophysiologies of earlier-onset glaucoma observed in ARS patients. *In chapter 4, I will examine the involvement of the FOXC1 transcription factor in the stress response pathway by characterizing a potential target gene that belongs to the heat shock protein 70 (HSP70) family of proteins, heat shock protein A6 (HSPA6; also known as HSP70B').* Even in the absence of stress, HSP70 proteins aid in folding of nascent and misfolded proteins. Environmental stresses cause proteins proteotoxic damage and thus, under stress conditions, there is a higher need for the chaperoning activity of HSP70 proteins. Under stress conditions, HSP70s do not normally aid in refolding of damaged proteins. Rather HSP70s facilitate the movement of the damaged proteins to the proteolytic system by preventing aggregation (132). Thus, HSPA6 is an

interesting FOXC1 target gene to examine because of the potential role in protecting cells under stress conditions.

A

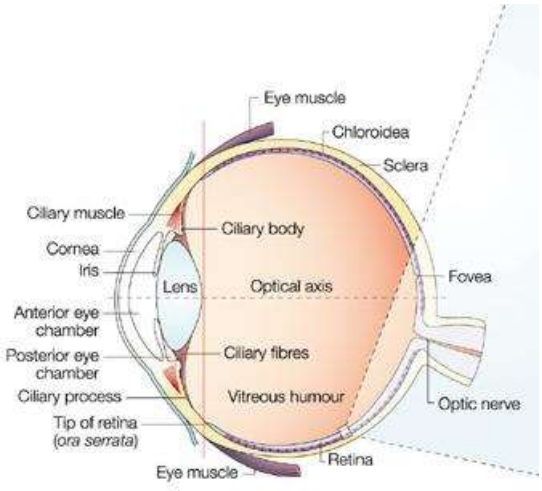
Eye muscle
Chloroidea
Sclera
Ciliary muscle
Ciliary body
Cornea
Iris
Lens
Optical axis
Fovea
Anterior eye chamber
Posterior eye chamber
Ciliary fibres
Ciliary process
Vitreous humour
Optic nerve
Tip of retina (ora serrata)
Retina
Eye muscle

B

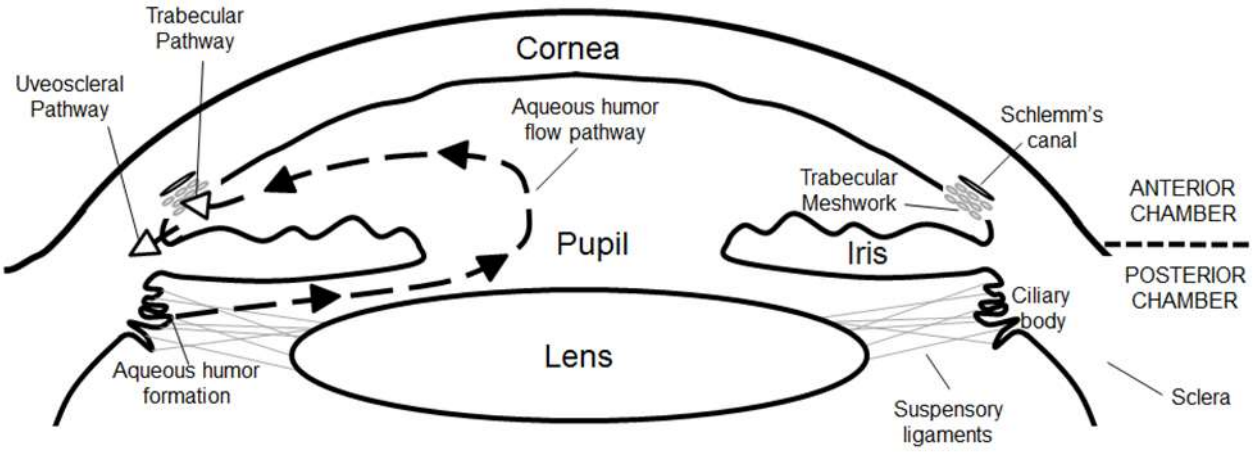
Trabecular Pathway
Cornea
Uveoscleral Pathway
Aqueous humor flow pathway
Schlemm's canal
Trabecular Meshwork
ANTERIOR CHAMBER
Pupil
Iris
POSTERIOR CHAMBER
Ciliary body
Lens
Aqueous humor formation
Suspensory ligaments
Sclera

Figure 1: Schematic diagram of human eye. A) The cross section shows the various tissues that make up the whole human eye. The vertical line divides the anterior and posterior segments of the eye. The retinal ganglion cells (RGCs) are located in the posterior segment within the retinal layer. The structures located in the anterior segment are important for maintaining intraocular pressure (IOP). Figure adapted from Graw (133). B) The schematic diagram shows the aqueous humor flow pathway. Aqueous humor is produced by the ciliary body in the posterior chamber and then flows into the anterior chamber. The majority of the aqueous humor will be drained from the eye via the trabecular pathway through the trabecular meshwork (TM) and Schlemm's canal. The rest of the aqueous humor is drained via the uveoscleral pathway. Increased resistance occurs when the TM and Schelmm's canal malfunction. This disruption in aqueous humor outflow leads to increased intraocular pressure (IOP), which is a major risk factor for developing glaucoma. Figure from Ito and Walter (1).

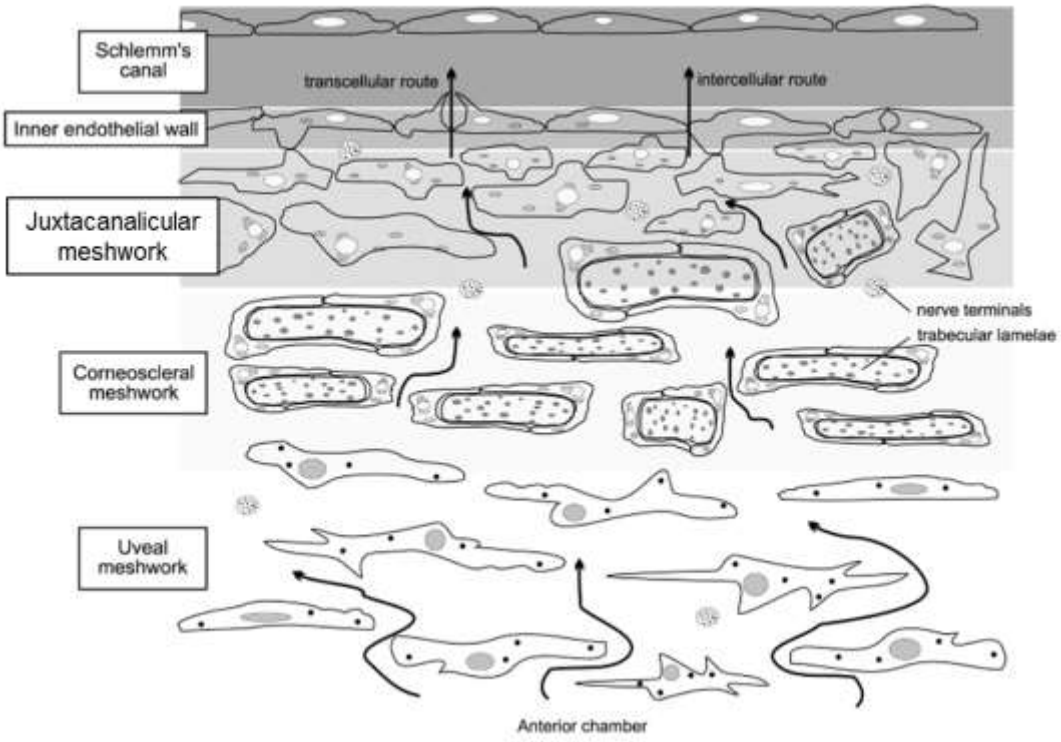
Schlemm's canal
transcellular route
intercellular route
Inner endothelial wall
Juxtacanalicular meshwork
nerve terminals
trabecular lamelae
Corneoscleral meshwork
Uveal meshwork
Anterior chamber

Figure 2: Schematic diagram of trabecular meshwork (TM). The aqueous humour flows through the three layers of the TM; uveal meshwork, corneoscleral meshwork, and the juxtacanalicular meshwork. Finally, the aqueous humor is drained from the eye through Schlemm's canal. Resistance to aqueous humour flow is suggested to increase as the intercellular spaces decrease in the three layers of the TM. Figure modified from Llobet *et al.* (48).

A

B

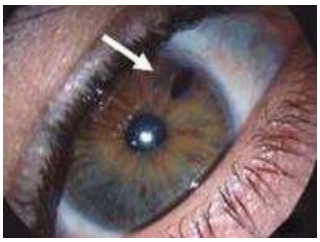

C

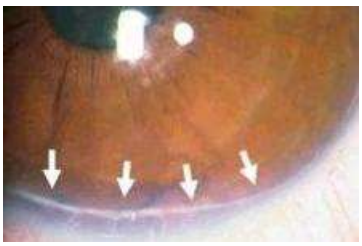

D

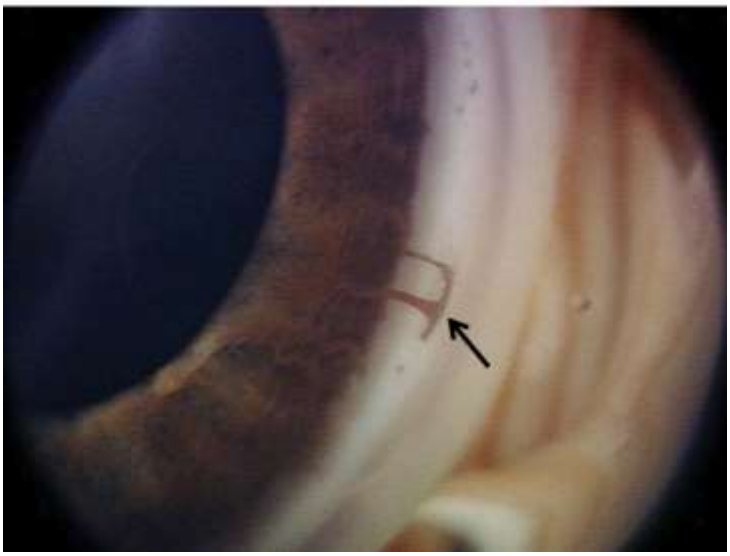

E

F

Figure 3: Ocular and systemic changes observed in Axenfeld-Rieger patients. A) Corectopia (displaced pupil) in the right eye is indicated by the arrow. B) Polycoria (extra hole is the iris) is indicated by the arrow. C) Posterior embryotoxon which results from a prominent Schwalbe's line is indicated by the arrows. D) Iridocorneal strands (arrow) can be observed. In addition to ocular anomalies, Axenfeld-Rieger patients can also have systemic defects including E) redundant preumbilical skin and F) dental anomalies such as hypodontia and microdontia. A to C were modified from Tumer *et al.* (66). D was modified from Chang *et al.* (134). E and F were modified from Lines *et al.* (135).

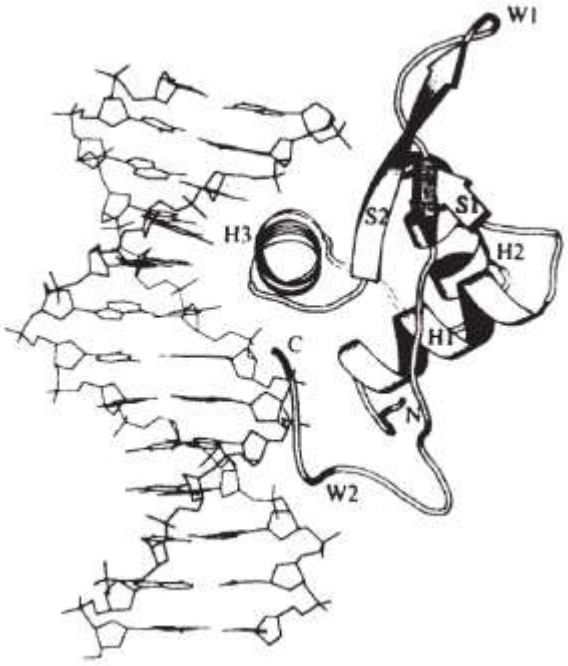
W1
S2
S1
H3
H2
H1
C
N
W2

Figure 4: Schematic diagram of the FOXA3 Forkhead Domain (FHD) bound to DNA. The FHD consists of three α-helices (H1, H2, H3) and three β-strands (S1, S2, S3). The helices are shown as coils while the sheets are represented as arrows. S2 and S3 delineate two wing-like loops (W1 and W2). H3 makes contact with the major groove of DNA while W2 makes contact with the minor groove of DNA. Figure from Clark *et al.* (76).

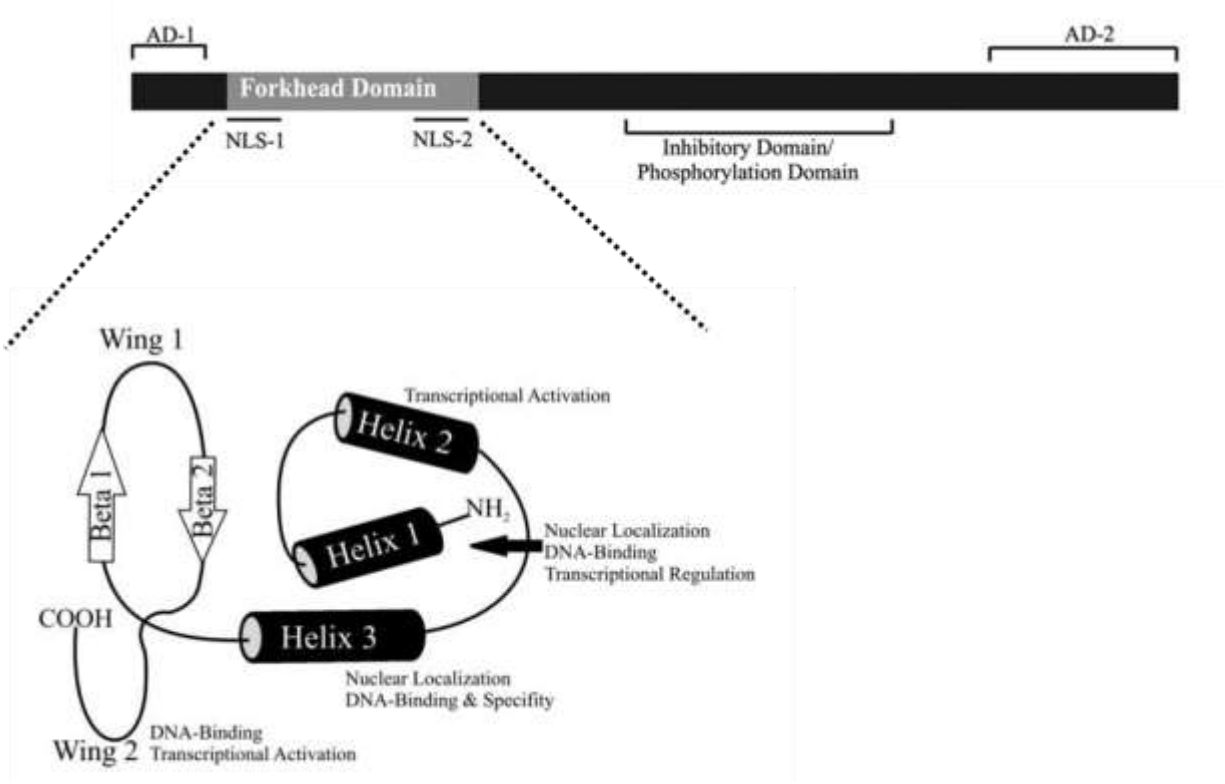
AD-1
AD-2
Forkhead Domain
NLS-1
NLS-2
Inhibitory Domain/
Phosphorylation Domain
Wing 1
Transcriptional Activation
Helix 2
Beta 1
Beta 2
NH2
Helix 1
Nuclear Localization
DNA-Binding
Transcriptional Regulation
COOH
Helix 3
Nuclear Localization
DNA-Binding & Specifity
Wing 2
DNA-Binding
Transcriptional Activation

Figure 5: Schematic diagram of FOXC1 functional domains. The Forkhead domain (FHD) is located between amino acid residues 69 and 178. Two nuclear localization domains (NLS-1, NLS-2) lie within the FHD. The transcriptional activation domains are located at amino acid residues 1-51 (AD-1) and 435-553 (AD-2). The inhibitory domain is located at amino acid residues 215-366). Figure modified from Berry *et al.* (81,136).

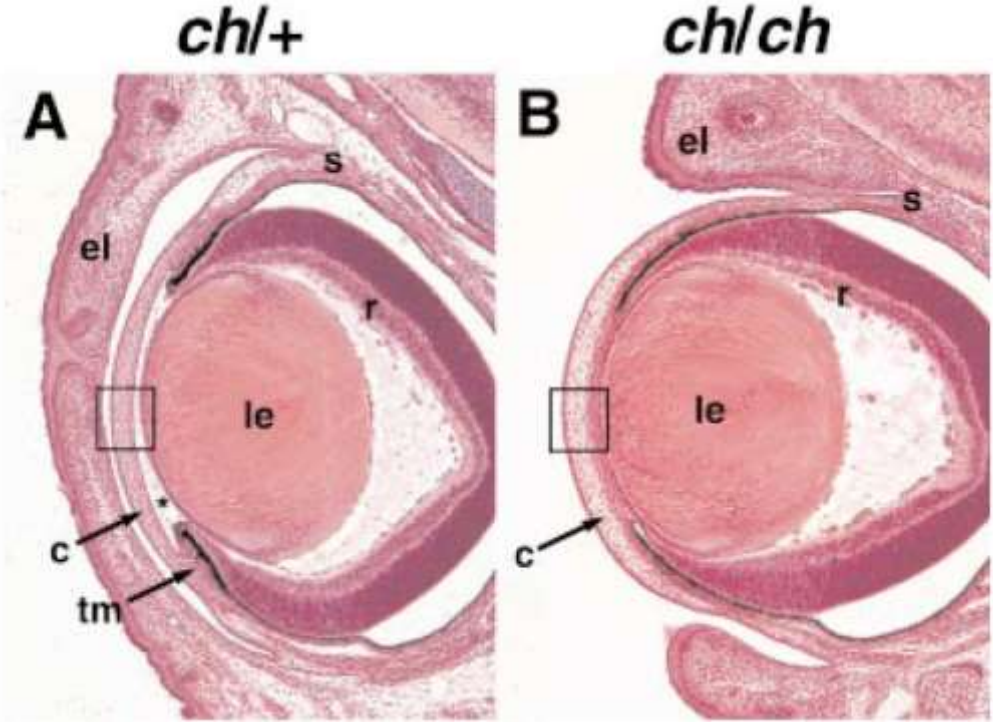
ch/+
ch/ch
A
B
el
s
r
le
c
tm
el
s
r
le
c

Figure 6: Ocular structures of heterozygous and homozygous congenital hydrocephalus (*ch*) mice at 17 dpc. *ch* mice have a point mutation in FoxC1,which results in a truncated protein lacking the Forkhead domain (FHD). Unlike in the heterozygous mice (*ch*/+), the anterior chamber (indicated by a (*) in A) does not form (square) in the homozygous mice (*ch/ch*). Abbreviations: c, cornea; el, endothelial layer; en, endothelium; le, lens; r, retina; s, sclera; tm, trabecular meshwork. Figure modified from Kidson *et al.* (88).

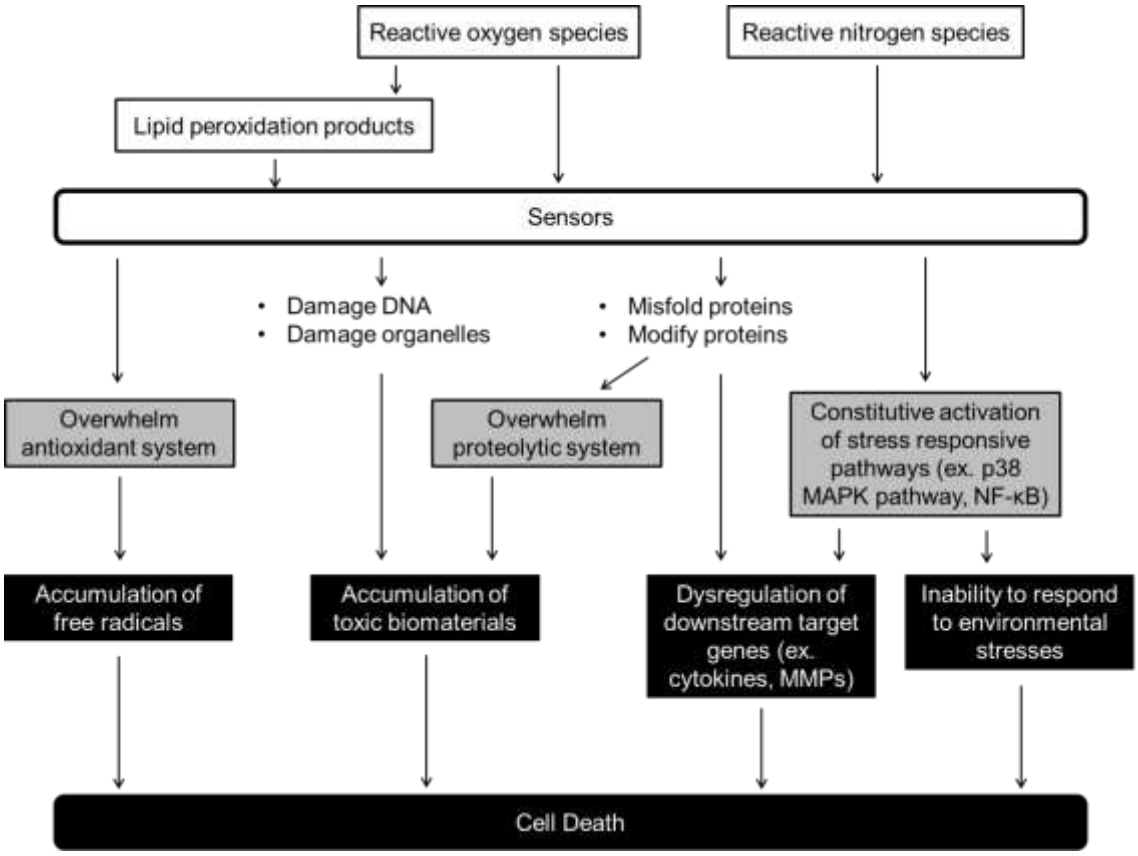
Reactive oxygen species
Reactive nitrogen species
Lipid peroxidation products
Sensors
• Damage DNA
• Damage organelles
• Misfold proteins
• Modify proteins
Overwhelm antioxidant system
Overwhelm proteolytic system
Constitutive activation of stress responsive pathways (ex. p38 MAPK pathway, NF-κB)
Accumulation of free radicals
Accumulation of toxic biomaterials
Dysregulation of downstream target genes (ex. cytokines, MMPs)
Inability to respond to environmental stresses
Cell Death

Figure 7: Overview of various oxidative stress-related effects on the cell, which would contribute to cell death. Figure from Ito and Walter (1).

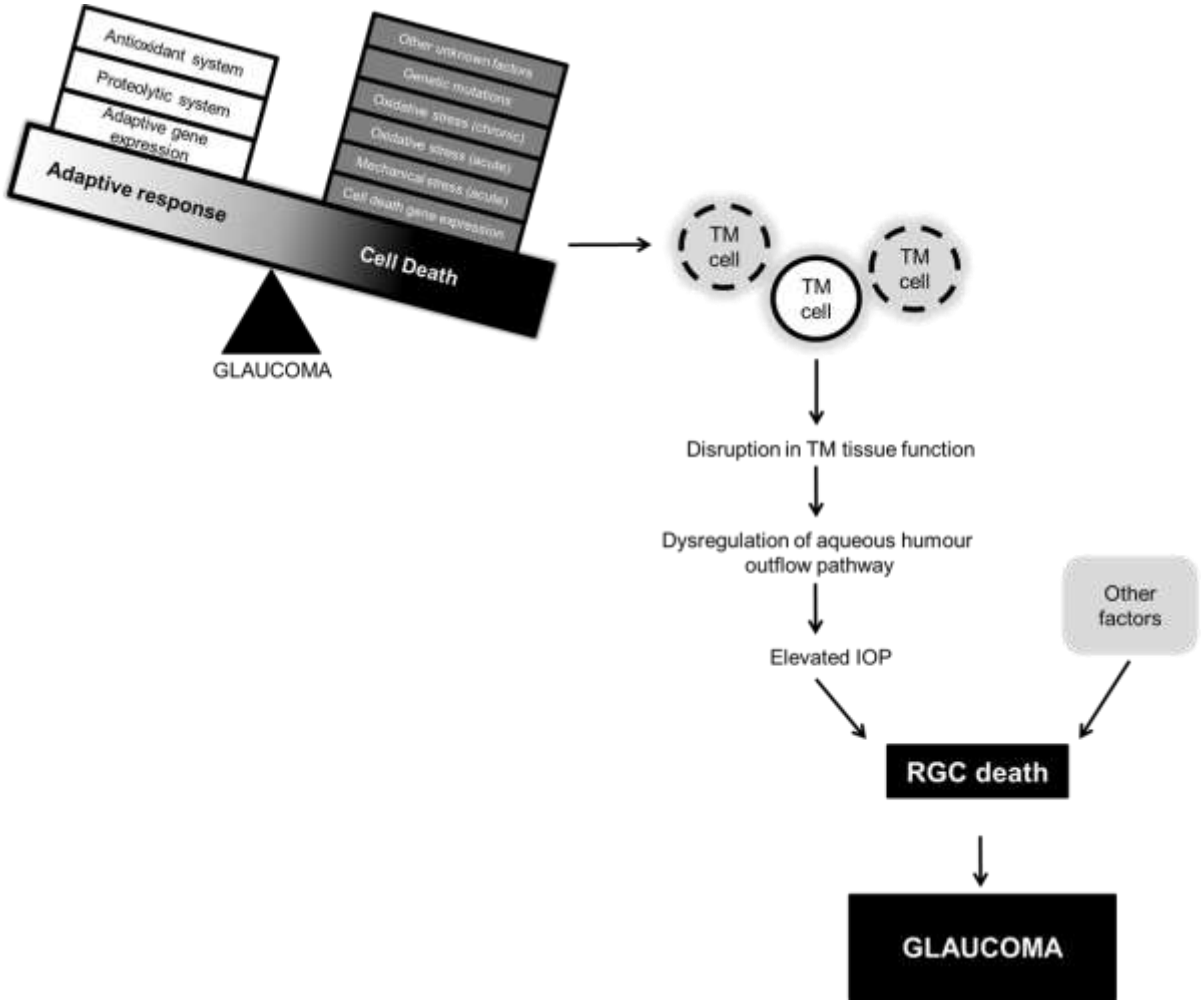
Antioxidant system
Proteolytic system
Adaptive gene expression
Adaptive response
Other unknown factors
Genetic mutations
Oxidative stress (chronic)
Oxidative stress (acute)
Mechanical stress (acute)
Cell death gene expression
Cell Death
GLAUCOMA
TM cell
TM cell
TM cell
Disruption in TM tissue function
Dysregulation of aqueous humour outflow pathway
Elevated IOP
Other factors
RGC death
GLAUCOMA

Figure 8. Trabecular meshwork of glaucoma phenotype. Similar to normal non-aging and aging conditions, trabecular meshwork (TM) cells are exposed to a variety of stresses. However, other unknown factors are present to initiate the cascade of events that lead to the development of glaucoma. Also, genetic mutations could compromise normal TM cell function. All of these factors are predicted to result in TM cell death (dotted circles) to the extent that the TM tissue is no longer able to function properly. Consequently, there will be dysregulation of aqueous humor drainage resulting in increased intraocular pressure (IOP), which would ultimately lead to retinal ganglion cell (RGC) death and glaucoma. Figure from Ito and Walter (1).

References

(1) Ito YA, Walter MA. **Genetics and environmental stress factor contributions to anterior segment malformations and glaucoma**. In: Rumelt S, editor. **Glaucoma – Basic and Clinical Aspects**: InTech; In Press.

(2) Quigley HA, Broman AT. The number of people with glaucoma worldwide in 2010 and 2020. Br J Ophthalmol 2006 Mar;90(3):262-267.

(3) Rudnicka AR, Mt-Isa S, Owen CG, Cook DG, Ashby D. Variations in primary open-angle glaucoma prevalence by age, gender, and race: a Bayesian meta-analysis. Invest Ophthalmol Vis Sci 2006 Oct;47(10):4254-4261.

(4) Leske MC. Open-angle glaucoma -- an epidemiologic overview. Ophthalmic Epidemiol 2007 Jul-Aug;14(4):166-172.

(5) Vrabec JP, Levin LA. The neurobiology of cell death in glaucoma. Eye (Lond) 2007 Dec;21 Suppl 1:S11-4.

(6) Almasieh M, Wilson AM, Morquette B, Cueva Vargas JL, Di Polo A. The molecular basis of retinal ganglion cell death in glaucoma. Prog Retin Eye Res 2012 Mar;31(2):152-181.

(7) Giblin FJ, McCready JP, Kodama T, Reddy VN. A direct correlation between the levels of ascorbic acid and H2O2 in aqueous humor. Exp Eye Res 1984 Jan;38(1):87-93.

(8) Bhuyan KC, Bhuyan DK. Regulation of hydrogen peroxide in eye humors. Effect of 3-amino-1H-1,2,4-triazole on catalase and glutathione peroxidase of rabbit eye. Biochim Biophys Acta 1977 May 26;497(3):641-651.

(9) Mark HH. Aqueous humor dynamics in historical perspective. Surv Ophthalmol 2010 Jan-Feb;55(1):89-100.

(10) Goel M, Picciani RG, Lee RK, Bhattacharya SK. Aqueous humor dynamics: a review. Open Ophthalmol J 2010 Sep 3;4:52-59.

(11) Brubaker RF. Measurement of Aqueous Flow By Fluorophotometry. The Glaucomas; 1989. p. 337.

(12) Millar C, Kaufman PL. Aqueous humor: Secretion and dynamics. In: Jaeger EA, Tasman W, editors. DUANE'S FOUNDATIONS OF CLINICAL OPHTHALMOLOGY: Philadelphia: Lippincott; 1995. p. 1.

(13) Hollows FC, Graham PA. Intra-ocular pressure, glaucoma, and glaucoma suspects in a defined population. Br J Ophthalmol 1966 Oct;50(10):570-586.

(14) Bill A. The aqueous humor drainage mechanism in the cynomolgus monkey (Macaca irus) with evidence for unconventional routes. Invest Ophthalmol 1965 Oct;4(5):911-919.

(15) Bill A, Hellsing K. Production and drainage of aqueous humor in the cynomolgus monkey (Macaca irus). Invest Ophthalmol 1965 Oct;4(5):920-926.

(16) Alm A, Nilsson SF. Uveoscleral outflow--a review. Exp Eye Res 2009 Apr;88(4):760-768.

(17) FINE BS. Observations on the Drainage Angle in Man and Rhesus Monkey: a Concept of the Pathogenesis of Chronic Simple Glaucoma. a Light and Electron Microscopic Study. Invest Ophthalmol 1964 Dec;3:609-646.

(18) Fine BS. Structure of the trabecular meshwork and the canal of Schlemm. Trans Am Acad Ophthalmol Otolaryngol 1966 Sep-Oct;70(5):777-790.

(19) Rohen JW, Futa R, Lutjen-Drecoll E. The fine structure of the cribriform meshwork in normal and glaucomatous eyes as seen in tangential sections. Invest Ophthalmol Vis Sci 1981 Oct;21(4):574-585.

(20) Lutjen-Drecoll E, Futa R, Rohen JW. Ultrahistochemical studies on tangential sections of the trabecular meshwork in normal and glaucomatous eyes. Invest Ophthalmol Vis Sci 1981 Oct;21(4):563-573.

(21) Underwood JL, Murphy CG, Chen J, Franse-Carman L, Wood I, Epstein DL, et al. Glucocorticoids regulate transendothelial fluid flow resistance and formation of intercellular junctions. Am J Physiol 1999 Aug;277(2 Pt 1):C330-42.

(22) Tripathi R. Tracing the bulk outflow route of cerebrospinal fluid by transmission and scanning electron microscopy. Brain Res 1974 Nov 22;80(3):503-506.

(23) Epstein DL, Rohen JW. Morphology of the trabecular meshwork and inner-wall endothelium after cationized ferritin perfusion in the monkey eye. Invest Ophthalmol Vis Sci 1991 Jan;32(1):160-171.

(24) Brilakis HS, Johnson DH. Giant vacuole survival time and implications for aqueous humor outflow. J Glaucoma 2001 Aug;10(4):277-283.

(25) Ascher KW. The aqueous veins: I. Physiologic importance of the visible elimination of intraocular fluid. Am J Ophthalmol. 1942;25:1174-1209.

(26) Lutjen-Drecoll E. New findings on the functional structure of the region of the angle of the chamber and its changes after glaucoma surgery (author's transl). Klin Monbl Augenheilkd 1973 Oct;163(4):410-419.

(27) Maepea O, Bill A. Pressures in the juxtacanalicular tissue and Schlemm's canal in monkeys. Exp Eye Res 1992 Jun;54(6):879-883.

(28) Ethier CR, Kamm RD, Palaszewski BA, Johnson MC, Richardson TM. Calculations of flow resistance in the juxtacanalicular meshwork. Invest Ophthalmol Vis Sci 1986 Dec;27(12):1741-1750.

(29) Seiler T, Wollensak J. The resistance of the trabecular meshwork to aqueous humor outflow. Graefes Arch Clin Exp Ophthalmol 1985;223(2):88-91.

(30) Acott TS, Kelley MJ. Extracellular matrix in the trabecular meshwork. Exp Eye Res 2008 Apr;86(4):543-561.

(31) Keller KE, Aga M, Bradley JM, Kelley MJ, Acott TS. Extracellular matrix turnover and outflow resistance. Exp Eye Res 2009 Apr;88(4):676-682.

(32) Woessner JF,Jr. Matrix metalloproteinases and their inhibitors in connective tissue remodeling. FASEB J 1991 May;5(8):2145-2154.

(33) Bradley JM, Vranka J, Colvis CM, Conger DM, Alexander JP, Fisk AS, et al. Effect of matrix metalloproteinases activity on outflow in perfused human organ culture. Invest Ophthalmol Vis Sci 1998 Dec;39(13):2649-2658.

(34) Page-McCaw A, Ewald AJ, Werb Z. Matrix metalloproteinases and the regulation of tissue remodelling. Nat Rev Mol Cell Biol 2007 Mar;8(3):221-233.

(35) Rohen JW, Lutjen E, Barany E. The relation between the ciliary muscle and the trabecular meshwork and its importance for the effect of miotics on aqueous outflow resistance. A study in two contrasting monkey species, Macaca irus and Cercopithecus aethiops. Albrecht Von Graefes Arch Klin Exp Ophthalmol 1967;172(1):23-47.

(36) Lutjen-Drecoll E, Wiendl H, Kaufman PL. Acute and chronic structural effects of pilocarpine on monkey outflow tissues. Trans Am Ophthalmol Soc 1998;96:171-91; discussion 192-5.

(37) Barany EH. The mode of action of miotics on outflow resistance. A study of pilocarpine in the vervet monkey Cercopithecus ethiops. Trans Ophthalmol Soc U K 1966;86:539-578.

(38) Gabelt BT, Kaufman PL. Changes in aqueous humor dynamics with age and glaucoma. Prog Retin Eye Res 2005 Sep;24(5):612-637.

(39) Toris CB, Yablonski ME, Wang YL, Camras CB. Aqueous humor dynamics in the aging human eye. Am J Ophthalmol 1999 Apr;127(4):407-412.

(40) BECKER B. The decline in aqueous secretion and outflow facility with age. Am J Ophthalmol 1958 Nov;46(5 Part 1):731-736.

(41) Gaasterland D, Kupfer C, Milton R, Ross K, McCain L, MacLellan H. Studies of aqueous humour dynamics in man. VI. Effect of age upon parameters of intraocular pressure in normal human eyes. Exp Eye Res 1978 Jun;26(6):651-656.

(42) Bloom JN, Levene RZ, Thomas G, Kimura R. Fluorophotometry and the rate of aqueous flow in man. I. Instrumentation and normal values. Arch Ophthalmol 1976 Mar;94(3):435-443.

(43) Brubaker RF, Nagataki S, Townsend DJ, Burns RR, Higgins RG, Wentworth W. The effect of age on aqueous humor formation in man. Ophthalmology 1981 Mar;88(3):283-288.

(44) Kupfer C. Clinical significance of pseudofacility. Sanford R. Gifford Memorial Lecture. Am J Ophthalmol 1973 Feb;75(2):193-204.

(45) Foster PJ, Alsbirk PH, Baasanhu J, Munkhbayar D, Uranchimeg D, Johnson GJ. Anterior chamber depth in Mongolians: variation with age, sex, and method of measurement. Am J Ophthalmol 1997 Jul;124(1):53-60.

(46) Rufer F, Schroder A, Klettner A, Frimpong-Boateng A, Roider JB, Erb C. Anterior chamber depth and iridocorneal angle in healthy White subjects: effects of age, gender and refraction. Acta Ophthalmol 2010 Dec;88(8):885-890.

(47) Lutjen-Drecoll E, Kaufman PL, Eichhorn M. Long-term timolol and epinephrine in monkeys. I. Functional morphology of the ciliary processes. Trans Ophthalmol Soc U K 1986;105 (Pt 2)(Pt 2):180-195.

(48) Llobet A, Gasull X, Gual A. Understanding trabecular meshwork physiology: a key to the control of intraocular pressure? News Physiol Sci 2003 Oct;18:205-209.

(49) Lutjen-Drecoll E. Morphological changes in glaucomatous eyes and the role of TGFbeta2 for the pathogenesis of the disease. Exp Eye Res 2005 Jul;81(1):1-4.

(50) Alvarado J, Murphy C, Juster R. Trabecular meshwork cellularity in primary open-angle glaucoma and nonglaucomatous normals. Ophthalmology 1984 Jun;91(6):564-579.

(51) Grierson I, Howes RC. Age-related depletion of the cell population in the human trabecular meshwork. Eye (Lond) 1987;1 (Pt 2)(Pt 2):204-210.

(52) Alvarado J, Murphy C, Polansky J, Juster R. Age-related changes in trabecular meshwork cellularity. Invest Ophthalmol Vis Sci 1981 Nov;21(5):714-727.

(53) Tschumper RC, Johnson DH. Trabecular meshwork cellularity. Differences between fellow eyes. Invest Ophthalmol Vis Sci 1990 Jul;31(7):1327-1331.

(54) Buller C, Johnson DH, Tschumper RC. Human trabecular meshwork phagocytosis. Observations in an organ culture system. Invest Ophthalmol Vis Sci 1990 Oct;31(10):2156-2163.

(55) Grierson I, Chisholm IA. Clearance of debris from the iris through the drainage angle of the rabbit's eye. Br J Ophthalmol 1978 Oct;62(10):694-704.

(56) Grierson I, Lee WR. Erythrocyte phagocytosis in the human trabecular meshwork. Br J Ophthalmol 1973 Jun;57(6):400-415.

(57) Johnson DH, Richardson TM, Epstein DL. Trabecular meshwork recovery after phagocytic challenge. Curr Eye Res 1989 Nov;8(11):1121-1130.

(58) Rohen JW, van der Zypen E. The phagocytic activity of the trabecularmeshwork endothelium. An electron-microscopic study of the vervet (Cercopithecus aethiops). Albrecht Von Graefes Arch Klin Exp Ophthalmol 1968;175(2):143-160.

(59) Shirato S, Murphy CG, Bloom E, Franse-Carman L, Maglio MT, Polansky JR, et al. Kinetics of phagocytosis in trabecular meshwork cells. Flow cytometry and morphometry. Invest Ophthalmol Vis Sci 1989 Dec;30(12):2499-2511.

(60) Zhou L, Li Y, Yue BY. Alteration of cytoskeletal structure, integrin distribution, and migratory activity by phagocytic challenge in cells from an ocular tissue--the trabecular meshwork. In Vitro Cell Dev Biol Anim 1999 Mar;35(3):144-149.

(61) Alvarado JA, Alvarado RG, Yeh RF, Franse-Carman L, Marcellino GR, Brownstein MJ. A new insight into the cellular regulation of aqueous outflow: how trabecular meshwork endothelial cells drive a mechanism that regulates the permeability of Schlemm's canal endothelial cells. Br J Ophthalmol 2005 Nov;89(11):1500-1505.

(62) Shifera AS, Trivedi S, Chau P, Bonnemaison LH, Iguchi R, Alvarado JA. Constitutive secretion of chemokines by cultured human trabecular meshwork cells. Exp Eye Res 2010 Jul;91(1):42-47.

(63) Rohen JW, Witmer R. Electrn microscopic studies on the trabecular meshwork in glaucoma simplex. Albrecht Von Graefes Arch Klin Exp Ophthalmol 1972;183(4):251-266.

(64) Idrees F, Vaideanu D, Fraser SG, Sowden JC, Khaw PT. A review of anterior segment dysgeneses. Surv Ophthalmol 2006 May-Jun;51(3):213-231.

(65) Sowden JC. Molecular and developmental mechanisms of anterior segment dysgenesis. Eye (Lond) 2007 Oct;21(10):1310-1318.

(66) Tumer Z, Bach-Holm D. Axenfeld-Rieger syndrome and spectrum of PITX2 and FOXC1 mutations. Eur J Hum Genet 2009 Dec;17(12):1527-1539.

(67) Strungaru MH, Dinu I, Walter MA. Genotype-phenotype correlations in Axenfeld-Rieger malformation and glaucoma patients with FOXC1 and PITX2 mutations. Invest Ophthalmol Vis Sci 2007 Jan;48(1):228-237.

(68) D'haene B, Meire F, Claerhout I, Kroes HY, Plomp A, Arens YH, et al. Expanding the spectrum of FOXC1 and PITX2 mutations and copy number changes in patients with anterior segment malformations. Invest Ophthalmol Vis Sci 2011 Jan 21;52(1):324-333.

(69) Phillips JC, del Bono EA, Haines JL, Pralea AM, Cohen JS, Greff LJ, et al. A second locus for Rieger syndrome maps to chromosome 13q14. Am J Hum Genet 1996 Sep;59(3):613-619.

(70) Lehmann OJ, Ebenezer ND, Jordan T, Fox M, Ocaka L, Payne A, et al. Chromosomal duplication involving the forkhead transcription factor gene FOXC1 causes iris hypoplasia and glaucoma. Am J Hum Genet 2000 Nov;67(5):1129-1135.

(71) Nishimura DY, Searby CC, Alward WL, Walton D, Craig JE, Mackey DA, et al. A spectrum of FOXC1 mutations suggests gene dosage as a mechanism for developmental defects of the anterior chamber of the eye. Am J Hum Genet 2001 Feb;68(2):364-372.

(72) Lehmann OJ, Ebenezer ND, Ekong R, Ocaka L, Mungall AJ, Fraser S, et al. Ocular developmental abnormalities and glaucoma associated with interstitial 6p25 duplications and deletions. Invest Ophthalmol Vis Sci 2002 Jun;43(6):1843-1849.

(73) Chanda B, Asai-Coakwell M, Ye M, Mungall AJ, Barrow M, Dobyns WB, et al. A novel mechanistic spectrum underlies glaucoma-associated chromosome 6p25 copy number variation. Hum Mol Genet 2008 Nov 15;17(22):3446-3458.

(74) Tonoki H, Harada N, Shimokawa O, Yosozumi A, Monzaki K, Satoh K, et al. Axenfeld-Rieger anomaly and Axenfeld-Rieger syndrome: clinical, molecular-cytogenetic, and DNA array analyses of three patients with chromosomal defects at 6p25. Am J Med Genet A 2011 Dec;155A(12):2925-2932.

(75) Benayoun BA, Caburet S, Veitia RA. Forkhead transcription factors: key players in health and disease. Trends Genet 2011 Jun;27(6):224-232.

(76) Clark KL, Halay ED, Lai E, Burley SK. Co-crystal structure of the HNF-3/fork head DNA-recognition motif resembles histone H5. Nature 1993 Jul 29;364(6436):412-420.

(77) van Dongen MJ, Cederberg A, Carlsson P, Enerback S, Wikstrom M. Solution structure and dynamics of the DNA-binding domain of the adipocyte-transcription factor FREAC-11. J Mol Biol 2000 Feb 18;296(2):351-359.

(78) Weigelt J, Climent I, Dahlman-Wright K, Wikstrom M. Solution structure of the DNA binding domain of the human forkhead transcription factor AFX (FOXO4). Biochemistry 2001 May 22;40(20):5861-5869.

(79) Pierrou S, Hellqvist M, Samuelsson L, Enerback S, Carlsson P. Cloning and characterization of seven human forkhead proteins: binding site specificity and DNA bending. EMBO J 1994 Oct 17;13(20):5002-5012.

(80) Berry FB, Skarie JM, Mirzayans F, Fortin Y, Hudson TJ, Raymond V, et al. FOXC1 is required for cell viability and resistance to oxidative stress in the eye through the transcriptional regulation of FOXO1A. Hum Mol Genet 2008 Feb 15;17(4):490-505.

(81) Berry FB, Saleem RA, Walter MA. FOXC1 transcriptional regulation is mediated by N- and C-terminal activation domains and contains a phosphorylated transcriptional inhibitory domain. J Biol Chem 2002 Mar 22;277(12):10292-10297.

(82) Berry FB, Mirzayans F, Walter MA. Regulation of FOXC1 stability and transcriptional activity by an epidermal growth factor-activated mitogen-activated protein kinase signaling cascade. J Biol Chem 2006 Apr 14;281(15):10098-10104.

(83) Fetterman CD, Mirzayans F, Walter MA. Characterization of a novel FOXC1 mutation, P297S, identified in two individuals with anterior segment dysgenesis. Clin Genet 2009 Sep;76(3):296-299.

(84) Gage PJ, Rhoades W, Prucka SK, Hjalt T. Fate maps of neural crest and mesoderm in the mammalian eye. Invest Ophthalmol Vis Sci 2005 Nov;46(11):4200-4208.

(85) Kume T, Deng KY, Winfrey V, Gould DB, Walter MA, Hogan BL. The forkhead/winged helix gene Mf1 is disrupted in the pleiotropic mouse mutation congenital hydrocephalus. Cell 1998 Jun 12;93(6):985-996.

(86) Hong HK, Lass JH, Chakravarti A. Pleiotropic skeletal and ocular phenotypes of the mouse mutation congenital hydrocephalus (ch/Mf1) arise from a winged helix/forkhead transcriptionfactor gene. Hum Mol Genet 1999 Apr;8(4):625-637.

(87) Grunenberg H. Congenital hydrocephalus in the mouse, a case of spurious pleiotropism. J Genet 1943;45.

(88) Kidson SH, Kume T, Deng K, Winfrey V, Hogan BL. The forkhead/winged-helix gene, Mf1, is necessary for the normal development of the cornea and formation of the anterior chamber in the mouse eye. Dev Biol 1999 Jul 15;211(2):306-322.

(89) Skarie JM, Link BA. FoxC1 is essential for vascular basement membrane integrity and hyaloid vessel morphogenesis. Invest Ophthalmol Vis Sci 2009 Nov;50(11):5026-5034.

(90) Acharya M, Huang L, Fleisch VC, Allison WT, Walter MA. A complex regulatory network of transcription factors critical for ocular development and disease. Hum Mol Genet 2011 Apr 15;20(8):1610-1624.

(91) Shields MB. Axenfeld-Rieger syndrome: a theory of mechanism and distinctions from the iridocorneal endothelial syndrome. Trans Am Ophthalmol Soc 1983;81:736-784.

(92) Alkemade PHH. Dysgenesis medoermalis of the iris and the cornea. A study of Rieger's syndrome and Peter's Anomaly. The Netherlands: Van Gorcum; 1969.

(93) Clark AF. The cell and molecular biology of glaucoma: biomechanical factors in glaucoma. Invest Ophthalmol Vis Sci 2012 May 4;53(5):2473-2475.

(94) Liton PB, Gonzalez P. Stress response of the trabecular meshwork. J Glaucoma 2008 Aug;17(5):378-385.

(95) Vittal V, Rose A, Gregory KE, Kelley MJ, Acott TS. Changes in gene expression by trabecular meshwork cells in response to mechanical stretching. Invest Ophthalmol Vis Sci 2005 Aug;46(8):2857-2868.

(96) Kumar DM, Agarwal N. Oxidative stress in glaucoma: a burden of evidence. J Glaucoma 2007 May;16(3):334-343.

(97) Ferreira SM, Lerner SF, Brunzini R, Evelson PA, Llesuy SF. Oxidative stress markers in aqueous humor of glaucoma patients. Am J Ophthalmol 2004 Jan;137(1):62-69.

(98) Wang WH, McNatt LG, Shepard AR, Jacobson N, Nishimura DY, Stone EM, et al. Optimal procedure for extracting RNA from human ocular tissues and expression profiling of the congenital glaucoma gene FOXC1 using quantitative RT-PCR. Mol Vis 2001 Apr 17;7:89-94.

(99) Izzotti A, Bagnis A, Sacca SC. The role of oxidative stress in glaucoma. Mutat Res 2006 Mar;612(2):105-114.

(100) Rose RC, Richer SP, Bode AM. Ocular oxidants and antioxidant protection. Proc Soc Exp Biol Med 1998 Apr;217(4):397-407.

(101) Bleau G, Giasson C, Brunette I. Measurement of hydrogen peroxide in biological samples containing high levels of ascorbic acid. Anal Biochem 1998 Oct 1;263(1):13-17.

(102) García-Castiñeiras S. Hydrogen peroxide in the aqueous humor: 1992-1997. 1998;17(4):335-343.

(103) Valko M, Leibfritz D, Moncol J, Cronin MT, Mazur M, Telser J. Free radicals and antioxidants in normal physiological functions and human disease. Int J Biochem Cell Biol 2007;39(1):44-84.

(104) McCord JM, Fridovich I. Superoxide dismutase. An enzymic function for erythrocuprein (hemocuprein). J Biol Chem 1969 Nov 25;244(22):6049-6055.

(105) KINSEY VE. Transfer of ascorbic acid and related compounds across the blood-aqueous barrier. Am J Ophthalmol 1947 Oct;30(10):1262-1266.

(106) BECKER B. Chemical composition of human aqueous humor; effects of acetazoleamide. AMA Arch Ophthalmol 1957 Jun;57(6):793-800.

(107) Reiss GR, Werness PG, Zollman PE, Brubaker RF. Ascorbic acid levels in the aqueous humor of nocturnal and diurnal mammals. Arch Ophthalmol 1986 May;104(5):753-755.

(108) Reddy VN, Giblin FJ, Lin LR, Chakrapani B. The effect of aqueous humor ascorbate on ultraviolet-B-induced DNA damage in lens epithelium. Invest Ophthalmol Vis Sci 1998 Feb;39(2):344-350.

(109) Schachtschabel DO, Binninger EA, Rohen JW. In vitro cultures of trabecular meshwork cells of the human eye as a model system for the study of cellular aging. Arch Gerontol Geriatr 1989 Nov-Dec;9(3):251-262.

(110) Guo MS, Wu YY, Liang ZB. Hyaluronic acid increases MMP-2 and MMP-9 expressions in cultured trabecular meshwork cells from patients with primary open-angle glaucoma. Mol Vis 2012;18:1175-1181.

(111) Knepper PA, Goossens W, Palmberg PF. Glycosaminoglycan stratification of the juxtacanalicular tissue in normal and primary open-angle glaucoma. Invest Ophthalmol Vis Sci 1996 Nov;37(12):2414-2425.

(112) Knepper PA, Goossens W, Hvizd M, Palmberg PF. Glycosaminoglycans of the human trabecular meshwork in primary open-angle glaucoma. Invest Ophthalmol Vis Sci 1996 Jun;37(7):1360-1367.

(113) Jampel HD, Moon JI, Quigley HA, Barron Y, Lam KW. Aqueous humor uric acid and ascorbic acid concentrations and outcome of trabeculectomy. Arch Ophthalmol 1998 Mar;116(3):281-285.

(114) Leite MT, Prata TS, Kera CZ, Miranda DV, de Moraes Barros SB, Melo LA,Jr. Ascorbic acid concentration is reduced in the secondary aqueous humour of glaucomatous patients. Clin Experiment Ophthalmol 2009 May;37(4):402-406.

(115) Lee P, Lam KW, Lai M. Aqueous humor ascorbate concentration and open-angle glaucoma. Arch Ophthalmol 1977 Feb;95(2):308-310.

(116) de Nadal E, Ammerer G, Posas F. Controlling gene expression in response to stress. Nat Rev Genet 2011 Nov 3;12(12):833-845.

(117) Porter KM, Epstein DL, Liton PB. Up-regulated expression of extracellular matrix remodeling genes in phagocytically challenged trabecular meshwork cells. PLoS One 2012;7(4):e34792.

(118) Jenner P. Oxidative stress in Parkinson's disease. Ann Neurol 2003;53 Suppl 3:S26-36; discussion S36-8.

(119) Zhou C, Huang Y, Przedborski S. Oxidative stress in Parkinson's disease: a mechanism of pathogenic and therapeutic significance. Ann N Y Acad Sci 2008 Dec;1147:93-104.

(120) Nunomura A, Perry G, Aliev G, Hirai K, Takeda A, Balraj EK, et al. Oxidative damage is the earliest event in Alzheimer disease. J Neuropathol Exp Neurol 2001 Aug;60(8):759-767.

(121) Pratico D, Uryu K, Leight S, Trojanoswki JQ, Lee VM. Increased lipid peroxidation precedes amyloid plaque formation in an animal model of Alzheimer amyloidosis. J Neurosci 2001 Jun 15;21(12):4183-4187.

(122) Reddy PH, McWeeney S, Park BS, Manczak M, Gutala RV, Partovi D, et al. Gene expression profiles of transcripts in amyloid precursor protein transgenic mice: up-regulation of mitochondrial metabolism and apoptotic genes is an early cellular change in Alzheimer's disease. Hum Mol Genet 2004 Jun 15;13(12):1225-1240.

(123) Wiseman H, Halliwell B. Damage to DNA by reactive oxygen and nitrogen species: role in inflammatory disease and progression to cancer. Biochem J 1996 Jan 1;313 (Pt 1)(Pt 1):17-29.

(124) Valko M, Rhodes CJ, Moncol J, Izakovic M, Mazur M. Free radicals, metals and antioxidants in oxidative stress-induced cancer. Chem Biol Interact 2006 Mar 10;160(1):1-40.

(125) Cai H, Harrison DG. Endothelial dysfunction in cardiovascular diseases: the role of oxidant stress. Circ Res 2000 Nov 10;87(10):840-844.

(126) Izzotti A, Sacca SC, Cartiglia C, De Flora S. Oxidative deoxyribonucleic acid damage in the eyes of glaucoma patients. Am J Med 2003 Jun 1;114(8):638-646.

(127) Sacca SC, Pascotto A, Camicione P, Capris P, Izzotti A. Oxidative DNA damage in the human trabecular meshwork: clinical correlation in patients with primary open-angle glaucoma. Arch Ophthalmol 2005 Apr;123(4):458-463.

(128) Sorkhabi R, Ghorbanihaghjo A, Javadzadeh A, Rashtchizadeh N, Moharrery M. Oxidative DNA damage and total antioxidant status in glaucoma patients. Mol Vis 2011 Jan 7;17:41-46.

(129) Caballero M, Liton PB, Challa P, Epstein DL, Gonzalez P. Effects of donor age on proteasome activity and senescence in trabecular meshwork cells. Biochem Biophys Res Commun 2004 Oct 22;323(3):1048-1054.

(130) Govindarajan B, Laird J, Salomon RG, Bhattacharya SK. Isolevuglandin-modified proteins, including elevated levels of inactive calpain-1, accumulate in glaucomatous trabecular meshwork. Biochemistry 2008 Jan 15;47(2):817-825.

(131) Ghanem AA, Arafa LF, El-Baz A. Oxidative stress markers in patients with primary open-angle glaucoma. Curr Eye Res 2010 Apr;35(4):295-301.

(132) Kampinga HH, Craig EA. The HSP70 chaperone machinery: J proteins as drivers of functional specificity. Nat Rev Mol Cell Biol 2010 Aug;11(8):579-592.

(133) Graw J. The genetic and molecular basis of congenital eye defects. Nat Rev Genet 2003 Nov;4(11):876-888.

(134) Chang TC, Summers CG, Schimmenti LA, Grajewski AL. Axenfeld-Rieger syndrome: new perspectives. Br J Ophthalmol 2012 Mar;96(3):318-322.

(135) Lines MA, Kozlowski K, Walter MA. Molecular genetics of Axenfeld-Rieger malformations. Hum Mol Genet 2002 May 15;11(10):1177-1184.

(136) Berry FB, Tamimi Y, Carle MV, Lehmann OJ, Walter MA. The establishment of a predictive mutational model of the forkhead domain through the analyses of FOXC2 missense mutations identified in patients with hereditary lymphedema with distichiasis. Hum Mol Genet 2005 Sep 15;14(18):2619-2627.

(137) Kaufmann E, Knochel W. Five years on the wings of fork head. Mech Dev 1996 Jun;57(1):3-20.

(138) Mears AJ, Jordan T, Mirzayans F, Dubois S, Kume T, Parlee M, et al. Mutations of the forkhead/winged-helix gene, FKHL7, in patients with Axenfeld-Rieger anomaly. Am J Hum Genet 1998 Nov;63(5):1316-1328.

(139) Nishimura DY, Swiderski RE, Alward WL, Searby CC, Patil SR, Bennet SR, et al. The forkhead transcription factor gene FKHL7 is responsible for glaucoma phenotypes which map to 6p25. Nat Genet 1998 Jun;19(2):140-147.

(140) Reese AB, Ellsworth RM. The anterior chamber cleavage syndrome. Arch Ophthalmol 1966 Mar;75(3):307-318.

(141) Weatherill JR, Hart CT. Familial hypoplasia of the iris stroma associated with glaucoma. Br J Ophthalmol 1969 Jul;53(7):433-438.

(142) Shields MB, Buckley E, Klintworth GK, Thresher R. Axenfeld-Rieger syndrome. A spectrum of developmental disorders. Surv Ophthalmol 1985 May-Jun;29(6):387-409.

(143) Feingold M, Shiere F, Fogels HR, Donaldson D. Rieger's syndrome. Pediatrics 1969 Oct;44(4):564-569.

(144) Fitch N, Kaback M. The Axenfeld syndrome and the Rieger syndrome. J Med Genet 1978 Feb;15(1):30-34.

(145) Chisholm IA, Chudley AE. Autosomal dominant iridogoniodysgenesis with associated somatic anomalies: four-generation family with Rieger's syndrome. Br J Ophthalmol 1983 Aug;67(8):529-534.

(146) Hiemisch H, Monaghan AP, Schutz G, Kaestner KH. Expression of the mouse Fkh1/Mf1 and Mfh1 genes in late gestation embryos is restricted to mesoderm derivatives. Mech Dev 1998 Apr;73(1):129-132.

(147) Kume T, Deng K, Hogan BL. Murine forkhead/winged helix genes Foxc1 (Mf1) and Foxc2 (Mfh1) are required for the early organogenesis of the kidney and urinary tract. Development 2000 Apr;127(7):1387-1395.

(148) Swiderski RE, Reiter RS, Nishimura DY, Alward WL, Kalenak JW, Searby CS, et al. Expression of the Mf1 gene in developing mouse hearts: implication in the development of human congenital heart defects. Dev Dyn 1999 Sep;216(1):16-27.

(149) Winnier GE, Kume T, Deng K, Rogers R, Bundy J, Raines C, et al. Roles for the winged helix transcription factors MF1 and MFH1 in cardiovascular development revealed by nonallelic noncomplementation of null alleles. Dev Biol 1999 Sep 15;213(2):418-431.

(150) Saleem RA, Banerjee-Basu S, Berry FB, Baxevanis AD, Walter MA. Analyses of the effects that disease-causing missense mutations have on the structure and function of the winged-helix protein FOXC1. Am J Hum Genet 2001 Mar;68(3):627-641.

(151) Saleem RA, Murphy TC, Liebmann JM, Walter MA. Identification and analysis of a novel mutation in the FOXC1 forkhead domain. Invest Ophthalmol Vis Sci 2003 Nov;44(11):4608-4612.

(152) Jin C, Marsden I, Chen X, Liao X. Dynamic DNA contacts observed in the NMR structure of winged helix protein-DNA complex. J Mol Biol 1999 Jun 18;289(4):683-690.

(153) Murphy TC, Saleem RA, Footz T, Ritch R, McGillivray B, Walter MA. The wing 2 region of the FOXC1 forkhead domain is necessary for normal DNA-binding and transactivation functions. Invest Ophthalmol Vis Sci 2004 Aug;45(8):2531-2538.

(154) Saleem RA, Banerjee-Basu S, Murphy TC, Baxevanis A, Walter MA. Essential structural and functional determinants within the forkhead domain of FOXC1. Nucleic Acids Res 2004 Aug 6;32(14):4182-4193.

(155) Blom N, Gammeltoft S, Brunak S. Sequence and structure-based prediction of eukaryotic protein phosphorylation sites. J Mol Biol 1999 Dec 17;294(5):1351-1362.

(156) Jans DA, Hubner S. Regulation of protein transport to the nucleus: central role of phosphorylation. Physiol Rev 1996 Jul;76(3):651-685.

(157) Schwoebel ED, Moore MS. The control of gene expression by regulated nuclear transport. Essays Biochem 2000;36:105-113.

(158) De Baere E, Beysen D, Oley C, Lorenz B, Cocquet J, De Sutter P, et al. FOXL2 and BPES: mutational hotspots, phenotypic variability, and revision of the genotype-phenotype correlation. Am J Hum Genet 2003 Feb;72(2):478-487.

(159) Katoh M, Katoh M. Human FOX gene family (Review). Int J Oncol 2004 Nov;25(5):1495-1500.

(160) Cvekl A, Tamm ER. Anterior eye development and ocular mesenchyme: new insights from mouse models and human diseases. Bioessays 2004 Apr;26(4):374-386.

(161) Hanson IM, Fletcher JM, Jordan T, Brown A, Taylor D, Adams RJ, et al. Mutations at the PAX6 locus are found in heterogeneous anterior segment malformations including Peters' anomaly. Nat Genet 1994 Feb;6(2):168-173.

(162) Nelson LB, Spaeth GL, Nowinski TS, Margo CE, Jackson L. Aniridia. A review. Surv Ophthalmol 1984 May-Jun;28(6):621-642.

(163) Mirzayans F, Pearce WG, MacDonald IM, Walter MA. Mutation of the PAX6 gene in patients with autosomal dominant keratitis. Am J Hum Genet 1995 Sep;57(3):539-548.

(164) Acharya M, Mookherjee S, Bhattacharjee A, Bandyopadhyay AK, Daulat Thakur SK, Bhaduri G, et al. Primary role of CYP1B1 in Indian juvenile-onset POAG patients. Mol Vis 2006 Apr 20;12:399-404.

(165) Ito YA, Footz TK, Murphy TC, Courtens W, Walter MA. Analyses of a novel L130F missense mutation in FOXC1. Arch Ophthalmol 2007 Jan;125(1):128-135.

(166) Berry FB, O'Neill MA, Coca-Prados M, Walter MA. FOXC1 transcriptional regulatory activity is impaired by PBX1 in a filamin A-mediated manner. Mol Cell Biol 2005 Feb;25(4):1415-1424.

(167) Melo F, Feytmans E. Assessing protein structures with a non-local atomic interaction energy. J Mol Biol 1998 Apr 17;277(5):1141-1152.

(168) Al-Shahwan S, Edward DP, Khan AO. Severe ocular surface disease and glaucoma in a newborn with aniridia. J AAPOS 2005 Oct;9(5):499-500.

(169) Stoilov I, Akarsu AN, Sarfarazi M. Identification of three different truncating mutations in cytochrome P4501B1 (CYP1B1) as the principal cause of primary congenital glaucoma (Buphthalmos) in families linked to the GLC3A locus on chromosome 2p21. Hum Mol Genet 1997 Apr;6(4):641-647.

(170) Johnston JA, Ward CL, Kopito RR. Aggresomes: a cellular response to misfolded proteins. J Cell Biol 1998 Dec 28;143(7):1883-1898.

(171) Khan AO, Aldahmesh MA, Al-Amri A. Heterozygous FOXC1 mutation (M161K) associated with congenital glaucoma and aniridia in an infant and a milder phenotype in her mother. Ophthalmic Genet 2008 Jun;29(2):67-71.

(172) Komatireddy S, Chakrabarti S, Mandal AK, Reddy AB, Sampath S, Panicker SG, et al. Mutation spectrum of FOXC1 and clinical genetic heterogeneity of Axenfeld-Rieger anomaly in India. Mol Vis 2003 Feb 18;9:43-48.

(173) Panicker SG, Sampath S, Mandal AK, Reddy AB, Ahmed N, Hasnain SE. Novel mutation in FOXC1 wing region causing Axenfeld-Rieger anomaly. Invest Ophthalmol Vis Sci 2002 Dec;43(12):3613-3616.

(174) Kopito RR. Aggresomes, inclusion bodies and protein aggregation. Trends Cell Biol 2000 Dec;10(12):524-530.

(175) Wetzel R. Mutations and off-pathway aggregation of proteins. Trends Biotechnol 1994 May;12(5):193-198.

(176) Markossian KA, Kurganov BI. Protein folding, misfolding, and aggregation. Formation of inclusion bodies and aggresomes. Biochemistry (Mosc) 2004 Sep;69(9):971-984.

(177) Ito YA, Footz TK, Berry FB, Mirzayans F, Yu M, Khan AO, et al. Severe molecular defects of a novel FOXC1 W152G mutation result in aniridia. Invest Ophthalmol Vis Sci 2009 Aug;50(8):3573-3579.

(178) Schwechter BR, Millet LE, Levin LA. Histone deacetylase inhibition-mediated differentiation of RGC-5 cells and interaction with survival. Invest Ophthalmol Vis Sci 2007 Jun;48(6):2845-2857.

(179) Noonan E, Giardina C, Hightower L. Hsp70B' and Hsp72 form a complex in stressed human colon cells and each contributes to cytoprotection. Exp Cell Res 2008 Aug 1;314(13):2468-2476.

(180) Yu H, Liu Z, Zhou H, Dai W, Chen S, Shu Y, et al. JAK-STAT pathway modulates the roles of iNOS and COX-2 in the cytoprotection of early phase of hydrogen peroxide preconditioning against apoptosis induced by oxidative stress. Neurosci Lett 2012 Nov 7;529(2):166-171.

(181) Leung TK, Rajendran MY, Monfries C, Hall C, Lim L. The human heat-shock protein family. Expression of a novel heat-inducible HSP70 (HSP70B') and isolation of its cDNA and genomic DNA. Biochem J 1990 Apr 1;267(1):125-132.

(182) Noonan EJ, Fournier G, Hightower LE. Surface expression of Hsp70B' in response to proteasome inhibition in human colon cells. Cell Stress Chaperones 2008 Spring;13(1):105-110.

(183) Noonan EJ, Place RF, Rasoulpour RJ, Giardina C, Hightower LE. Cell number-dependent regulation of Hsp70B' expression: evidence of an extracellular regulator. J Cell Physiol 2007 Jan;210(1):201-211.

(184) Calnan DR, Brunet A. The FoxO code. Oncogene 2008 Apr 7;27(16):2276-2288.

(185) Ray PS, Wang J, Qu Y, Sim MS, Shamonki J, Bagaria SP, et al. FOXC1 is a potential prognostic biomarker with functional significance in basal-like breast cancer. Cancer Res 2010 May 15;70(10):3870-3876.

(186) Kroemer G, Galluzzi L, Vandenabeele P, Abrams J, Alnemri ES, Baehrecke EH, et al. Classification of cell death: recommendations of the Nomenclature Committee on Cell Death 2009. Cell Death Differ 2009 Jan;16(1):3-11.

(187) Kaufmann SH, Desnoyers S, Ottaviano Y, Davidson NE, Poirier GG. Specific proteolytic cleavage of poly(ADP-ribose) polymerase: an early marker of chemotherapy-induced apoptosis. Cancer Res 1993 Sep 1;53(17):3976-3985.

(188) Tewari M, Quan LT, O'Rourke K, Desnoyers S, Zeng Z, Beidler DR, et al. Yama/CPP32 beta, a mammalian homolog of CED-3, is a CrmA-inhibitable protease that cleaves the death substrate poly(ADP-ribose) polymerase. Cell 1995 Jun 2;81(5):801-809.

(189) Lindahl T, Satoh MS, Poirier GG, Klungland A. Post-translational modification of poly(ADP-ribose) polymerase induced by DNA strand breaks. Trends Biochem Sci 1995 Oct;20(10):405-411.

(190) Herceg Z, Wang ZQ. Failure of poly(ADP-ribose) polymerase cleavage by caspases leads to induction of necrosis and enhanced apoptosis. Mol Cell Biol 1999 Jul;19(7):5124-5133.

(191) Lemaire C, Andreau K, Souvannavong V, Adam A. Inhibition of caspase activity induces a switch from apoptosis to necrosis. FEBS Lett 1998 Mar 27;425(2):266-270.

(192) Akerfelt M, Morimoto RI, Sistonen L. Heat shock factors: integrators of cell stress, development and lifespan. Nat Rev Mol Cell Biol 2010 Aug;11(8):545-555.

(193) Brocchieri L, Conway de Macario E, Macario AJ. hsp70 genes in the human genome: Conservation and differentiation patterns predict a wide array of

overlapping and specialized functions. BMC Evol Biol 2008 Jan 23;8:19-2148-8-19.

(194) Wisniewska M, Karlberg T, Lehtio L, Johansson I, Kotenyova T, Moche M, et al. Crystal structures of the ATPase domains of four human Hsp70 isoforms: HSPA1L/Hsp70-hom, HSPA2/Hsp70-2, HSPA6/Hsp70B', and HSPA5/BiP/GRP78. PLoS One 2010 Jan 11;5(1):e8625.

(195) Hageman J, van Waarde MA, Zylicz A, Walerych D, Kampinga HH. The diverse members of the mammalian HSP70 machine show distinct chaperone-like activities. Biochem J 2011 Apr 1;435(1):127-142.

(196) Chow AM, Mok P, Xiao D, Khalouei S, Brown IR. Heteromeric complexes of heat shock protein 70 (HSP70) family members, including Hsp70B', in differentiated human neuronal cells. Cell Stress Chaperones 2010 Sep;15(5):545-553.

(197) Saleh A, Srinivasula SM, Balkir L, Robbins PD, Alnemri ES. Negative regulation of the Apaf-1 apoptosome by Hsp70. Nat Cell Biol 2000 Aug;2(8):476-483.

(198) Beere HM, Wolf BB, Cain K, Mosser DD, Mahboubi A, Kuwana T, et al. Heat-shock protein 70 inhibits apoptosis by preventing recruitment of procaspase-9 to the Apaf-1 apoptosome. Nat Cell Biol 2000 Aug;2(8):469-475.

(199) Beere HM, Green DR. Stress management - heat shock protein-70 and the regulation of apoptosis. Trends Cell Biol 2001 Jan;11(1):6-10.

(200) Kim HE, Jiang X, Du F, Wang X. PHAPI, CAS, and Hsp70 promote apoptosome formation by preventing Apaf-1 aggregation and enhancing nucleotide exchange on Apaf-1. Mol Cell 2008 Apr 25;30(2):239-247.

(201) Ravagnan L, Gurbuxani S, Susin SA, Maisse C, Daugas E, Zamzami N, et al. Heat-shock protein 70 antagonizes apoptosis-inducing factor. Nat Cell Biol 2001 Sep;3(9):839-843.

(202) Wang J, Ray PS, Sim MS, Zhou XZ, Lu KP, Lee AV, et al. FOXC1 regulates the functions of human basal-like breast cancer cells by activating NF-kappaB signaling. Oncogene 2012 Nov 8;31(45):4798-4802.

(203) Huang L, Chi J, Berry FB, Footz TK, Sharp MW, Walter MA. Human p32 is a novel FOXC1-interacting protein that regulates FOXC1 transcriptional activity in ocular cells. Invest Ophthalmol Vis Sci 2008 Dec;49(12):5243-5249.

(204) Berry FB, Lines MA, Oas JM, Footz T, Underhill DA, Gage PJ, et al. Functional interactions between FOXC1 and PITX2 underlie the sensitivity to

FOXC1 gene dose in Axenfeld-Rieger syndrome and anterior segment dysgenesis. Hum Mol Genet 2006 Mar 15;15(6):905-919.

(205) Zhou BB, Elledge SJ. The DNA damage response: putting checkpoints in perspective. Nature 2000 Nov 23;408(6811):433-439.

(206) Zhang B, Chambers KJ, Faller DV, Wang S. Reprogramming of the SWI/SNF complex for co-activation or co-repression in prohibitin-mediated estrogen receptor regulation. Oncogene 2007 Nov 1;26(50):7153-7157.

(207) Balciunas D, Galman C, Ronne H, Bjorklund S. The Med1 subunit of the yeast mediator complex is involved in both transcriptional activation and repression. Proc Natl Acad Sci U S A 1999 Jan 19;96(2):376-381.

(208) Mann M, Ong SE, Gronborg M, Steen H, Jensen ON, Pandey A. Analysis of protein phosphorylation using mass spectrometry: deciphering the phosphoproteome. Trends Biotechnol 2002 Jun;20(6):261-268.

Chapter 2. Analyses of a Novel L130F Missense Mutation in FOXC1

This chapter was published in:

Ito YA, Footz TK, Murphy TC, Courtens W, and Walter MA. Analyses of a novel L130F missense mutation in FOXC1. (2007). *Arch Ophthalmol*. 125(1):128-135.

Note: All experiments were carried out by Y.A. Ito except for the *in silico* analysis presented in Figure 7, which was carried out by T.K. Footz. The clinical examination of the patient was carried out by W. Courtens.

Introduction

The forkhead box (FOX) family of transcription factors, including FOXC1, share an evolutionarily conserved 110–amino acid sequence known as the *forkhead domain* (FHD) (137). This DNA-binding motif is composed of 1 minor and 3 major α-helixes and 2 β-strands (137). The 2 β-strands form 2 loops that wrap around the DNA, giving the FHD its characteristic winglike structure (76).

Patients with *FOXC1* mutations mapping to chromosome 6p25 are affected with human Axenfeld-Rieger Syndrome (ARS) (138,139). This genetic disease is transmitted in an autosomal dominant manner and is highly penetrant. The FOXC1 protein is expressed in many of the developing ocular tissues in the anterior chamber of the mouse eye (88). Mutations in *FOXC1* result in malformations in the anterior chamber of the human eye that include iridogoniodysgenesis, iris hypoplasia, corectopia, polycoria, a prominent Schwalbe line, and iridocorneal tissue adhesions (135,140,141). The most serious consequence of ARS is that approximately 50% of patients develop glaucoma (142). In addition to the ocular defects, patients with ARS can have systemic defects, including maxillary hypoplasia, hypodontia, and a protruding umbilicus (143-145).

Correct FOXC1 expression is crucial for embyrogenesis and, in particular, for the normal development of the skeletal, cardiovascular, urogenital, and ocular tissues (85,146-149). Furthermore, FOXC1 continues

to be expressed in several adult tissues, including the eyes, brain, heart, and kidneys (148). Because the spatial and temporal patterns for FOXC1 expression have been observed to coincide with the differentiation of specific tissues (148), mutations in the *FOXC1* gene usually result in gross morphological defects.

For normal development, not only does FOXC1 need to be expressed in the appropriate spatial and temporal patterns, but the level of FOXC1 expression must be strictly regulated (150). Thus, ARS can result from either a loss-of-function mutation, in which FOXC1 expression is less than the critical lower threshold of 80% of wild-type activity levels, or a mutation causing FOXC1 expression to exceed the upper threshold of 150% (150). No strong genotype-phenotype correlation has been established, which suggests that the process for developing a particular phenotype in a patient with a mutation of the *FOXC1* gene is a complex one (151).

We have identified a novel *FOXC1* missense mutation, L130F, in 2 related individuals with ARS. The hydrophobic L130 residue is located in helix 3 of the FHD. Helix 3 is referred to as the *recognition helix* because it interacts with the major groove of DNA (152). Previous studies have found that missense mutations that occur within helix 3 disrupt DNA binding and subsequent transcriptional activation (136). Thus, we performed a molecular analysis to examine how the disease-causing L130F mutation disrupts *FOXC1* function. Molecular analyses of *FOXC1* missense

mutations such as L130F will provide further insight into how disruptions in *FOXC1* lead to human ARS and will give new possibilities for the development of treatments for this disease.

Materials and Methods

Reports of Patients

This research adhered to the tenets of the Declaration of Helsinki. Patient samples and information were collected with informed consent as specified by the University of Alberta Ethics Board. The L130F mutation was identified in a white woman (patient 1) and her son (patient 2). Patient 1 was diagnosed as having ARS at 27 years of age, after her son was diagnosed as having ARS and glaucoma at 2 months of age. Patient 1 had no dental or facial abnormalities. An ophthalmological examination revealed that patient 1 had iris hypoplasia, a prominent Schwalbe line, and peripheral anterior synechiae, but no glaucoma. Patient 2 was diagnosed as having ARS because he had corectopia and hypertelorism. He had a slight excess of skin at the umbilical region. Results of the ophthalmological examination disclosed a posterior embryotoxon. Patient 2 also had an intraocular pressure of 14 mm Hg, but abnormally high cup-disc ratios of 0.85 and 0.80 for the left and right eyes, respectively. Both patients were bilaterally affected. The maternal grandparents did not have the L130F mutation, indicating a de novo mutation in patient 1.

Mutation Detection

The *FOXC1* gene was amplified as previously described (138). Polymerase chain reaction products were gel purified, extracted on separation columns (Qiagen, Valencia, Calif), and sequenced directly by using a phosphorus 33–labeled terminator cycle sequencing kit (Amersham Biosciences, Baie d'Urfe, Quebec). In addition, the polymerase chain reaction products were sequenced using a 3130 × l genetic analyzer (Applied Biosystems Inc, Foster City, Calif) to generate chromatograms and to confirm the observations from the manual sequencing experiments.

Plasmid

The *FOXC1* pcDNA4 His/Max B (Invitrogen, Carlsbad, Calif) has been described previously (150). Briefly, the FOXC1 cDNA (a gift from P. Carlsson) was repaired at the 3` end and was subcloned into EcoRI–XbaI sites in the pcDNA4 His/Max B plasmid. Site-directed mutagenesis was performed using a mutagenesis kit (QuickChange; Strategene, La Jolla, Calif) with the addition of 10% dimethylsulfoxide. The mutagenic primer sequences for L130F were as follows: forward, 5′-agc atc cgc cac aac ttc tcg ctc aac gag tgc-3′; reverse, 5′-gca ctc gtt gag cga gaa gtt gtg gcg gat gct-3′. Potential mutant constructs were sequenced with the 3130 × l genetic analyzer. Confirmed mutants were subcloned into the *FOXC1* pcDNA4 His/Max vector and resequenced.

Cell culture

We cultured COS-7 cells and HeLa cells in Dulbecco modified Eagle medium and 10% fetal bovine serum at 37°C and 5% carbon dioxide (CO_2).

Immunoblot analysis and calf intestinal alkaline phosphatase treatment

The COS-7 cells (10^6 cells per 100-mm plate) were transfected with 4 µg of *FOXC1* tagged with Xpress epitope (Invitrogen) using commercially available reagent (Fugene 6; Roche, Indianapolis, Ind). Forty-eight hours after transfection, the proteins were extracted and resolved on a 10% sodium dodecyl sulfate polyacrylamide gel electrophoresis (SDS-PAGE) gel. The proteins were detected by immunoblotting using an anti-Xpress antibody (1:10 000 dilution; Invitrogen) against the pcDNA4 His/Max vector–encoded N-terminal Xpress tag and visualized with chemiluminescent substrate (Supersignal West Pico; Pierce Biotechnology, Rockford, Ill). Protein extracts were incubated with 20 U of calf intestinal alkaline phosphatase (CIP) (Invitrogen) with or without 11µM sodium vanadate for 1 hour in a 37°C water bath. An equal amount of 2 × SDS-PAGE loading buffer was added, and the proteins were then resolved on a 10% SDS-PAGE gel and visualized by immunoblotting as described.

Immunofluorescence

The COS-7 cells (2×10^5 cells per 35-mm well) were grown and transfected directly on coverslips with 1 μg of Xpress-epitope–tagged *FOXC1*. The COS-7 cells were also transfected with the pcDNA4 His/Max vector as a control experiment. Twenty-four hours after transfection, the localization of the FOXC1 protein was visualized by incubating the coverslips with anti-Xpress antibody and antimouse Cy3–conjugated secondary antibody. The position of the nucleus was visualized by staining with 4′,6-diamidine-2-phenylindole (DAPI). First, a total of 480 cells transfected with wild-type *FOXC1* were scored for nuclear or cytoplasmic staining or both. Then, a total of 623 cells transfected with L130F were scored.

Electrophoretic mobility shift assay

The amount of L130F protein in the COS-7 cell extracts was equalized to wild-type FOXC1 levels by inspection of the proteins detected by immunoblotting. The protein extracts were incubated for 30 minutes at room temperature with 1.25mM dithiothreitol, 0.3 μg of sheared salmon sperm DNA, 0.125 μg of poly dI/dC (Sigma-Aldrich Corp, St Louis, Mo), and 80 000 counts per minute of phosphorus 32 (^{32}P)–deoxycytidine triphosphate–labeled double-stranded DNA containing the following *FOXC1* binding site (shown underlined): forward, 5′-gatccaaa gtaaataaa caacaga-3′; reverse, 5′-gatctctgttg tttatttac tttg-3′ (150). After prerunning the

6% polyacrylamide gel containing Tris-glycine-EDTA buffer for 15 minutes, the electrophoretic mobility shift assay (EMSA) reaction products were subjected to electrophoresis. As a control, the COS-7 cells were transfected with the pcDNA4 His/Max vector. Also, a mock EMSA reaction was carried out with just the ^{32}P-deoxycytidine triphosphate–labeled double-stranded DNA to ensure that the EMSA was specific for the ability of the FOXC1 protein to bind to DNA.

Dual luciferase assay

HeLa cells (4×10^4 cells per 15-mm well) were cotransfected with 100 ng of the *FOXC1* pcDNA4 His/Max construct, 20 ng of the pGL3-TK construct with 6× FOXC1 binding sites (150), and 1 ng of the pRL-TK control plasmid. Forty-eight hours after transfection, the luciferase assays were carried out using the dual luciferase assay kit (Promega Corp, Madison, Wis). Each experiment was done in triplicate and was performed 3 times. As a control, the HeLa cells were transfected with the pcDNA4 His/Max empty vector instead of the *FOXC1* pcDNA4 His/Max construct.

Modeling

In silico mutagenesis of the *FOXC2* FHD model was performed using the Swiss-PdbViewer (*http://ca.expasy.org/spdbv/*), and the models were evaluated with the atomic nonlocal environment assessment (ANOLEA) Swiss model server (*http://swissmodel.expasy.org/anolea/*), as

described previously (153). The molecular modeling was carried out by T.K. Footz.

Results

The *FOXC1* gene was screened for mutations by direct sequence analysis of polymerase chain reaction products of patient DNA. A heterozygous C-to-T transition at codon position 130 (388C>T; L130F) that results in a leucine-to-phenylalanine change was detected in patients 1 and 2 (Figure 1). Sequencing of the patients' DNA and 100 healthy control chromosomes suggest that the L130F mutation is not present in the healthy population.

Immunoblotting indicated that a plasmid containing a complementary DNA encoding *FOXC1* with the L130F mutation and transfected into COS-7 cells was capable of expressing the L130F protein, which was approximately the same size as the wild-type protein (approximately 65 kDa) (Figure 2A). Thus, the relative stability of L130F protein expression was similar to that of the wild-type protein. However, the L130F construct repeatedly produced a pattern of immunoreactive degradation products that differed from the wild-type construct pattern (Figure 2B). Similar to the wild-type sample, the L130F protein bands occurred as a doublet (Figure 2A). Both bands were slightly shifted so that it had a lower molecular weight than either of the wild-type bands,

suggesting that the L130F protein was modified differently than the wild-type protein. Because FOXC1 is known to be phosphorylated (81), we examined whether the L130F mutation affected protein phosphorylation. When the L130F protein was incubated with calf intestinal alkaline phosphatase, the higher-molecular-weight band was eliminated (Figure 3). When the L130F protein was incubated with the phosphatase inhibitor sodium vanadate, the doublet was restored. This finding indicated that phosphorylation of the L130F (and wild type) protein was responsible for the occurrence of the immunoreactive doublet bands.

Immunofluorescent microscopy was performed to determine whether the L130F protein was able to localize to the nucleus. Only 33.7% of the L130F proteins localized exclusively to the nucleus, compared with 92.5% for the wild-type proteins (Figure 4). The COS-7 cells transfected with the pcDNA4 His/Max vector showed no staining with Cy3 (data not shown), indicating that the immunofluorescence observed was specific for the FOXC1 protein. These data indicate that the L130F mutation severely disrupts the ability of the FOXC1 protein to localize to the nucleus.

The DNA-binding ability of the L130F protein, expressed in the COS-7 cells, was determined by EMSA results. For the wild-type protein, the amount of protein-DNA complexes that formed increased as the amount of protein was increased (Figure 5). In contrast, the L130F protein showed a greatly reduced capacity to bind DNA, even when the amount of protein added to the EMSA reaction was increased (Figure 5), indicating

that this mutation significantly disrupts the normal DNA-binding capacity of the FOXC1 protein.

The ability of the L130F protein, expressed in the HeLa cells, to activate expression of a luciferase reporter containing 6 consensus FOXC1 binding sites was determined. Wild-type FOXC1 was able to activate expression of the luciferase reporter (Figure 6). The transactivation potential of the mutant protein was reduced 3-fold compared with wild-type FOXC1 (Figure 6). The transactivation potential of L130F is comparable to the transactivation potential of the empty expression vector, indicating that the L130F mutation severely disrupts the ability of the FOXC1 protein to activate a reporter gene.

Finally, molecular modeling of the FOXC1 FHD was performed to predict which amino acid residue contacts would be disrupted by the L130F mutation. The first model layer of the nuclear magnetic resonance–solved structure file of FOXC2 (77) was used as a homology model for FOXC1 because of its near-perfect sequence identity over the FHDs; the only differences are that FOXC1 contains aspartate residues at positions 96 and 117, whereas FOXC2 has glutamate residues. In this homology model, L130 was mutated to phenylalanine *in silico* to predict structural defects in the L130F molecule via the ANOLEA mean force potential calculations. We compared the results with those for I87M (Figure 7) and indicate that, although the side chains of I87 and L130 are normally involved in the same hydrophobic cluster, mutations at these positions

may produce different effects. When I87 was changed to a methionine residue, the ANOLEA scores for M87, I104, I126, L130, F136, and W152 were all affected, whereas the effect of L130F was limited to positions 87, 130, and 152. Although recombinant *FOXC1* harboring a mutation at position I87 does not produce a stable protein (154), recombinant *FOXC1* harboring an L130F mutation was recoverable in whole-cell extracts (Figure 2A). Thus, the sum of the ANOLEA energy differences for any single mutation model does not necessarily predict the degree of stability of the expressed recombinant protein. Nevertheless, the model is able to predict that the L130F mutation will result in severe disruptions to *FOXC1* function.

Discussion

The disruption of *FOXC1* function by the novel disease-causing L130F mutation demonstrates the importance of helix 3 in *FOXC1* function. Helix 3 of the FOXC1 protein interacts with the major groove of DNA and confers DNA-binding specificity. However, molecular modeling predicts that the L130 residue does not make direct contact with DNA (data not shown). Rather, the L130 residue is thought to be oriented toward the hydrophobic core and forms a pocket with other residues, including I87, I104, I126, F136, and W152 (154). Missense mutations that substitute a differently charged amino acid, such as R127H, appear to

disrupt the electrostatic charge of the FHD and thus greatly reduce the affinity of the mutant protein for DNA (151). Missense mutations such as I126E and I126K, which introduce a hydrophilic residue into the hydrophobic core, also disrupt *FOXC1*-DNA interactions (154). Although the interaction of the phenylalanine residue in place of the leucine residue at codon position 130 preserves the neutrally charged and hydrophobic nature of this position, the EMSA results indicate that the L130F mutation nevertheless reduces the ability of the mutant protein to bind DNA (Figure 5). The phenylalanine residue is bulkier and thus it is likely that the L130F mutation disrupts the helix 3 structure so that this helix can no longer fit into the major groove of the DNA. As a result, helix 3 of the FOXC1 protein may no longer be able to interact with DNA. The L130F mutation also reduces the transactivation potential to residual levels (Figure 5). This is consistent with the EMSA results that indicate that the L130F protein cannot bind DNA because DNA binding is a prerequisite for transactivation.

The FOXC1 protein is thought to be tightly regulated by posttranslational modifications (82). One of the ways that the FOXC1 protein is regulated is by phosphorylation (81). Previous research has determined that the phosphorylated residues of FOXC1 lie within the inhibitory domain, which is located within amino acid residues 215 through 366 (81,155). Recently, the ERK1/2 mitogen-activated protein kinase–dependent phosphorylation of FOXC1 at the S272 residue was

determined to stabilize FOXC1 by preventing the recruitment of degradation factors or, conversely, by recruiting stabilization factors (82). Because leucine and phenylalanine are amino acids that cannot become phosphorylated, the L130F missense mutation will not directly affect the phosphorylation state of the residue at position 130. However, the L130F protein was found to migrate at an apparently reduced molecular weight compared with the wild-type protein (Figure 2A), suggesting that the mutant and wild-type proteins are differentially phosphorylated. The bulkier nature of the phenylalanine residue appears to cause enough localized structural distortion to prevent the linear amino acid sequence from folding properly. Thus, the altered topology of the L130F protein may hinder the normal recognition and regulation by protein kinases.

Mutations in *FOXC2* cause hereditary lymphedema with distichiasis (136). The FHD of *FOXC1* and *FOXC2* have 98% sequence homology (136). An R121H missense mutation in helix 3 of the *FOXC2* FHD displayed a similar migration pattern to that of the L130F mutation in *FOXC1* (136). The R121H and L130F proteins displayed a faster migration than did wild-type FOXC2 and wild-type FOXC1, respectively (136). Also, when treated with calf intestinal alkaline phosphatase, R121H and L130F displayed mobilities equal to those of wild-type FOXC2 and wild-type FOXC1, respectively (136). In both cases, the mutant proteins are predicted to not be phosphorylated to the full extent of the wild-type proteins. This similarity demonstrates how small changes in helix 3 of the

FHD can result in great changes by altering the overall structure of the FOXC2 or FOXC1 protein.

The immunofluorescence results indicate that most of the L130F proteins are unable to localize to the nucleus (Figure 4), which is surprising because L130F is not in the regions of *FOXC1* known to be directly involved in nuclear localization (81). Also, previous experiments have shown that, in many cases, substitution of a differently charged amino acid at any position disrupts the ability of the protein to localize to the nucleus to a greater extent than a substitution involving amino acids with the same charge (153). For example, a *FOXC1* missense mutation involving 2 neutrally charged amino acid residues, I126A, resulted in the localization of 77% of the I126A proteins to the nucleus (154). However, when the I126 residue was replaced with a negatively charged glutamic acid residue or a positively charged lysine residue, none of the mutant proteins localized to the nucleus (154). This was not the case with the L130F mutation. Although leucine and phenylalanine are both neutrally charged, immunofluorescence showed that the L130F mutation severely disrupted the normal localization of the protein to the nucleus. Only 33.7% of the L130F proteins are able to localize exclusively to the nucleus. Because of the L130F mutation, the overall topology of the L130F protein may be altered in a manner that prevents the nuclear localization signal and nuclear localization accessory signal from being properly detected. However, the alteration in the phosphorylation pattern in the L130F protein

may also contribute to the reduction in the transport of the mutant protein to the nucleus, because phosphorylation appears to regulate the nuclear transport of many transcription factors (156,157).

Consistent with findings from previous studies (138,139), a single missense mutation in *FOXC1* identified within a single family had variable phenotypic consequences. In the case of the 2 related individuals with the L130F mutation in *FOXC1*, both individuals were diagnosed as having ARS. However, the mother had a mild form of the disease, whereas her son was severely affected and was diagnosed as having glaucoma at just 2 months of age. Stochastic events during development are likely to result in variable expression of downstream targets of FOXC1 in regard to the timing, location, and level of expression. Thus, although tight regulation of FOXC1 is essential for proper development, environmental factors and modifier genes may also contribute to phenotypic variability (150).

Investigation of the L130F mutation also gives important insight into the likely effects of mutations of other *FOX* genes. A mutation equivalent to L130F has been found in the *FOXL2* gene (158), where a C-to-T transition at codon position 106 (553C>T; L106F) was detected in a patient with blepharophimosis-ptosis-epicanthus inversus syndrome (158). The leucine residue at position 130 in *FOXC1*, which is equivalent to that at position 106 in *FOXL2*, is highly conserved in other *FOX* genes. There are at least 43 members in the human *FOX* gene family (159), and this L130 residue is found in 24 of those genes (158). As for L130F, we predict

that the L106F *FOXL2* mutation is also likely to disrupt protein function severely. A mutation of this conserved leucine residue is likely to lead to adverse functional consequences in all FOX proteins.

In this study, we report the identification of a novel missense mutation in *FOXC1*, L130F. The severe disruption of *FOXC1* function as a result of the disease-causing L130F mutation is consistent with previously studied missense mutations located within helix 3 (136). The L130F *FOXC1* mutation is one of the most disruptive *FOXC1* mutations studied because this mutation disrupts nuclear localization and impairs DNA binding, which subsequently impedes transcriptional activation. Thus, the analysis of the L130F missense mutation provides further insight into how disruptions in the *FOXC1* FHD lead to human ARS.

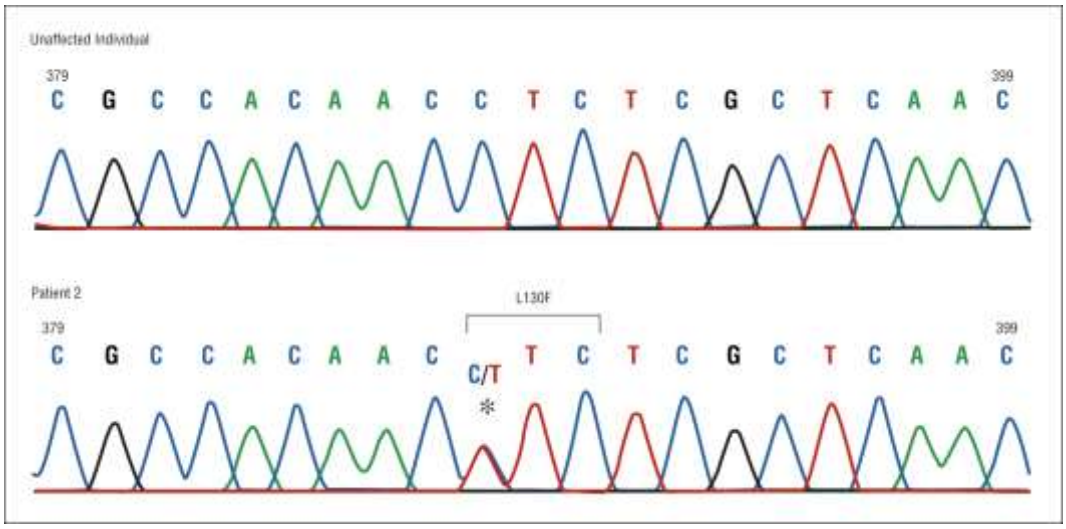
Unaffected Individual
379
399
C G C C A C A A C C T C T C G C T C A A C
Patient 2
L130F
379
399
C G C C A C A A C C/T T C T C G C T C A A C

Figure 1: Identification of the L130F mutation in the *FOXC1* (forkhead box C1) gene. The chromatogram shows the genomic DNA sequence of an unaffected individual and patient 2. Patient 2 has a heterozygous C-to-T transition that results in a leucine-to-phenylalanine change at codon position 130.

A

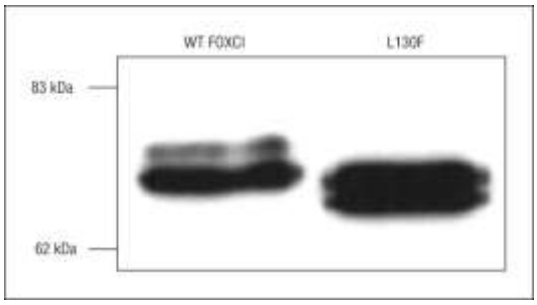

B

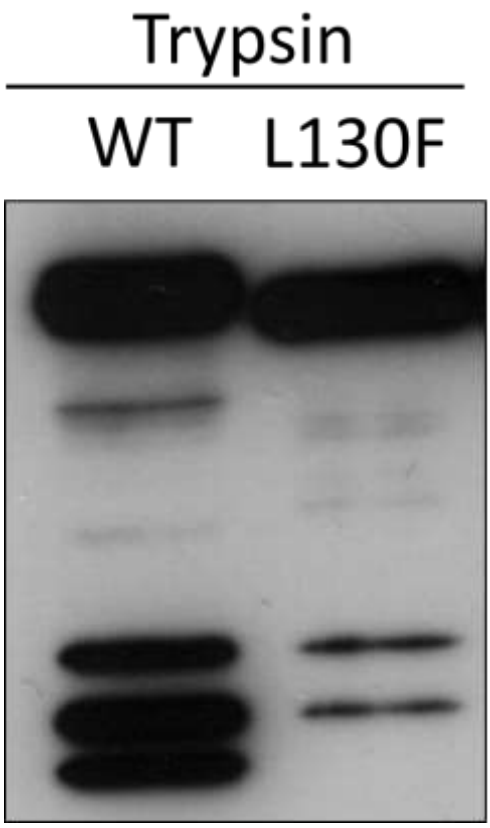

Figure 2: The L130F mutation in the *FOXC1* (forkhead box C1) gene does not affect protein stability. The Xpress (Invitrogen, Carlsbad, Calif) epitope–tagged wild-type (WT) FOXC1 and L130F, transfected into COS-7 cells, were detected by immunoblotting. A) The L130F protein is expressed at levels similar to those of WT FOXC1 protein. Both occurred as a doublet at approximately 65 kDa. The protein size marker is indicated to the left. B) Trypsin digest of the WT and L130F protein extracts results in different digestion products.

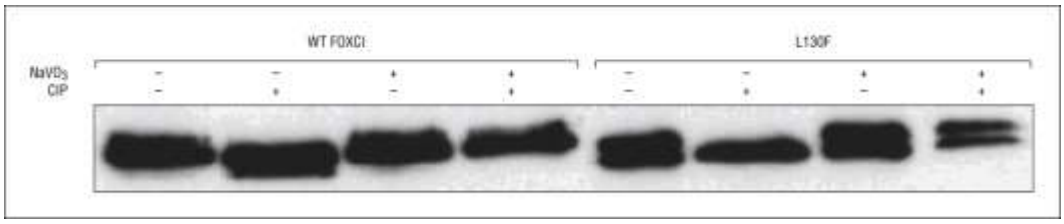
WT FOXC1
L130F
NaVO3
CIP

Figure 3: The L130F mutation in the *FOXC1* (forkhead box C1) gene alters phosphorylation of wild-type (WT) FOXC1 protein. In this immunoblot, the disappearance of the higher-molecular-weight bands on incubation with calf intestinal alkaline phosphatase (CIP) and their appearance with the inhibition of CIP by sodium vanadate ($NaVO_3$) indicated that the WT FOXC1 and L130F proteins are both phosphorylated.

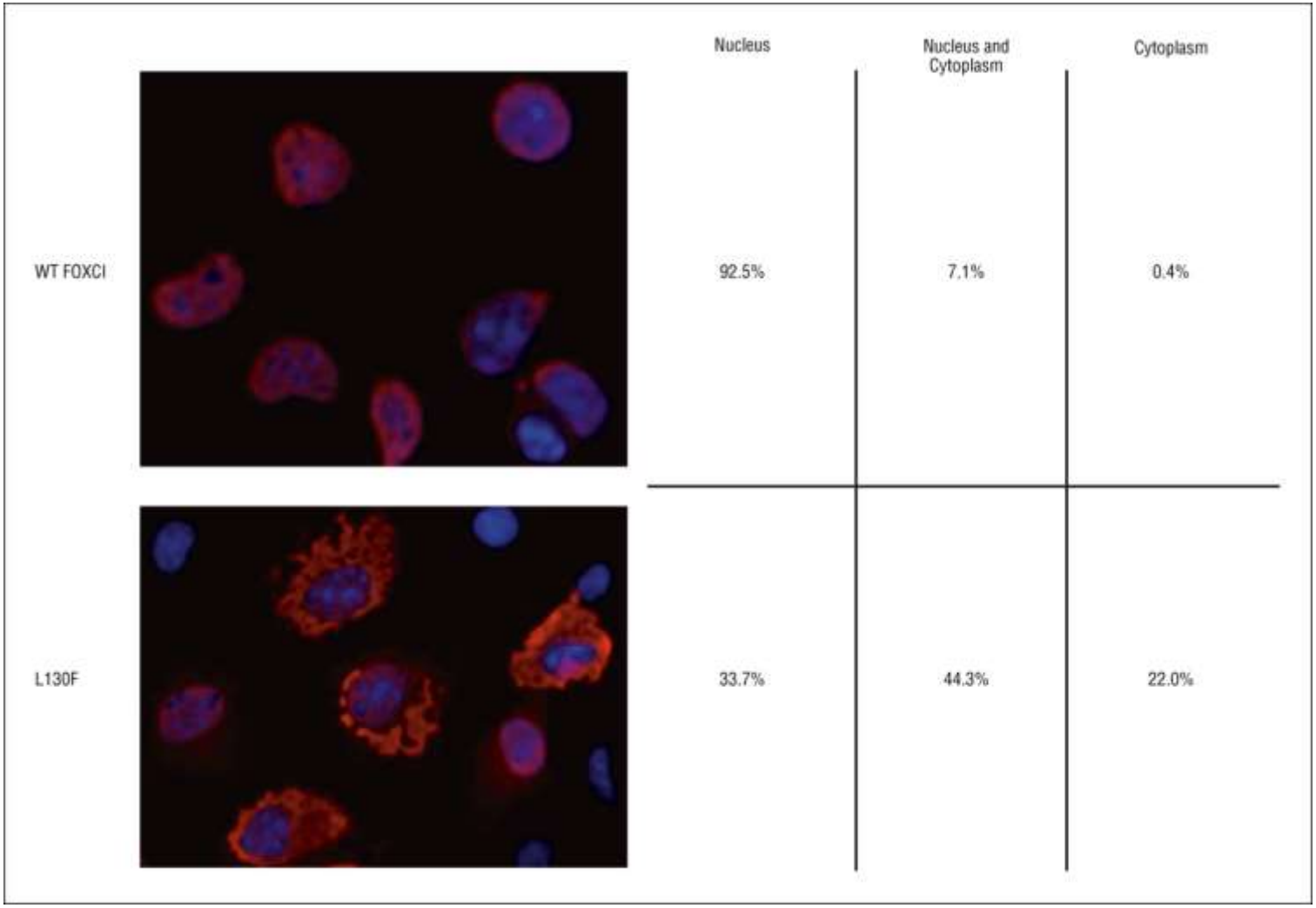
Nucleus
Nucleus and Cytoplasm
Cytoplasm
WT FOXCI
92.5%
7.1%
0.4%
L130F
33.7%
44.3%
22.0%

Figure 4: The L130F mutation in the *FOXC1* (forkhead box C1) gene disrupts efficient nuclear localization of the FOXC1 protein. The L130F proteins, visualized by Cy3 fluorescence (red) during microscopy, showed reduced localization to the nucleus, visualized by 4′,6-diamidine-2-phenylindole staining (blue), compared with wild-type (WT) FOXC1. A total of 480 cells and 623 cells were counted for WT FOXC1 and L130F, respectively.

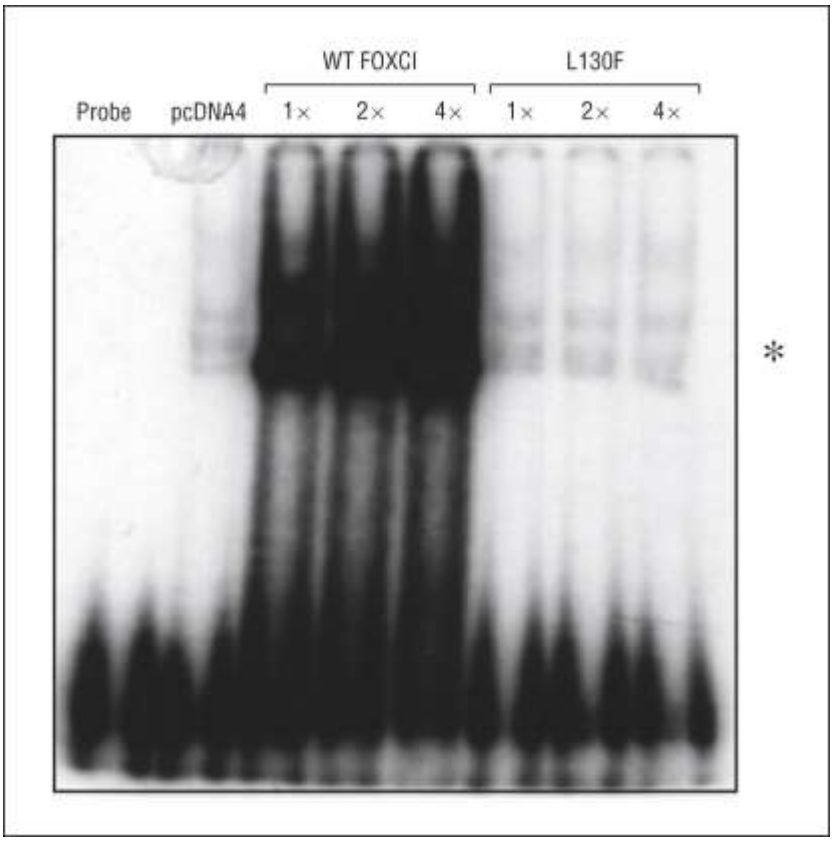
WT FOXCI
L130F
Probe
pcDNA4
1×
2×
4×
1×
2×
4×
*

Figure 5: The L130F mutation in the *FOXC1* (forkhead box C1) gene impairs DNA binding. The wild-type (WT) FOXC1 and L130F proteins were incubated with phosphorus 32-deoxycytidine triphosphate–labeled double-stranded DNA containing FOXC1-binding sites. Unlike WT FOXC1, which formed protein-DNA complexes (*), the electrophoretic mobility shift assay showed, with this autoradiogram, that the L130F protein was unable to bind to DNA even at high concentrations.

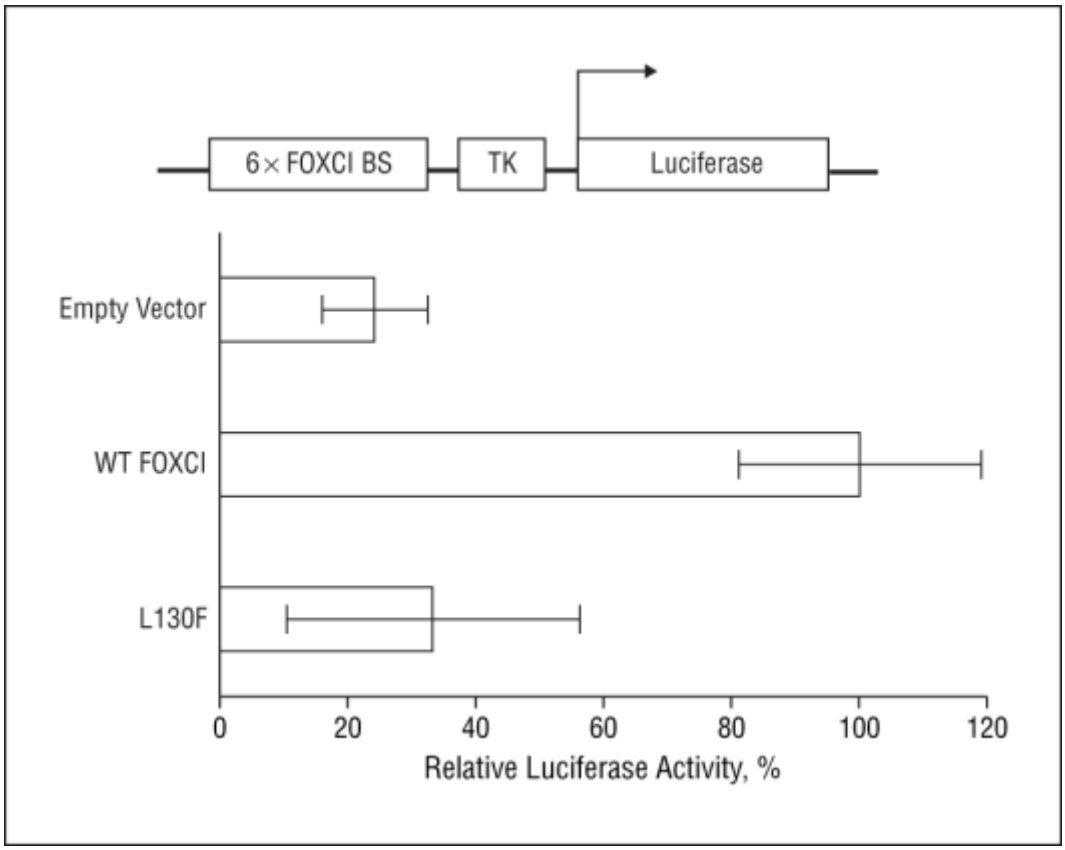
6× FOXCI BS
TK
Luciferase
Empty Vector
WT FOXCI
L130F
0
20
40
60
80
100
120
Relative Luciferase Activity, %

Figure 6: The L130F mutation in the *FOXC1* (forkhead box C1) gene impairs transcriptional activation. The L130F protein transactivated the luciferase reporter with 6× FOXC1 binding sites (BS) (above the graph) at residual levels. The data show mean luciferase values, normalized to *Renilla* luciferase, from a representative experiment carried out in triplicate. Error bars are the standard error of the mean. WT indicates wild type.

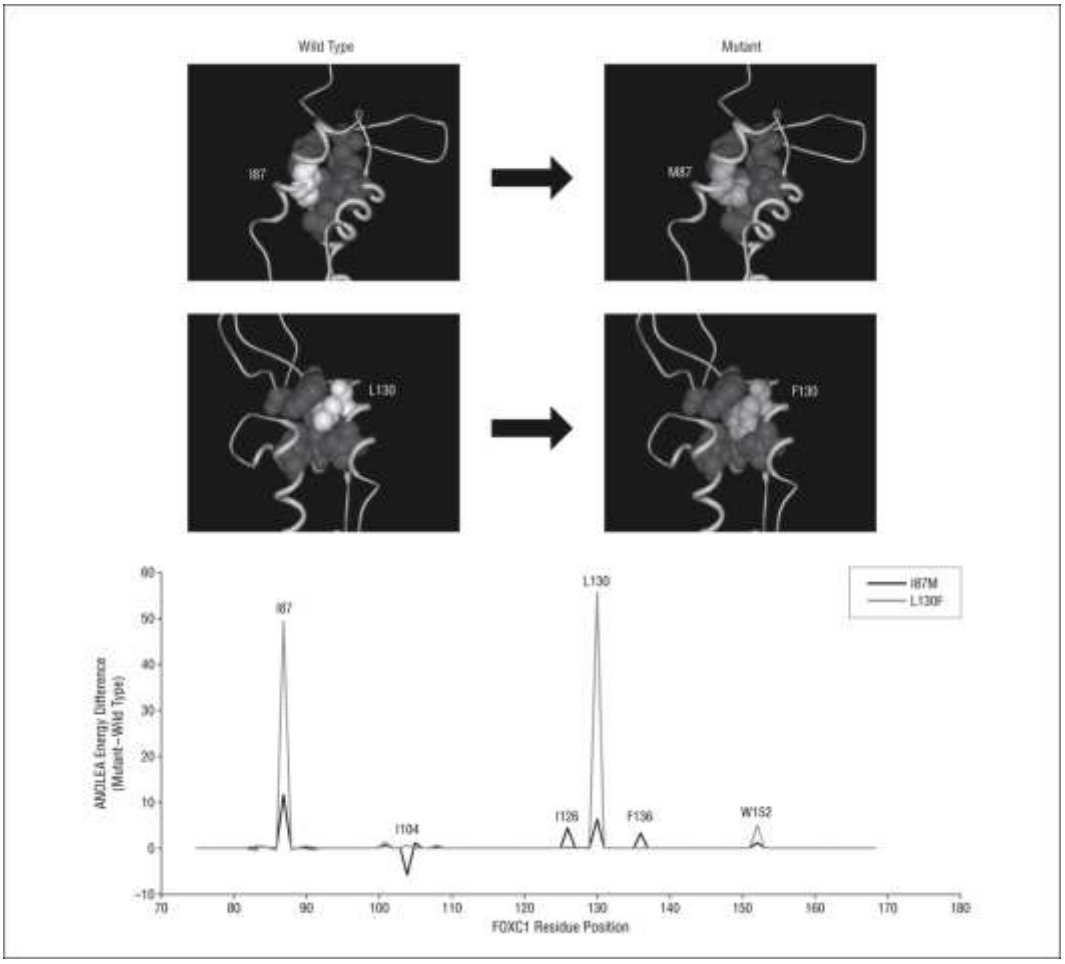
Wild Type
Mutant
I87
M87
L130
F130
I87M
L130F
ANOLEA Energy Difference
(Mutant – Wild Type)
I87
L130
I104
I126
F136
W152
FOXC1 Residue Position

Figure 7: Molecular models and scatterplot of *in silico* analysis of the L130F mutation in the *FOXC1* (forkhead box C1) gene. The FOXC2-derived homology model of FOXC1 shows the protein backbone (ribbon), mutated residues (gray), and unmutated residues (white). The wild-type and mutant-equivalent models were submitted to an atomic nonlocal environment assessment (ANOLEA) Swiss model server. Energy differences are in E/*k*T units, where E represents energy; *k*, the Boltzmann constant; and T, absolute temperature. The *in silico* analysis was carried out by T.K. Footz.

References

(1) Kaufmann E, Knochel W. Five years on the wings of fork head. Mech Dev 1996 Jun;57(1):3-20.

(2) Clark KL, Halay ED, Lai E, Burley SK. Co-crystal structure of the HNF-3/fork head DNA-recognition motif resembles histone H5. Nature 1993 Jul 29;364(6436):412-420.

(3) Mears AJ, Jordan T, Mirzayans F, Dubois S, Kume T, Parlee M, et al. Mutations of the forkhead/winged-helix gene, FKHL7, in patients with Axenfeld-Rieger anomaly. Am J Hum Genet 1998 Nov;63(5):1316-1328.

(4) Nishimura DY, Swiderski RE, Alward WL, Searby CC, Patil SR, Bennet SR, et al. The forkhead transcription factor gene FKHL7 is responsible for glaucoma phenotypes which map to 6p25. Nat Genet 1998 Jun;19(2):140-147.

(5) Kidson SH, Kume T, Deng K, Winfrey V, Hogan BL. The forkhead/winged-helix gene, Mf1, is necessary for the normal development of the cornea and formation of the anterior chamber in the mouse eye. Dev Biol 1999 Jul 15;211(2):306-322.

(6) Lines MA, Kozlowski K, Walter MA. Molecular genetics of Axenfeld-Rieger malformations. Hum Mol Genet 2002 May 15;11(10):1177-1184.

(7) Reese AB, Ellsworth RM. The anterior chamber cleavage syndrome. Arch Ophthalmol 1966 Mar;75(3):307-318.

(8) Weatherill JR, Hart CT. Familial hypoplasia of the iris stroma associated with glaucoma. Br J Ophthalmol 1969 Jul;53(7):433-438.

(9) Shields MB, Buckley E, Klintworth GK, Thresher R. Axenfeld-Rieger syndrome. A spectrum of developmental disorders. Surv Ophthalmol 1985 May-Jun;29(6):387-409.

(10) Feingold M, Shiere F, Fogels HR, Donaldson D. Rieger's syndrome. Pediatrics 1969 Oct;44(4):564-569.

(11) Fitch N, Kaback M. The Axenfeld syndrome and the Rieger syndrome. J Med Genet 1978 Feb;15(1):30-34.

(12) Chisholm IA, Chudley AE. Autosomal dominant iridogoniodysgenesis with associated somatic anomalies: four-generation family with Rieger's syndrome. Br J Ophthalmol 1983 Aug;67(8):529-534.

(13) Hiemisch H, Monaghan AP, Schutz G, Kaestner KH. Expression of the mouse Fkh1/Mf1 and Mfh1 genes in late gestation embryos is restricted to mesoderm derivatives. Mech Dev 1998 Apr;73(1):129-132.

(14) Kume T, Deng K, Hogan BL. Murine forkhead/winged helix genes Foxc1 (Mf1) and Foxc2 (Mfh1) are required for the early organogenesis of the kidney and urinary tract. Development 2000 Apr;127(7):1387-1395.

(15) Kume T, Deng KY, Winfrey V, Gould DB, Walter MA, Hogan BL. The forkhead/winged helix gene Mf1 is disrupted in the pleiotropic mouse mutation congenital hydrocephalus. Cell 1998 Jun 12;93(6):985-996.

(16) Swiderski RE, Reiter RS, Nishimura DY, Alward WL, Kalenak JW, Searby CS, et al. Expression of the Mf1 gene in developing mouse hearts: implication in the development of human congenital heart defects. Dev Dyn 1999 Sep;216(1):16-27.

(17) Winnier GE, Kume T, Deng K, Rogers R, Bundy J, Raines C, et al. Roles for the winged helix transcription factors MF1 and MFH1 in cardiovascular development revealed by nonallelic noncomplementation of null alleles. Dev Biol 1999 Sep 15;213(2):418-431.

(18) Saleem RA, Banerjee-Basu S, Berry FB, Baxevanis AD, Walter MA. Analyses of the effects that disease-causing missense mutations have on the structure and function of the winged-helix protein FOXC1. Am J Hum Genet 2001 Mar;68(3):627-641.

(19) Saleem RA, Murphy TC, Liebmann JM, Walter MA. Identification and analysis of a novel mutation in the FOXC1 forkhead domain. Invest Ophthalmol Vis Sci 2003 Nov;44(11):4608-4612.

(20) Jin C, Marsden I, Chen X, Liao X. Dynamic DNA contacts observed in the NMR structure of winged helix protein-DNA complex. J Mol Biol 1999 Jun 18;289(4):683-690.

(21) Berry FB, Tamimi Y, Carle MV, Lehmann OJ, Walter MA. The establishment of a predictive mutational model of the forkhead domain through the analyses of FOXC2 missense mutations identified in patients with hereditary lymphedema with distichiasis. Hum Mol Genet 2005 Sep 15;14(18):2619-2627.

(22) Murphy TC, Saleem RA, Footz T, Ritch R, McGillivray B, Walter MA. The wing 2 region of the FOXC1 forkhead domain is necessary for normal DNA-binding and transactivation functions. Invest Ophthalmol Vis Sci 2004 Aug;45(8):2531-2538.

(23) Berry FB, Saleem RA, Walter MA. FOXC1 transcriptional regulation is mediated by N- and C-terminal activation domains and contains a phosphorylated transcriptional inhibitory domain. J Biol Chem 2002 Mar 22;277(12):10292-10297.

(24) van Dongen MJ, Cederberg A, Carlsson P, Enerback S, Wikstrom M. Solution structure and dynamics of the DNA-binding domain of the adipocyte-transcription factor FREAC-11. J Mol Biol 2000 Feb 18;296(2):351-359.

(25) Saleem RA, Banerjee-Basu S, Murphy TC, Baxevanis A, Walter MA. Essential structural and functional determinants within the forkhead domain of FOXC1. Nucleic Acids Res 2004 Aug 6;32(14):4182-4193.

(26) Berry FB, Mirzayans F, Walter MA. Regulation of FOXC1 stability and transcriptional activity by an epidermal growth factor-activated mitogen-activated protein kinase signaling cascade. J Biol Chem 2006 Apr 14;281(15):10098-10104.

(27) Blom N, Gammeltoft S, Brunak S. Sequence and structure-based prediction of eukaryotic protein phosphorylation sites. J Mol Biol 1999 Dec 17;294(5):1351-1362.

(28) Jans DA, Hubner S. Regulation of protein transport to the nucleus: central role of phosphorylation. Physiol Rev 1996 Jul;76(3):651-685.

(29) Schwoebel ED, Moore MS. The control of gene expression by regulated nuclear transport. Essays Biochem 2000;36:105-113.

(30) De Baere E, Beysen D, Oley C, Lorenz B, Cocquet J, De Sutter P, et al. FOXL2 and BPES: mutational hotspots, phenotypic variability, and revision of the genotype-phenotype correlation. Am J Hum Genet 2003 Feb;72(2):478-487.

(31) Katoh M, Katoh M. Human FOX gene family (Review). Int J Oncol 2004 Nov;25(5):1495-1500.

Chapter 3. Severe molecular defects of a novel FOXC1 W152G mutation result in aniridia

This chapter was published in:

Ito YA, Footz TK, Berry FB, Mirzayans F, Yu M, Khan AO, and Walter MA. Severe molecular defects of a novel FOXC1 W152G mutation result in aniridia. (2009). *Invest Ophthalmol Vis Sci.* 50(8):3573-3579.

Note: All experiments were carried out by Y.A. Ito except for the *in silico* analysis presented in Figure 5, which was carried out by T.K. Footz. The clinical examination of the patient, presented in Figure 1A-1C, was carried out by A.O. Khan.

Introduction

The anterior segment of the eye consists of structures—iris, trabecular meshwork, Schlemm's canal—that are important for maintaining proper flow of aqueous humor. Many of these structures, including the iris stroma and the trabecular meshwork, are derived from the periocular mesenchyme. Differentiation of the periocular mesenchyme during development is under the influence of several transcription factors, including paired box 6 (PAX6) and FOXC1 (160). Mutations in *PAX6* and *FOXC1* have been suggested to prevent the proper interaction of surface and neural ectodermal cells with neural crest-derived mesenchymal cells during development (160), resulting in anterior segment dysgenesis. Specifically, mutations in *PAX6* have been implicated in aniridia (absence of the iris) (161), whereas mutations in *FOXC1* cause Axenfeld-Rieger Syndrome (ARS) (138). ARS includes a variety of ocular anomalies that affect the iris (hypoplasia, corectopia, polycoria, and peripheral anterior synechia) and other ocular structures. Patients with aniridia or ARS are at a high risk for glaucoma (144,162), a progressively blinding condition that is usually associated with elevated intraocular pressure.

FOXC1 belongs to the *F*orkhead B*ox* family of transcription factors, which are characterized by a highly conserved DNA-binding Forkhead Domain (FHD). The FHD consists of three α-helices and two β-strands. Each β-strand is followed by a winglike loop. All missense mutations identified to date lie within the FHD. Molecular analyses of several of these

FOXC1 missense mutations suggest that the different subdomains within the FHD may have specific functional roles (154).

A novel *FOXC1* missense mutation, W152G, was identified in a newborn boy with aniridia and congenital glaucoma. In this report, the W152G mutation was analyzed to understand how molecular defects in FOXC1 contribute to the development of ocular malformations, including aniridia. Furthermore, molecular analysis of the W152G mutation highlights the importance of having efficient quality control machinery within the cell that is able to regulate improperly folded protein.

Materials and Methods

Mutation Detection

The research adhered to the tenets of the Declaration of Helsinki. *PAX6* and *FOXC1* were amplified as previously described (138,163). *CYP1B1* was amplified using previously published primers (164) and DNA polymerase (KAPAHiFi; Kapa Biosystems, Inc., Woburn, MA). Polymerase chain reaction (PCR) products were gel purified and extracted on separation columns (Qiagen, Valencia, CA). The coding regions of *PAX6, CYP1B1*, and *FOXC1* were sequenced using a genetic analyzer (3130*xl*; Applied Biosystems Inc., Foster City, CA) as previously described (165).

Plasmid

Site-directed mutagenesis was performed (QuikChange mutagenesis kit; Stratagene, La Jolla, CA) with the addition of 10% dimethylsulfoxide. Mutagenic primer sequences for W152G were as follows: forward, 5′-ggcaagggcagctacgggacgctggacccgg-3′; reverse, 5′-ccgggtccagcgtcccgtagctgcccttgcc-3′. Potential mutant constructs were sequenced. Confirmed mutants were subcloned into the *FOXC1* pcDNA4 His/Max vector (Invitrogen, Burlington, ON, Canada) (150), and the entire insert was resequenced.

Cell Culture

COS-7 cells, HeLa cells, and nonpigmented ciliary epithelial cells were cultured in high-glucose Dulbecco's modified Eagle's medium (DMEM) and supplemented with 10% fetal bovine serum (FBS). Immortalized human trabecular meshwork (HTM) cells were cultured in low-glucose DMEM and 10% FBS.

Immunoblot Analysis

COS-7 or HeLa cells were transfected with 4 μg epitope-tagged (Xpress; Invitrogen) *FOXC1* (10) with the use of a reagent (Fugene 6; Roche, Mississauga, ON, Canada). Whole-cell extracts were prepared 48 hours after transfection, as described previously (82). The proteins were resolved on an SDS-PAGE gel, transferred to a nitrocellulose membrane, and probed with the appropriate antibodies as described previously (82).

Epitope-tagged (Xpress; Invitrogen) FOXC1 was detected with anti–epitope-tagged (Xpress; Invitrogen) antibody (1:10,000). For the phosphorylation experiments, protein extracts were incubated with 20 U calf intestinal alkaline phosphatase (CIP; Invitrogen), with or without 11 μM sodium vanadate ($NaVO_3$), for 1 hour at 37°C before being resolved on an SDS-PAGE gel. Protein extracts were partially digested by incubation with 1.7 μM trypsin at 37°C for 5 minutes. Digestion products were resolved on an SDS-PAGE gel and were detected using a rabbit polyclonal antibody raised against FOXC1 (1:2000; Abcam, Cambridge, MA).

Immunofluorescence

Cells were grown and transfected directly on coverslips with 1 μg epitope-tagged (Xpress; Invitrogen) *FOXC1* as previously described (150). Either 24 hours or 48 hours after transfection, the cells were fixed with 2% paraformaldehyde for 15 minutes and were processed for immunofluorescence as previously described (166). The formation of protein aggregates was further analyzed by treatment of HTM cells with 20 μM MG132 and/or 0.01 μg/μL nocodazole 14 hours before processing for immunofluorescence. The FOXC1 protein was visualized by incubation with anti–epitope-tagged (Xpress; Invitrogen) antibody and anti–mouse Cy3-conjugated secondary antibody (Jackson ImmunoResearch, West Grove, PA) while the nucleus was visualized by incubation with DAPI. At least 100 cells were scored for each experimental group.

Electrophoretic Mobility Shift Assay (EMSA)

The amount of W152G protein in COS-7 whole cell extracts was equalized to wild-type (WT) FOXC1 levels by inspection of the proteins detected by immunoblotting. EMSA was performed as described previously (150).

Transactivation Assay

The FOXC1 luciferase reporter assay was performed as described previously (166). Each experiment was conducted three times in triplicate. Proper expression of all expression vectors was first verified by parallel immunoblot analysis.

Modeling

In silico mutagenesis of the FOXC2 FHD model (98% identical with the FOXC1 FHD) was performed with Swiss-Pdb Viewer (http://ca.expasy.org/spdbv/) and was evaluated with the Atomic Non-Local Environment Assessment (ANOLEA) server (http://www.swissmodel.expasy.org/anolea/) (167) as described previously (165). The *in silico* analysis was carried out by T.K. Footz.

Results

A newborn boy had severe ocular malformations including bilateral megalocornea and opacity, aniridia, and congenital glaucoma (Figures 1A

1B 1C) (168). The patient had no recorded family history of ocular disease. Given that aniridia has been associated with mutations in *PAX6*, we screened *PAX6* by direct sequence analysis of PCR products from the patient DNA. However, no *PAX6* mutations were found. Screening of *CYP1B1*, a gene that has been implicated in primary congenital glaucoma (169), identified the following polymorphisms: rs2617266TT, rs10012GG, rs1056827TT, rs1056836CC, rs1056837CC, and rs1800440AG. All six alterations in *CYP1B1* have been reported to be non–disease-causing SNPs and thus, were unlikely to have contributed to the negative phenotypes in this patient. Subsequently, we screened *FOXC1* for mutations. A heterozygous T-to-G transversion at codon position 152 (c.454T>G; W152G) was identified (Figure 1D). This mutation was confirmed by sequencing both strands of the amplified product. The W152G mutation was not present in 100 normal control chromosomes. This is the first reported case of a mutation involving an amino acid residue within β-strand 2 of the FOXC1 FHD and extends the phenotypic consequence of *FOXC1* mutations to include aniridia.

To examine how the W152G mutation alters FOXC1 function, the W152G mutation was introduced into the *FOXC1* cDNA by site-directed mutagenesis. The W152G protein is stable enough to be detected by immunoblot analysis (Figure 2A). As we have previously reported, the WT FOXC1 protein migrates as multiple bands because of phosphorylated forms of the protein (81). The W152G protein also occurred as multiple

bands. However, one of the mutant bands had faster mobility than the WT bands. The WT and W152G FOXC1 proteins were incubated with calf intestinal alkaline phosphatase (CIP) to confirm that the multiple bands were attributed to phosphorylated forms of the FOXC1 protein. When the WT and W152G protein lysates were incubated with CIP, the presence of the upper band was reduced (Figure 2B). Based on these data, we conclude that the W152G mutant protein may be folded or phosphorylated differently from the WT protein. Because neither tryptophan nor glycine can be phosphorylated, any difference in phosphorylation was not attributed to direct phosphorylation changes of this residue at position 152. Rather, changes that affected the entire protein structure, such as misfolding of the protein, could have been responsible. To examine this possibility, the WT and W152G FOXC1 proteins were partially digested with trypsin. Incubation of the protein lysates with trypsin resulted in the disappearance of nearly all the full-length WT bands, whereas the full-length W152G bands were still visible (Figure 2C, left), indicating that W152G results in a mutant FOXC1 protein with decreased accessibility to trypsin. This fact plus the observation of different digestion products of WT compared with W152G FOXC1 proteins suggest that there are differences in the overall structure of the WT and mutant proteins (Figure 2C ,right).

The DNA-binding ability of the W152G protein was examined by EMSA. The ability to bind to DNA is essential for FOXC1 to function as an effective transcription factor and to regulate the expression of other genes.

As expected, the WT protein was able to bind to the FOXC1 binding site (Figure 3A). However, the W152G protein was unable to bind even when the protein level was increased (Figure 3A). Based on the EMSA results, we conclude that the W152G mutation greatly disrupts the DNA-binding ability of the mutant FOXC1 protein.

A reporter assay was conducted in HeLa cells to examine the ability of the W152G protein to activate a luciferase reporter gene containing six copies of the consensus FOXC1 binding sites. The transactivation ability of W152G was only 3% of WT FOXC1, similar to that of the empty expression vector (Figure 3B).

The ability of the W152G FOXC1 protein to localize to the nucleus was examined by immunofluorescence. More than 90% of HTM cells showed exclusive nuclear localization of the FOXC1 WT protein (Figure 4A). However, there was a dramatic reduction in the number of HTM cells with exclusive nuclear localization of the W152G FOXC1 protein (10.3%) compared with the WT protein (92%; Figure 4A). Most cells showed localization of the W152G protein to both the nucleus and the cytoplasm. Interestingly, the W152G mutant proteins formed aggregated complexes in the cytoplasm in approximately 30% of cells (Figure 4A). Aggregated complexes in the cytoplasm have been observed for one other FOXC1 mutation, L130F (165). To examine whether the protein aggregates are part of aggresomes, we treated the cells with MG132, a proteasomal inhibitor known to induce the formation of aggresomes (170). Because

microtubules are essential for the formation of aggresomes, the cells were also treated with nocodazole, which disrupts microtubules (170). The MG132 and nocodazole treatments did not affect the nuclear localization of the WT protein (Table 1; Figure 4B). MG132 treatment did not affect the formation of protein aggregates for either the W152G or the L130F mutation (Table 1). Interestingly, fully formed aggresomes were observed in MG132-treated HTM cells expressing L130F (Figure 4B). Nocodazole treatment with or without MG132 decreased the percentage of cells with protein aggregates from 46.2% in untreated cells to 35.8% and 33.3%, respectively, for the L130F mutation. These results further verify that the L130F proteins form aggresomes. For the W152G mutation, adding nocodazole with or without MG132 did not decrease the number of cells with protein aggregates, suggesting that the protein aggregates formed by the W152G protein are not microtubule-dependent inclusion bodies (Table 1; Figure 4B). Although both W152G and L130F result in the formation of protein aggregates in the cytoplasm, aggresome formation was only observed for the L130F mutation. These results suggest that the two mutant FOXC1 proteins are processed in the cell by different mechanisms.

FOXC2-based homology models (165) of the FOXC1 FHD bearing the L130F and W152G mutations were analyzed to determine potential effects on protein structure. Figure 5B shows a comparison of ANOLEA mean force potentials calculated for the mutations compared with WT. The analysis indicated that the L130F mutation was predicted to have

unfavorable effects (i.e., higher ANOLEA scores) on the residues at positions 87, 130, and 152. However, W152G affects a different set of residues, namely those at positions 98, 99, 130, 136, 138, and 152. Therefore, it appears that W152G may cause a more profound disturbance to the structure of an important hydrophobic pocket of the FHD than L130F. This difference in the predicted effects on FOXC1 structure is consistent with the more severe molecular and phenotypic consequences of the W152G mutation.

Discussion

In this study, we identified a novel *FOXC1* missense mutation, W152G, in a patient with aniridia and congenital glaucoma (Figure 1A). This finding of a *FOXC1* mutation causing aniridia is supported by a recent report of another patient with aniridia with a FOXC1 M161K mutation (171). However, FOXC1 M161K mutations were previously identified in two other patients, both of whom had ARS (iris hypoplasia, a prominent Schwalbe line, peripheral anterior synechiae) rather than aniridia (172,173), indicating phenotypic variability in patients with FOXC1 M161K mutations. Distinguishing between the distinct phenotypes that can apparently rise from the same FOXC1 M161K mutation would be of interest for future studies.

This study on the FOXC1 W152G mutation is the first examination of the molecular consequences of an aniridia-causing *FOXC1* mutation. In addition, this is the first time a mutation has been found in a residue within β-strand 2 of the FOXC1 FHD. Interestingly, molecular modeling by Saleem *et al.* (150) predicted that the W152 residue forms highly conserved pairwise interactions with other hydrophobic amino acid residues, such as I87 and L130. These hydrophobic residues are involved in the formation of a hydrophobic core within the FHD. In addition to the novel W152G mutation, two mutations involving amino acid residues that form this hydrophobic core have been reported. Both I87M and L130F result in severe disruptions to normal FOXC1 protein function, including defects in protein stability, nuclear localization, and DNA binding (150,165). Thus, amino acid residues involved in the formation of the hydrophobic core appear to be particularly important for the FOXC1 protein function.

Mutations often lead to the synthesis of misfolded proteins. Tryptophan and glycine are hydrophobic and neutrally charged amino acid residues. Despite these similarities, the W152G mutation appears to distort the protein structure by preventing the linear amino acid chain from folding properly. Molecular modeling predicts that substituting tryptophan with the much smaller glycine residue at codon position 152 results in a protein in a less energetically favorable state (Figure 5). Such an energetically unfavorable state would be predicted to result in a misfolded protein. Supporting this prediction is the partial digest with trypsin that

resulted in different digestion products between the WT and W152G proteins, thus indicating the proteins are folded differently (Figure 2C). The W152G mutation could result in the exposure of normally hidden trypsin sites or, alternatively, could result in normally exposed trypsin sites becoming inaccessible. This may explain how trypsin cleaves the mutant protein at different sites compared with the WT protein, resulting in different digestion products (Figure 2C). Thus, consistent with the molecular modeling prediction, the W152G mutation appears to alter the overall topology of the FOXC1 protein.

Misfolding of the mutant FOXC1 protein has severe consequences on normal FOXC1 protein function. Immunofluorescence results showed that most of the W152G proteins were unable to localize exclusively to the nucleus (Figure 4A). These results were surprising because the W152G mutation is not located within the known nuclear localization signal (NLS) or nuclear localization accessory signal (NLAS) (81). FOXC1 mutations involving substitution of amino acid residues with the same charge usually result in milder nuclear localization defects than mutations that introduce an amino acid residue with a different charge (154). The altered topology of the W152G protein could prevent the correct detection of the NLS and NLAS, preventing the protein from localizing to the nucleus. Interestingly, nocodazole treatment with or without MG132 decreased the number of cells with L130F protein aggregates (Table 1; Figure 4B). Nevertheless, disassembling these protein aggregates did not result in increased

exclusive nuclear localization of the L130F protein. Thus, at least in the case of the L130F mutation, the protein aggregates do not appear to contribute to the severity of the nuclear localization defect.

Many of the molecular defects caused by the *W152G* mutation are similar to the molecular defects observed with the *L130F* mutation. The W152G and the L130F mutant proteins are phosphorylated differently than the WT protein, have a nuclear localization defect, and cannot bind to DNA (165). In both cases, the net result is that the ability of FOXC1 to regulate gene expression is impaired. Despite these similarities, however, the *W152G* mutation and the *L130F* mutation cause different phenotypes. The *W152G* mutation causes aniridia and congenital glaucoma (168). The *L130F* mutation was found in a woman with a mild form of ARS and no glaucoma (165). Her son was diagnosed with a severe form of ARS (corectopia, hypertelorism, posterior embryotoxon) and congenital glaucoma (165). A possible explanation for the difference in phenotype is that the L130F mutant proteins form aggresomes but the W152G proteins do not. In normal cells, the protein quality control machinery prevents the accumulation of protein aggregates by promoting correct folding of proteins through chaperone activity and continuously degrading misfolded proteins before protein aggregates can form (174). Misfolding of the protein often results in the incorrect exposure of hydrophobic surfaces that are usually buried in the protein core (175). When the misfolded form of the protein persists, such as when a mutation causes the misfolding, protein

aggregates may form primarily through the incorrect intermolecular interaction of the hydrophobic surfaces of the misfolded proteins (176). Because such protein aggregates are stable complexes that can be pathogenic (174), some cells form aggresomes to protect against potentially toxic protein aggregates (170). Aggresomes are cytoplasmic inclusion bodies that form when protein aggregates are transported by microtubules to the microtubule organizing center (170). They may form when the capacity of the proteasomal degradation pathway is exceeded (170). Kopito (174) suggests that concentrating the protein aggregates into aggresomes may promote the degradation of aggregates by autophagy, thereby providing an alternative route for the cell to discard potentially toxic protein aggregates. Thus, although the *L130F* mutation results in protein aggregates in approximately 18% more cells than the *W152G* mutation (Table 1; Figure 4B), these cells may be able more effectively to discard the protein aggregates by forming aggresomes. As a result of an inability to participate in this additional degradation pathway, the *W152G* mutation may cause a more severe phenotype than the *L130F* mutation. The inability of the W152G protein aggregates to form aggresomes along with the numerous other molecular defects of the W152G protein may underlie the aniridia phenotype that results from the *FOXC1 W152G* mutation.

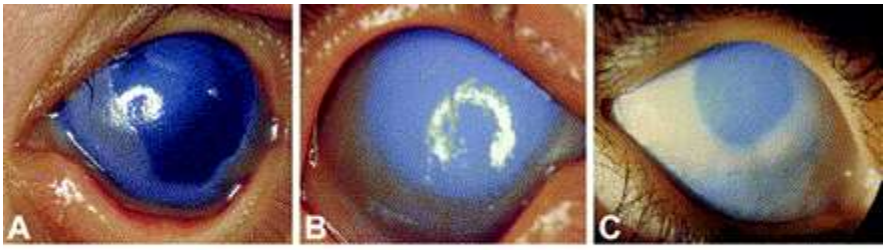

D.

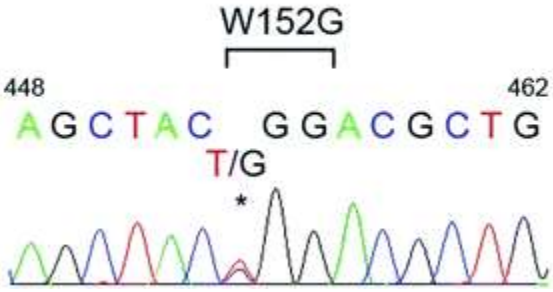

Figure 1: *FOXC1 W152G* mutation identified in a patient with aniridia. (A) At 2 weeks of age, abnormal elevated thickened limbal tissue and diffused corneal haze (stromal scarring, stromal edema, and epithelial edema) are observed. (B) At 2 months of age, the abnormal tissue is no longer distinct, there is no elevation of limbal tissue, and pannus is present ×360°. (C) At 5 months of age, the pannus is replaced by scarring. The photographs are reprinted from Al-Shahwan S, Edward DP, Khan AO. Severe ocular surface disease and glaucoma in a newborn with aniridia. *J AAPOS*. 2005;9:499–500. (D) The chromotagram shows the genomic DNA sequence of the patient in (A–C). The patient has a heterozygous T-to-G transversion that results in a tryptophan-to-glycine change at codon position 152.

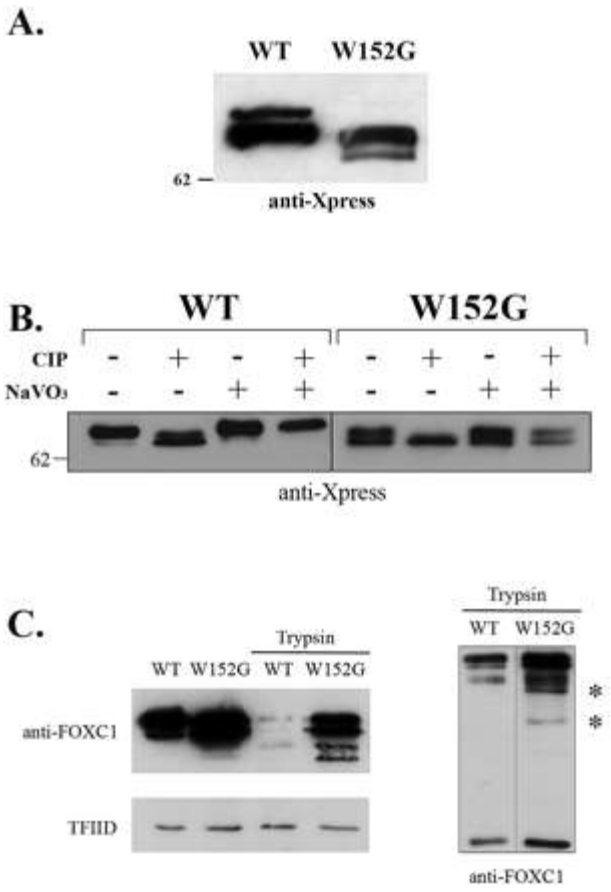
A.
WT
W152G
62
anti-Xpress
B.
WT
W152G
CIP
NaVO3
62
anti-Xpress
C.
Trypsin
WT W152G WT W152G
anti-FOXC1
TFIID
Trypsin
WT W152G
anti-FOXC1

Figure 2: **Expression analysis of WT and W152G FOXC1 cDNAs in transfected COS cells.** (A) WT FOXC1 and W152G recombinant proteins were detected by immunoblotting. WT and W152G occurred as multiple bands, but the migration pattern of W152G was altered. (B) Treatment with CIP and $NaVO_3$ indicates that the upper band is attributed to phosphorylated forms of the protein for WT and W152G. (C, *left*) The immunoblot has equal protein loading. W152G is more resistant than WT when partially digested with trypsin. *Right*: to visualize the digestion products for WT and W152G, the immunoblot was loaded with equal protein expression levels. *Asterisks*: different digestion products between the WT and W152G proteins.

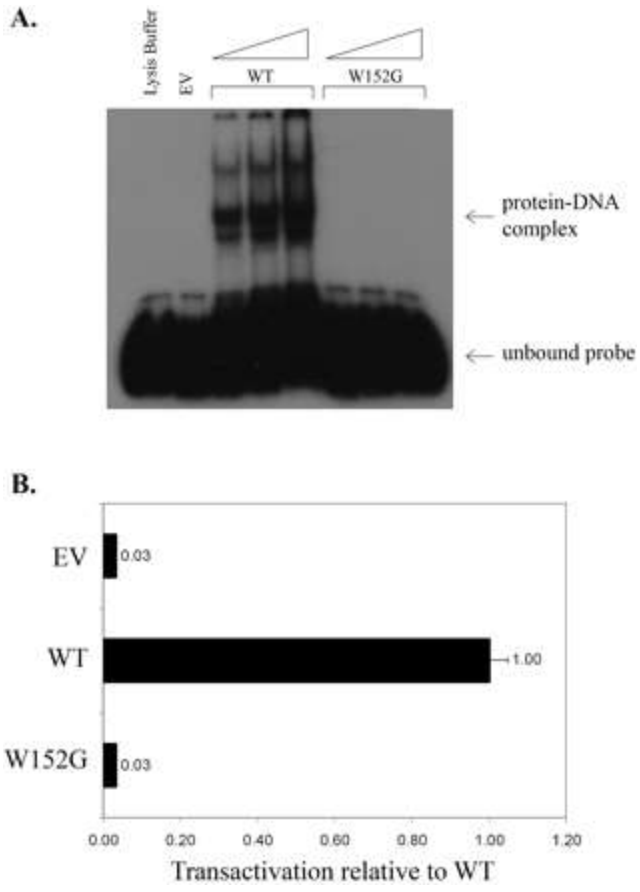
A.
Lysis Buffer
EV
WT
W152G
protein-DNA complex
unbound probe
B.
EV
WT
W152G
0.03
1.00
0.03
0.00
0.20
0.40
0.60
0.80
1.00
1.20
Transactivation relative to WT

Figure 3: Molecular defects of the FOXC1 W152G mutant protein. (A) Whole-cell extracts from COS cells transfected with FOXC1 WT or FOXC1 W152G expression vectors were incubated with a radioactively labeled FOXC1 consensus binding site oligonucleotide probe. FOXC1 WT formed protein-DNA complexes, but FOXC1 W152G did not form protein-DNA complexes even when the amount of the FOXC1 W152G protein was increased. (B) The FOXC1 W152G mutant protein was unable to transactivate a firefly luciferase reporter gene with six copies of the in vitro-derived FOXC1-binding site. Firefly luciferase values were normalized to a *Renilla* luciferase control. Mean luciferase values from a representative experiment transfected in triplicate are shown. Error bars represent the SEM.

A.

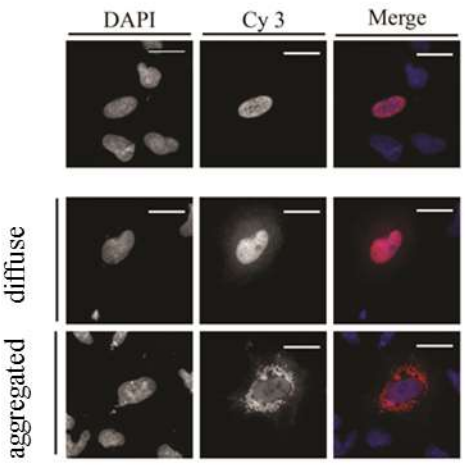

	Exclusive Localization (%)		Nucleus+Cytoplasm (%)	
	Nucleus	Cytoplasm	Diffuse	Aggregated
WT	92.0	0	8.0	0
W152G	10.3	0.4	60.1	29.2

B.

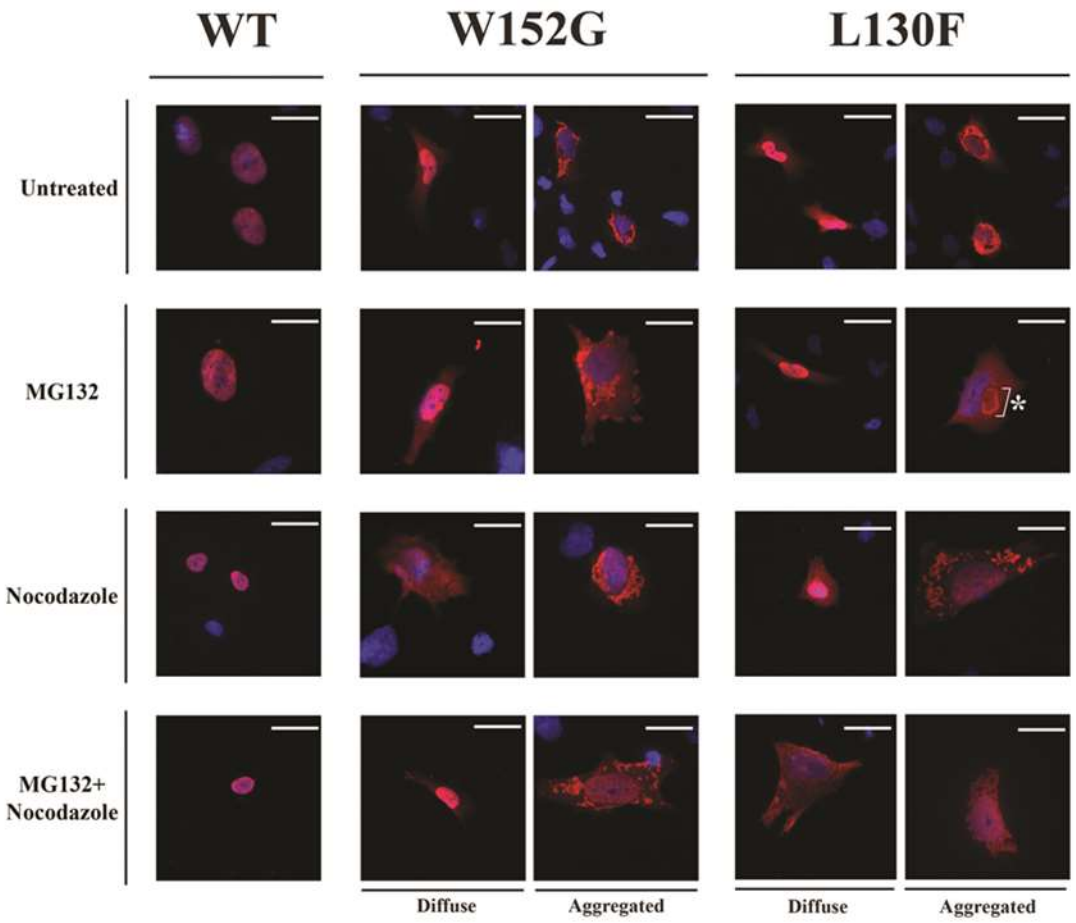

Figure 4: Localization patterns of FOXC1 W152G and FOXC1 L130F proteins in HTM cells. (A) Most FOXC1 WT-expressing cells displayed a nuclear-exclusive pattern (*top*). However, 60.1% of FOXC1 W152G-expressing cells displayed a diffused pattern of mutant protein in the cytoplasm (*middle*), and 29.2% of cells displayed an aggregated pattern of proteins in the cytoplasm (*bottom*). (B) Neither MG132 nor nocodazole treatment affected the ability of the FOXC1 WT protein to localize exclusively to the nucleus. Neither MG132 nor nocodazole treatment of HTM cells transfected with FOXC1 W152G changed the characteristics of the protein aggregates. *Asterisk*: MG132 treatment induced the formation of aggresomes in HTM cells transfected with FOXC1 L130F (MG132, aggregated). Interestingly, although protein aggregates were still present in the cytoplasm of HTM cells treated with nocodazole (with or without MG132), the protein aggregates appeared to be more dispersed (compare nocodazole aggregated panel and MG132+nocodazole aggregated panel with untreated aggregated panel). *Blue*: DAPI-stained nuclei. *Red*: Cy3 fluorescence of epitope-tagged recombinant FOXC1 proteins. Scale bars, 10 μm.

A.

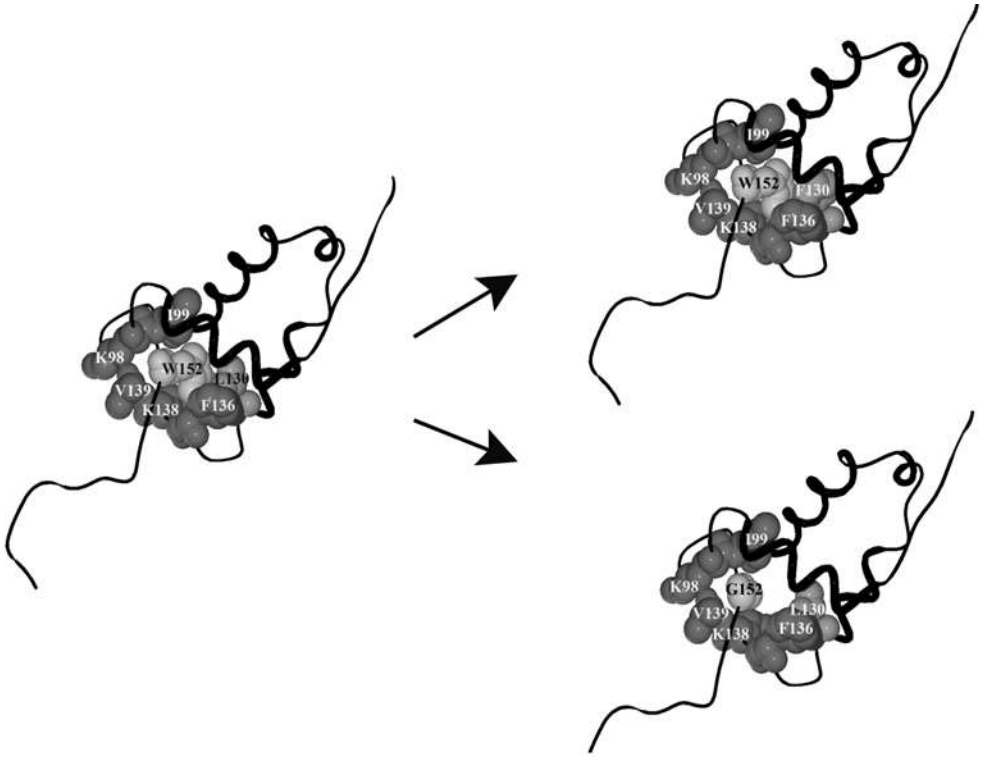
I99
K98
W152
L130
V139
K138
F136
I99
K98
W152
F130
V139
K138
F136
I99
K98
G152
L130
V139
K138
F136

B.

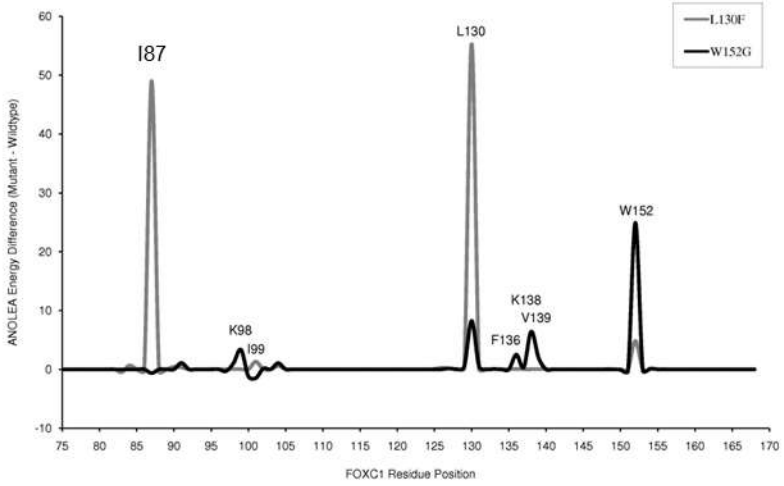
L130F
W152G
I87
L130
W152
K138
V139
K98
I99
F136
ANOLEA Energy Difference (Mutant - Wildtype)
FOXC1 Residue Position
60
50
40
30
20
10
0
-10
75
80
85
90
95
100
105
110
115
120
125
130
135
140
145
150
155
160
165
170

Figure 5: Comparison of W152G and L130F molecular models. (A) *In silico* mutagenesis shows that replacement of the bulky W152 side chain with glycine may result in suboptimal packing in the FHD hydrophobic core. The protein backbone is depicted in *black*, unmutated residues in *dark gray*, and position 152 in *light gray*. WT and mutant models were submitted to the ANOLEA Swiss model server. (B) Peaks on the scatter plot represent amino acid positions that experience an altered pseudoenergy state, as calculated by ANOLEA, as a result of the indicated mutation. The *in silico* analysis was carried out by T.K. Footz.

Table 1: Summary of subcellular localization of the WT and W152G FOXC1 protein in HTM cells treated with or without MG132 and nocodazole 48h post-transfection

	Number of cells counted	Exclusive Localization (%)		Nucleus + Cytoplasm (%)	
		Nucleus	Cytoplasm	Diffuse	Aggregated
WT untreated	107	84.1	0	15.9	0
WT+MG132	120	83.3	0	16.7	0
WT+NOC	132	84.8	0	15.2	0
WT+MG132+NOC	120	82.5	0	17.5	0
L130F untreated	104	15.4	0	38.5	46.2
L130F+MG132	104	12.5	0	37.5	50.0
L130F+NOC	102	3.9	0	62.7	33.3
L130F+MG132 +NOC	106	13.2	0	50.9	35.8
W152G untreated	113	5.3	0	66.4	28.3
W152G+MG132	107	0	0.9	72.0	27.1
W152G+NOC	111	1.8	0	64.0	34.2
W152G+MG132 +NOC	109	8.3	0	56.9	34.9

References

(1) Cvekl A, Tamm ER. Anterior eye development and ocular mesenchyme: new insights from mouse models and human diseases. Bioessays 2004 Apr;26(4):374-386.

(2) Hanson IM, Fletcher JM, Jordan T, Brown A, Taylor D, Adams RJ, et al. Mutations at the PAX6 locus are found in heterogeneous anterior segment malformations including Peters' anomaly. Nat Genet 1994 Feb;6(2):168-173.

(3) Mears AJ, Jordan T, Mirzayans F, Dubois S, Kume T, Parlee M, et al. Mutations of the forkhead/winged-helix gene, FKHL7, in patients with Axenfeld-Rieger anomaly. Am J Hum Genet 1998 Nov;63(5):1316-1328.

(4) Fitch N, Kaback M. The Axenfeld syndrome and the Rieger syndrome. J Med Genet 1978 Feb;15(1):30-34.

(5) Nelson LB, Spaeth GL, Nowinski TS, Margo CE, Jackson L. Aniridia. A review. Surv Ophthalmol 1984 May-Jun;28(6):621-642.

(6) Saleem RA, Banerjee-Basu S, Murphy TC, Baxevanis A, Walter MA. Essential structural and functional determinants within the forkhead domain of FOXC1. Nucleic Acids Res 2004 Aug 6;32(14):4182-4193.

(7) Mirzayans F, Pearce WG, MacDonald IM, Walter MA. Mutation of the PAX6 gene in patients with autosomal dominant keratitis. Am J Hum Genet 1995 Sep;57(3):539-548.

(8) Acharya M, Mookherjee S, Bhattacharjee A, Bandyopadhyay AK, Daulat Thakur SK, Bhaduri G, et al. Primary role of CYP1B1 in Indian juvenile-onset POAG patients. Mol Vis 2006 Apr 20;12:399-404.

(9) Ito YA, Footz TK, Murphy TC, Courtens W, Walter MA. Analyses of a novel L130F missense mutation in FOXC1. Arch Ophthalmol 2007 Jan;125(1):128-135.

(10) Saleem RA, Banerjee-Basu S, Berry FB, Baxevanis AD, Walter MA. Analyses of the effects that disease-causing missense mutations have on the structure and function of the winged-helix protein FOXC1. Am J Hum Genet 2001 Mar;68(3):627-641.

(11) Berry FB, Mirzayans F, Walter MA. Regulation of FOXC1 stability and transcriptional activity by an epidermal growth factor-activated mitogen-

activated protein kinase signaling cascade. J Biol Chem 2006 Apr 14;281(15):10098-10104.

(12) Berry FB, O'Neill MA, Coca-Prados M, Walter MA. FOXC1 transcriptional regulatory activity is impaired by PBX1 in a filamin A-mediated manner. Mol Cell Biol 2005 Feb;25(4):1415-1424.

(13) Melo F, Feytmans E. Assessing protein structures with a non-local atomic interaction energy. J Mol Biol 1998 Apr 17;277(5):1141-1152.

(14) Al-Shahwan S, Edward DP, Khan AO. Severe ocular surface disease and glaucoma in a newborn with aniridia. J AAPOS 2005 Oct;9(5):499-500.

(15) Stoilov I, Akarsu AN, Sarfarazi M. Identification of three different truncating mutations in cytochrome P4501B1 (CYP1B1) as the principal cause of primary congenital glaucoma (Buphthalmos) in families linked to the GLC3A locus on chromosome 2p21. Hum Mol Genet 1997 Apr;6(4):641-647.

(16) Berry FB, Saleem RA, Walter MA. FOXC1 transcriptional regulation is mediated by N- and C-terminal activation domains and contains a phosphorylated transcriptional inhibitory domain. J Biol Chem 2002 Mar 22;277(12):10292-10297.

(17) Johnston JA, Ward CL, Kopito RR. Aggresomes: a cellular response to misfolded proteins. J Cell Biol 1998 Dec 28;143(7):1883-1898.

(18) Khan AO, Aldahmesh MA, Al-Amri A. Heterozygous FOXC1 mutation (M161K) associated with congenital glaucoma and aniridia in an infant and a milder phenotype in her mother. Ophthalmic Genet 2008 Jun;29(2):67-71.

(19) Komatireddy S, Chakrabarti S, Mandal AK, Reddy AB, Sampath S, Panicker SG, et al. Mutation spectrum of FOXC1 and clinical genetic heterogeneity of Axenfeld-Rieger anomaly in India. Mol Vis 2003 Feb 18;9:43-48.

(20) Panicker SG, Sampath S, Mandal AK, Reddy AB, Ahmed N, Hasnain SE. Novel mutation in FOXC1 wing region causing Axenfeld-Rieger anomaly. Invest Ophthalmol Vis Sci 2002 Dec;43(12):3613-3616.

(21) Kopito RR. Aggresomes, inclusion bodies and protein aggregation. Trends Cell Biol 2000 Dec;10(12):524-530.

(22) Wetzel R. Mutations and off-pathway aggregation of proteins. Trends Biotechnol 1994 May;12(5):193-198.

(23) Markossian KA, Kurganov BI. Protein folding, misfolding, and aggregation. Formation of inclusion bodies and aggresomes. Biochemistry (Mosc) 2004 Sep;69(9):971-984.

Chapter 4. Analysis of the role of the FOXC1 transcription factor in stress response through the regulation of HSPA6

Introduction

In the previous two chapters, I examined the molecular consequences of two FOXC1 mutations, L130F and W152G. Mutations in FOXC1 disrupt the normal functioning of the FOXC1 protein including its ability to localize to the nucleus, bind DNA, and/or transactivate a reporter gene. Thus, FOXC1 mutations are predicted to result in dysregulation of downstream target genes, which would have negative consequences on the cell. Recent studies have begun to identify genes that are regulated by FOXC1. Microarray analysis using a hormone-responsive FOXC1 construct has identified a large number of potential target genes of FOXC1 (80). Identifying target genes of FOXC1 is an effective strategy for determining specific pathways that FOXC1 is involved in. By characterizing FOXO1a as a FOXC1 target gene, Berry *et al.* observed that FOXC1 appears to mediate the stress response pathway. In addition, knocking down FOXC1 in HTM cells sensitizes cells to H_2O_2-induced oxidative stress.

The potential involvement of FOXC1 in the stress response pathway is particularly interesting. Since FOXC1 continues to be expressed in the adult TM (98), FOXC1 may be involved in mediating the TM's stress response by regulating stress-responsive genes. TM cells are exposed to various environmental stresses including mechanical and oxidative stresses. TM cells have various cellular defense mechanisms that enable these cells to respond and adapt in a dynamic environment.

However, chronic stress conditions have been suggested to overwhelm the cellular defense mechanisms, resulting in TM cell death. The death of TM cells will subsequently lead to the elevation of IOP due to inefficient aqueous humor drainage, and the development of a glaucoma phenotype.

In the present chapter, I examine the role of FOXC1 in mediating the stress response by regulating a stress-responsive target gene, HSPA6 (also known as HSP70B'). The majority of the following experiments are carried out in human trabecular meshwork (HTM) cells because FOXC1 has been shown to be expressed in adult TM. Also, the death of TM cells is predicted to be a contributing factor to the elevation of IOP. Since ROS are present in aqueous humor, TM cells are constantly exposed to oxidative stress conditions. Thus, in the following experiments, HTM cells were exposed to different severities of H_2O_2-induced acute oxidative stress to investigate the role of FOXC1 in stress response. A two-step H_2O_2 treatment, where cells were first pre-conditioned with a non-lethal dose of H_2O_2, was used to examine the potential for HTM cells to acquire cytoprotection. HTM cells are an appropriate model to use to examine HSPA6 function because HSPA6 is not present in conventional model organisms.

Materials and Methods

Mammalian cell culture and transfection

Human trabecular meshwork (HTM) cells were grown in Dulbecco's modified Eagle's medium (DMEM; Invitrogen), supplemented with 10% fetal bovine serum. Twenty-four hours pre-transfection, plates were seeded at the following densities so that transfections would be carried out at 30 to 50% confluency: 10^6 cells/100mm plate (10mL media); $2x10^5$ cells/25mm well (3mL media). Plasmid transfections were performed using a TransIT-LT1 (Mirus) transfection reagent to DNA ratio of 5:1, according to the manufacturer's protocol. Four micrograms and 0.8 µg of DNA were used for transfection of cells plated on 100mm plates and 6-well plates, respectively. siRNA transfections were performed using 12.5 µL of Lipofectamine 2000 (Invitrogen) per 100mm plate, according to the manufacturer's protocol (Table 1).

Plasmids

A FOXC1 pcDNA4-Xpress His/Max B (Invitrogen) plasmid was used. The FOXC1 L130F, W152G, and S131L mutant constructs were previously assembled (150,165,177).

The HSPA6 full length cDNA (DNASU Plasmid Repository) was subcloned into the pcDNA3.1/nV5-DEST vector (Invitrogen) in-frame to the V5 epitope by gateway technology. All vectors were sequenced to

confirm that no nucleotide changes were introduced into the cDNA and that the cDNAs were in-frame to the epitopes.

Two-step hydrogen peroxide (H_2O_2) treatment

Twenty-four hours post-transfection, cells were treated with 500 µM H_2O_2 for 2 hours, then allowed to recover in fresh media. Approximately 22 hours post-recovery, the cells were treated with 1000 µM H_2O_2 for 2 hours, then allowed to recover in fresh media for approximately 22 hours before analysis (Figure 1).

Heat shock treatment

Approximately 48h post-transfection, HTM cells were heat shocked at 44°C for 2h. Cells were allowed to recover in fresh media pre-warmed to 37°C for ~22h before analysis.

Trypan blue staining

HTM cells were plated onto 6-well plates and transfected with either a plasmid or siRNA. Twenty-four hours post-transfection, cells were exposed to the two-step H_2O_2 treatment before harvesting. Cells were trypsinized, then resuspended in 750 µL PBS. Cell viability was analyzed by mixing equal volumes of resuspended cells with 0.4% trypan blue (GIBCO BRL). After addition of trypan blue, the cells were immediately analyzed by loading onto a haemocytometer. For each sample, cells in eight 1 mm^2 squares were counted.

Protein analysis

For immunoblot analysis of endogenous FOXC1 protein, cells were harvested by scraping, lysed using Levin lysis buffer (1% IGEPAL CA-630, 0.5% sodium deoxycholate, 0.1% SDS, PBS) (178), and sonicated. For immunoblot analysis of all other proteins, cells were harvested by scraping, lysed using nuclear lysis buffer (20mM Hepes (pH 7.6), 500mM NaCl, 1.5mM MgCl2, 0.1% Triton-X 100, 20% glycerol, 1mM dithiothreitol, 1mM phenylmethylsulfonylfluoride, 0.5% protease inhibitor cocktail (Sigma)), and sonicated.

Protein lysates were resolved on a 10% sodium dodecyl sulfate gel and detected by immunoblotting with the appropriate primary and secondary antibodies (Table 2).

Realtime qPCR

After H_2O_2 treatment, total RNA was isolated from HTM cells using Trizol (Invitrogen). Two micrograms of total RNA was reverse transcribed using M-MLV Reverse Transcriptase according to the manufacturer's protocol (Invitrogen). The reverse transcribed product was treated with DNase I (Invitrogen). The QuantiTect SYBR Green PCR assay (Applied Biosystems) was used to quantitate FOXC1 RNA levels using the following primers: Forward 5'-CGGGTTGGAAAGGGATATTTA-3' and Reverse 5'-CAAAATGTTCTGCTCCTCTCG-3'. The Applied Biosystems 9700HT Thermal Cycler was used. The experiment was repeated three

times with each reaction conducted in triplicates each time. The FOXC1 RNA levels were compared to HPRT1 RNA levels, which served as an endogenous control, using the comparative $\Delta\Delta C_T$ method.

Dual Luciferase Assay

HeLa cells (4×10^4 cells per 15-mm well) were cotransfected with 160ng of the FOXC1 pcDNA4 His/Max expression vector, 60ng of the pGL3-TK reporter vector with the synthetic FOXC1 binding sites, and 5ng of the pRL-TK control vector. 160ng of the pcDNA4 His/Max empty vector and 60ng of the pGL3-TK reporter vector with no FOXC1 binding sites was used as controls to ensure that transactivation was specific to FOXC1. Transfections were performed using a TransIT-LT1 (Mirus) transfection reagent to DNA ratio of 3:1, according to the manufacturer's protocol. Twenty-four hours post-transfection, HeLa cells were subjected to the two-step H_2O_2 treatment. Twenty-two hours post-recovery, the luciferase assays were carried out using the dual luciferase assay kit according to the manufacturer's protocol (Promega). Each experiment was done in triplicate and was performed three times.

Northern blot analysis

Human trabecular meshwork (HTM) cells were transfected with 50nM control siRNA or 50nM FOXC1 siRNA (Table 1; Dharmacon). Forty-eight hours post-transfection, total RNA was isolated from HTM cells using Trizol (Invitrogen). Twenty to thirty µg of RNA was analyzed by Northern

blot on a formaldehyde agarose gel. The level of 28S ribosomal RNA was determined by visualization with the addition of ethidium bromide to the gel. A HSPA6 DNA fragment, unique to the 5` untranslated region of HSPA6, was PCR amplified using the following primers: Forward 5'-caa ggt gcg cgt atg cta c-3' and Reverse 5'-gct cat tga tga tcc gca aca c-3'. This HSPA6 DNA fragment was labeled with ^{32}P-dCTP by random primer labeling (Invitrogen) and hybridized to a Hybond-N membrane (Amersham Biosciences) using ExpressHyb Hybridization solution (BD Biosciences). HSPA6 RNA levels were normalized to 28S levels and quantified using ImageJ.

ChIP Analysis

Approximately 2.5x10^7 HTM cells were used for each ChIP reaction. HTM cells, grown to confluency, were crosslinked with1% formaldehyde for 10 minutes. The crosslinking reaction was stopped by the addition of 0.125M glycine. Cells were lysed in lysis buffer (5mM PIPES pH8.0, 85mM KCl, 0.5% IPEGAL CA-630, 1mM PMSF, 1:200 mammalian protease inhibitor cocktail (Sigma)) and homogenized by passage through a Dounce homogenizer (B pestle) six times. The cells were further lysed in nuclear lysis buffer [50mM Tris HCl pH 8.0, 10mM EDTA, 1% SDS, 1mM PMSF, 1:200 mammalian protease inhibitor cocktail]. The DNA was sheared to approximately 800bp by sonication. The sonicated lysates were pre-cleared with Protein A/G PLUS-Agarose beads (Santa Cruz Biotechnology). The sonicated, pre-cleared lysates

were incubated with 4µg of FOXC1 antibody (ORIGENE), 4µg of Histone H3 acetylated at lysine 9 antibody (Cell Signaling Technology), or rabbit IgG (Invitrogen) overnight. Protein beads were added to each sample for 1 hour and collected. The collected beads were washed three times with wash buffer (0.1%SDS, 1% Triton X-100, 2mM EDTA, 150mM NaCl, 20mM Tris-HCl pH 8.0) and once with final wash buffer (0.1%SDS, 1% Triton X-100, 2mM EDTA, 500mM NaCl, 20mM Tris-HCl pH 8.0). The protein-DNA complexes were eluted from the beads with elution buffer [1% SDS, 100mM $NaHCO_3$]. The protein was digested with the addition of proteinase K. The DNA was purified using the PCR cleanup protocol (QIAGEN). The purified DNA was eluted in 100µL of MilliQ water.

The sonicated, pre-cleared lysate was diluted to 1 in 100 for analysis as the “input” sample. For each PCR reaction, 1-5µL of the purified DNA (ie. ChIP reaction) was used as template. The primers sequences that were used for the ChIP-PCR are summarized in Table 3.

Results

FOXC1 levels decrease after exposure to H_2O_2-induced oxidative stress

Endogenous FOXC1 protein levels decreased after HTM cells were subjected to H_2O_2-induced oxidative stress (Figure 2A). HTM cells were subjected to three different H_2O_2 treatments as outlined in Figure 1.

Preconditioning with a non-lethal dose of H_2O_2 often results in increased tolerance to a second lethal dose of H_2O_2, a process known as cytoprotection (179,180). However, HTM cells under the present experimental conditions did not appear to acquire cytoprotective properties. Thus, in this section, the three H_2O_2 treatments are referred to as 'low dose', 'high dose', and 'severe dose'. FOXC1 protein levels did not recover even after 48 hours post-treatment, as observed with the 'low dose' samples. Also, the decrease in FOXC1 protein levels is not dependent on the severity of the H_2O_2 treatment since all three examined treatment conditions resulted in lower FOXC1 protein levels. Similarly, FOXC1 RNA levels significantly decreased in response to H_2O_2-induced oxidative stress (Figure 2B). FOXC1 levels from HTM total RNA were quantified by qPCR and normalized to HPRT1 RNA levels. Relative to untreated HTM samples, all three examined H_2O_2 treatment conditions resulted in a significant decrease in FOXC1 levels (p-value<0.01, Student's t-test). The ability of FOXC1 to transactivate a luciferase reporter gene with a synthetic FOXC1 binding site was also examined using HeLa cells. FOXC1 was able to transactivate the luciferase reporter gene under 'no H_2O_2' conditions (Figure 3A). However, the transactivation ability was reduced after exposure of HeLa cells to oxidative stress, most likely due to decreases in FOXC1 levels (Figure 3B). These experiments indicate that FOXC1 mRNA, protein levels, and activity all decrease after

exposure of cells to oxidative stress, and suggest that FOXC1 itself is a stress-responsive transcription factor.

FOXC1 appears to be an anti-apoptotic protein

The biological consequence of decreasing FOXC1 levels was examined by knocking down FOXC1 in HTM cells using siRNA against FOXC1. The efficiency of FOXC1 knockdown was confirmed by immunoblotting (Figure 4A). To distinguish between viable and non-viable cells, HTM cells were stained with trypan blue after treatment with H_2O_2. Under untreated conditions with normal FOXC1 levels, 78% of cells were viable (Figure 4B). However there were significantly less viable cells (69%) when FOXC1 was knocked down under 'no H_2O_2' conditions (p-value<0.01, Student's t-test). Also, relative to the control siRNA-transfected cells, there were significantly less viable cells in FOXC1 siRNA-transfected cells after exposure to a 'low dose' or 'high dose' of H_2O_2 (p-value<0.01, Student's t-test). Since decreasing FOXC1 levels are associated with increased cell death, FOXC1 appears to play a role in preventing cell death under both normal and oxidative stress conditions. Interestingly, relative to control siRNA-transfected cells with normal FOXC1 levels, FOXC1 knockdown did not result in more cell death under 'severe stress' conditions. These results are in contrast with the 'no H_2O_2', 'low dose', and 'high dose' conditions where FOXC1 knockdown results in increased cell death relative to control siRNA-transfected cells.

Two apoptotic markers, cleaved PARP-1 and cleaved caspase-7, were examined by immunoblot analysis to determine whether or not apoptosis is the mode of cell death that is occurring when FOXC1 is knocked down. Cleavage of PARP-1 is a hallmark of apoptosis and requires several caspases, including caspase-7, to become cleaved (Figure 5). In cells transfected with control siRNA and thus, with normal FOXC1 levels, there was an increase in both cleaved PARP-1 and cleaved caspase 7 protein levels as the intensity of the H_2O_2 treatment increased (Figures 5C,5D). When FOXC1 was knocked down, there was a significant increase in cleaved PARP-1 protein levels after exposure to both 'low dose' and 'high dose' oxidative stress conditions, suggesting that FOXC1 is anti-apoptotic. Similarly, cleaved caspase 7 protein levels significantly increased when FOXC1 was knocked in cells exposed to a 'high dose' and 'severe dose' of H_2O_2. Examination of these apoptotic markers thus suggest that FOXC1 plays a role in mediating the apoptotic cell death pathway.

HSPA6 is a target gene of the FOXC1 transcription factor

FOXC1 may mediate the apoptotic pathway by regulating downstream target genes that are involved in the stress response pathway. Berry *et al.* identified a number of potential FOXC1 target genes that are known to be involved in stress response, including HSP27 and HSPA6 (refer to Figure 1 of Appendix for results on HSP27) (80). In order to further examine the role of FOXC1 in mediating the stress response,

HSPA6, which is a member of the stress-responsive HSP70 family of proteins, was analyzed. Berry *et al.* identified HSPA6 as a potential target gene of FOXC1 by microarray analysis (80). Also, Berry *et al.* showed that in non-pigmented ciliary epithelial (NPCE) cells, overexpressing FOXC1 increased HSPA6 RNA levels, thus confirming HSPA6 as a target gene of FOXC1. In the present study, HSPA6 was further validated as a target gene of FOXC1 in HTM cells by Northern blot analysis. FOXC1 knockdown resulted in a significant decrease in HSPA6 RNA levels compared to control siRNA-transfected cells (p-value = 0.01, Student's t-test) (Figure 6A). Chromatin Immunoprecipitation (ChIP) assay was used to identify a FOXC1 binding site (BS1) located ~4800bp upstream of the HSPA6 transcription start site (Figure 6B; refer to Figure 2 of Appendix for expanded view of the upstream region of HSPA6). Another FOXC1 binding site (BS2), located less than 300bp downstream of FOXC1 BS1, did not bind FOXC1 when examined by ChIP analysis (Figure 6B). Finally, a 300bp region (BS3) located ~1300bp upstream of the transcription start site that includes two consensus FOX binding sites was examined. ChIP-PCR indicates FOXC1 is able to bind to the BS3 region (Figure 6B). To further validate HSPA6 as a downstream target of FOXC1, HSPA6 protein levels were examined in HTM cells with decreased FOXC1 levels. HSPA6 has been shown to have little or no basal protein expression and is only induced upon exposure to extreme conditions of stress (179,181-183). HSPA6 protein was not detected by immunoblot analysis under normal

untreated conditions (Figure 7A). In fact, neither single doses (500μM = 'low dose' or 1000μM = 'high dose') of H_2O_2 resulted in HSPA6 protein detection. However, HSPA6 protein was detected after two treatments of H_2O_2 (500μM followed by 1000μM = 'severe dose'). Thus, the two-step H_2O_2 treatment appears to result in a severe oxidative stress condition necessary to detect HSPA6 protein. In addition, HSPA6 protein levels increased 76% when FOXC1 was knocked down after exposure to the 'severe dose' ($p = 0.02$, Student's t-test) (Figure 7B). Taken together, these experiments confirm that HSPA6 is a direct target gene of the FOXC1 transcription factor.

HSPA6 is an anti-apoptotic protein under conditions of severe oxidative stress

Members of the HSP70 family of proteins typically have a protective role in cells. Cell death levels, as determined by trypan blue staining, did not change when FOXC1 was knocked down in HTM cells exposed to a 'severe dose' of H_2O_2 (Figure 4B). The highest levels of HSPA6 protein was observed under the same conditions (Figure 7B). To further examine the role of HSPA6, HSPA6 was knocked down in HTM cells by transfection with siRNA against HSPA6 (Figure 8A). After exposure to a 'severe dose' of H_2O_2, there were significantly more trypan blue positive cells in HSPA6 siRNA-transfected cells (64.7%) compared to control siRNA-transfected cells (58.7%) (p-value = 0.0027, Student's t-test) (Figure 8B). The increase in cell death when HSPA6 is knocked down thus

suggests that the HSPA6 protein may play a role in protecting cells and/or preventing cell death under severe oxidative stress conditions.

Examination of cleaved PARP-1 protein levels by immunoblotting indicated that there was significantly more of this apoptotic marker when HSPA6 was knocked down in cells exposed to the 'severe dose' of H_2O_2 (Figure 8C). However, there was a significant decrease in cleaved caspase-7 protein levels when HSPA6 was knocked down (Figure 8D). To examine this phenomenon further, HTM cells were heat shocked at 44°C for 2h as an alternative severe stress. After a 44°C heat shock treatment, HSPA6 protein was detected (Figure 8A). Similar to the oxidative stress treatment, heat shock treatment increased cleaved PARP-1 protein levels but not cleaved caspase-7 protein levels when HSPA6 was knocked down (Figure 8E). In these experiments, the cleavage of PARP-1 does not seem to require the activity of caspase-7. These results suggest that HSPA6 is an anti-apoptotic protein when present under severe stress conditions.

To further examine the potentially protective role of HSPA6, HSPA6 was overexpressed in HTM cells. Compared to empty vector-transfected cells, overexpression of HSPA6 resulted in a statistically significant 7.2% increase in cell viability after HTM cells were exposed to a 'high dose' of H_2O_2 (p-value = 0.0028, Student's t-test) (Figure 9A). HSPA6 overexpression did not alter cell viability after HTM cells were exposed to the 'low dose' and 'severe dose' of H_2O_2. Interestingly, immunoblot analysis indicated that HSPA6 protein levels were lower in cells treated

with ‘low dose’ and ‘severe dose’ treatments of H_2O_2 compared to cells that were untreated or treated with the ‘high dose’ of H_2O_2 (Figure 9B). These results suggest that when HSPA6 is present under stress conditions, HSPA6 may have a protective function.

FOXC1 mutants decrease viability of cells

Disease-causing FOXC1 mutations have previously been shown to alter the molecular characteristics of the protein including the ability of the mutant FOXC1 protein to localize to the nucleus, bind DNA, and/or transactivate a reporter gene (150,151,153,165,177). Thus, FOXC1 mutations are thought to alter the ability of the FOXC1 transcription factor to regulate expression of other genes including stress-responsive genes such as HSPA6. However, the consequence of specific FOXC1 mutations on cell viability has not been examined. In this study, cell viability was quantified in oxidatively stressed HTM cells overexpressing three FOXC1 mutants: L130F, W152G, and S131L (Table 4). Overexpressing wild type FOXC1 in HTM cells resulted in a significant 10.5% increase in cell viability compared to the empty vector-transfected cells when both types of transfected cells were treated with a ‘high dose’ of H_2O_2 (p-value = 0.003, Student’s t-test) (Figure 10A). There was no difference in cell viability when FOXC1 was overexpressed in HTM cells when cells were untreated, or exposed to a ‘low dose’ or ‘severe dose’ of H_2O_2. In the absence of oxidative stress, cells overexpressing the L130F, W152G, or S131L FOXC1 mutation had significantly decreased cell viability compared to

cells overexpressing wild type FOXC1 ($p < 0.01$ for all three mutations, Student's t-test) (Figure 10B). In addition, relative to wild type FOXC1-transfected cells, there was increased cell death in HTM cells overexpressing the three FOXC1 mutants after treatment with either the 'low dose' or 'high dose' of H_2O_2 ($p < 0.01$ for all three mutations, Student's t-test). However, the number of viable cells under 'severe dose' conditions were not significantly different between wild type FOXC1 and all three FOXC1 mutants examined. Finally, immunoblot analysis showed a decrease in both wild type and mutant exogenous FOXC1 protein levels after HTM cells were exposed to H_2O_2 (Figure 10C). Thus, the stress-responsive nature of the wild type FOXC1 transcription factor, in which FOXC1 levels are decreased in response to oxidative stress, was not altered by the three examined FOXC1 mutants.

Discussion

FOXC1 is a stress-responsive transcription factor

FOXC1 appears to be a stress-responsive transcription factor. Under H_2O_2-induced oxidative stress conditions, endogenous FOXC1 protein and RNA levels are significantly decreased (Figure 2). The decrease in FOXC1 levels in response to oxidative stress appears to be regulated at the transcript level. The decrease in FOXC1 mRNA levels in

response to oxidative stress may be caused by changes in transcription levels or alternatively, due to a decrease in mRNA.

My experiments showed that not only do endogenous FOXC1 protein levels decrease in response to oxidative stress, but the levels of exogenous FOXC1 proteins also decrease as well (Figure 3b and 9C). Thus, oxidative stress could also affect the stability of FOXC1 protein. External stimuli including oxidative stress have been shown to affect the localization of another FOX protein, FOXO, through post-translational modifications (PTMs). PTMs of FOX proteins play key roles in determining factors such as subcellular localization, DNA binding ability, and protein levels. In the case of FOXO transcription factors, various PTMs have been proposed to create a “FOXO code” that specifies the subsequent activity of the FOXO protein (184). Although oxidative stress does not alter nuclear localization of exogenous FOXC1 protein (data not shown), other factors such as protein stability could be affected through PTMs. Phosphorylation of the FOXC1 serine 272 residue has been suggested to promote FOXC1 protein stability by preventing the recruitment of degradation factors or promoting the recruitment of stabilization factors (82). *Thus, my experiments show that oxidative stress decreases FOXC1 at the transcript and protein levels, which I hypothesize will result in downregulation of downstream target genes (Figure 2B).*

FOXC1, apoptosis, and cell death

Results from the present study are in agreement with previously published research indicating that FOXC1 is anti-apoptotic (80,185). FOXC1 expression in adult eyes, specifically within TM cells, may be necessary for maintaining homeostasis since knocking down FOXC1 increased cell death even in the absence of H_2O_2 treatment (Figure 4B). Also, exposing HTM cells to low and high oxidative stress conditions resulted in elevated levels of cleaved caspase-7 and cleaved PARP-1 protein suggesting that a decrease in FOXC1 activates the apoptotic pathway (Figures 4C and 4D). Thus, the elevated levels of cell death observed in FOXC1 knockdown cells stained with trypan blue is likely due to apoptotic cell death as opposed to other modes of cell death such as necrosis.

Morphologically, apoptosis is characterized by cell shrinkage, condensation and fragmentation of chromatin, plasma membrane blebbing, and disintegration of the cell into apoptotic bodies (186). Phagocytes are thought to engulf the apoptotic bodies *in vivo*. Regulated physiological apoptosis is essential for maintaining homeostasis and tissue survival in multicellular organisms. The caspase family of cysteine proteases become activated by death stimuli and co-ordinates the apoptotic pathway that will ultimately result in the removal of the cell from its environment (Figure 5). The initiator caspases (ex. caspase-8, caspase-9, caspase-10) function upstream of the effector caspases (ex.

caspase-3, caspase-6, caspase-7). The initiator caspases respond to various death stimuli to activate the effector caspases that are responsible for proteolytic cleavage of specific substrates including PARP-1 (Figure 5). The cleavage of PARP-1 is a hallmark of caspase-dependent apoptosis (187,188). Under normal conditions, PARP-1 functions in DNA damage repair. In response to death stimuli, activated cleaved effector caspases cleave the 113 kDa PARP-1 protein, which results in the generation of a 89 kDa fragment and a 24 kDa fragment. The 89 kDa fragment is no longer able to bind to and repair damaged DNA (187). The 24 kDa fragment irreversibly binds to DNA strand breaks to inhibit DNA repair enzymes including uncleaved PARP-1. In the presence of severely damaged DNA, PARP-1 activity is elevated. PARP-1 undergoes auto-modification by forming poly(ADP-ribose) polymers which requires NAD^+ (189). Since synthesis of NAD^+ requires ATP, prolonged overactivation of PARP-1 depletes intracellular ATP levels. Depletion of ATP levels induces an alternate mode of cell death, necrosis. Morphologically, necrosis is characterized by an increase in cell volume resulting in the rupture of the plasma membrane (186). The subsequent unregulated leakage of the intracellular content is suggested to be detrimental to the overall health of the tissue. Thus, cleavage of PARP-1 to generate the 24 kDa fragment serves as an essential regulatory mechanism to ensure that cells will undergo cell death via the apoptotic pathway. In fact, inhibition of

caspases which prevent PARP-1 from being cleaved induces a switch from apoptosis to necrosis (190,191).

There is a decrease in the number of TM cells with age and in the glaucoma phenotype (50-52). Whether cell death occurs by apoptosis or necrosis is currently unknown. Nevertheless, the loss of TM cells is predicted to impair TM tissue function that in turn compromises the regulation of aqueous humor. *My experiments show that FOXC1 is an anti-apoptotic protein and thus, decreasing FOXC1 levels result in increased cell death under oxidative stress conditions. Fluctuations in FOXC1 levels in response to oxidative stress may thus be a contributing factor to TM cell death in both individuals with and without FOXC1 mutations.*

FOXC1 mediates stress response pathway through regulation of HSPA6

Depending on the severity of oxidative stress, FOXC1 may have a different effect on HTM cells. Decreased levels of FOXC1 protein resulted in decreased cell viability under normal, low dose, and high dose oxidative stress conditions. However, under severe oxidative stress conditions, knocking down FOXC1 did not alter cell viability (Figure 4B). Thus, FOXC1 may regulate a different set of genes depending on the presence and/or severity of stress. My experiments show that the FOXC1 transcription factor mediates the stress response by regulating HSPA6, a HSP70

protein that appears to function only after exposure of cells to severe stress. In agreement with preliminary data from a previous study (80), results from the present study indicate that HSPA6 is a downstream target of FOXC1. Under normal non-stress conditions, FOXC1 overexpression results in increased HSPA6 RNA levels while FOXC1 knockdown results in decreased HSPA6 RNA levels (80) (Figure 6A). ChIP analysis identified FOXC1 binding sites in the upstream region of the HSPA6 gene (Figure 6B) suggesting that FOXC1 is able to directly bind to this site and promote HSPA6 transcription. Under normal non-stress conditions, HSPA6 RNA is present but does not appear to be translated into protein (Figure 7A). It is possible that FOXC1 is necessary to maintain HSPA6 RNA so that RNA can be quickly translated into protein in response to severe stress. A quick response to stress is often essential in minimizing the potential damage that can be caused to a cell.

Under normal non-stress conditions in which no HSPA6 protein is detected, knocking down FOXC1 results in decreased HSPA6 RNA levels. In contrast, under severe oxidative stress conditions, FOXC1 knockdown results in an increase in HSPA6 protein levels (Figure 7B). Under severe stress conditions, the regulation of HSPA6 protein by FOXC1 could be masked by alternative regulatory factors. Heat shock proteins have heat shock elements (HSEs) that bind heat shock transcription factors (HSFs) (192). HSFs are principal regulators of the heat shock response, but are also activated in response to a variety of stresses other than heat shock

including oxidative stress, proteasomal stress, and chemical agents. HSPA6 has a HSE which binds HSF1 (183). Upon exposure to stress, HSF1 is activated and results in the induction of HSPA6 transcription (183). Thus, HSF1 activation may mask the effects of FOXC1 on HSPA6. Also, the decrease in FOXC1 levels in response to severe oxidative stress may be sensed by the cell as an additional source of stress, resulting in further activation of HSFs. Alternatively, FOXC1 binding could directly result in increased HSPA6 protein after exposure to severe oxidative stress. The mechanism of this switch in regulation is unclear, but may involve the recruitment of co-factors, PTMs of FOXC1, and/or binding to alternate binding sites. *Thus, HSPA6 appears to be under complex regulation by FOXC1, which is highly dependent on the environmental stress conditions.*

HSPA6 has a protective role in HTM cells

In humans, the HSP70 family consists of at least 17 distinct genes that are translated into proteins (193). HSPA6 homologs have been identified only in a subset of mammals including *Saguinus oedipus*, *Sus scrofa*, *Bos taurus*, *Gorilla gorilla, Pongo abelii*, and *Homo sapiens*. No HSPA6 homologs have been identified in rodents or fish precluding further analysis in conventional model organisms. Thus, HTM cells are an appropriate model to use to examine HSPA6 function.

Even in the absence of stress, HSP70 proteins aid in folding of nascent and misfolded proteins. Environmental stresses cause proteotoxic

damage and thus, there is a higher need for the chaperoning activity of HSP70 proteins. However, under stress conditions, refolding of proteins may no longer be possible due to extensive proteotoxic damage. In these cases, HSP70s aid degradation of damaged proteins by preventing aggregation so that the damaged proteins can be transported to the proteolytic system (132).

Similar to other HSP70s, HSPA6 contains an N-terminal ATPase binding domain, a linker domain, and a C-terminal substrate binding domain (SBD) (194). HSP70 proteins bind and release client proteins from the SBD in a cycle dependent on ATPase activity. To date, no *bona fide* client/substrate protein has been identified for HSPA6. Thus, although *in vitro* studies suggest that HSPA6 may have chaperoning ability (195), whether HSPA6 functions as a molecular chaperone *in vivo* is currently unknown.

HSPA6 is strictly stress-inducible with little to no basal expression (179,181,182). HSPA6 is expressed only under severe stress conditions such as exposure to a lethal heat shock or treatment with a proteasomal inhibitor, MG132 (181,182). In the present study, we showed that HSPA6 protein is only detected after exposure of HTM cells to two consecutive treatments of H_2O_2 (='severe stress') (Figure 7A). Preconditioning with a non-lethal dose of stress including heat shock or H_2O_2, has been shown to result in increased tolerance to a subsequent lethal stress in other cells lines, a process often referred to as cytoprotection or thermotolerance in

the case of exposure to heat shock stress (179,180). HSPA6 has been shown to be necessary for human colon cells, HT-29 and CRL-1807, to acquire cytoprotection in response to heat shock (182). Knocking down HSPA6 in human colon cells exposed to thermal stress resulted in a decrease in the number of proliferative cells. However, under the experimental conditions in the present study, HTM cells did not acquire cytoprotection after preconditioning with a non-lethal dose of H_2O_2.

Despite the difference in the role of HSPA6 in acquiring cytoprotection in the previous study of human colon cells (182) and my study of ocular cells, HSPA6 appears to have a protective effect on both types of cells. Overexpressing HSPA6 had a protective effect on cells under 'high dose' oxidative stress conditions (Figure 9A). Exogenous HSPA6 may not have had any effect on cell viability in the other oxidative stress conditions because HSPA6 protein levels decreased with the low dose and severe dose H_2O_2 treatments (Figure 9B). The decrease in exogenous HSPA6 protein after cells were exposed to the 'severe dose' of H_2O_2 was unexpected because endogenous HSPA6 protein was only detected under 'severe stress' conditions (Figure 7A).

Exogenous HSPA6 did not have an effect on cell viability under normal conditions (Figure 9A) suggesting that other stress-induced factors may be required for HSPA6 protein to function as a molecular chaperone. HSP70 proteins typically do not function alone as chaperones. The HSP70 chaperone machinery requires many co-factors including J proteins. J

proteins, also known as HSP40s, bind and deliver client proteins to HSP70 and stimulate HSP70's ATPase activity (reviewed by Kampinga and Craig (132)). Recombinant HSPA6 has been shown to bind to various members of the J protein family (195). Chow *et al.* observed that HSPA6 was only able to interact with a J protein co-factor after human neuronal cells, SH-5Y5Y, were treated with celasterol, a reagent that induces expression of heat shock proteins (196). Thus, without induction of HSPA6 by stress or chemical reagent, J proteins appear to not be mobilized to participate in the HSP70 chaperone machinery.

In addition to HSP70 proteins' role as molecular chaperones, the HSP70 family of proteins also function as signalling molecules that interact with various components of the apoptotic pathway. First, HSP70 is suggested to prevent apoptosis by interacting with apoptotic protease activating factor 1 (Apaf-1) (197-200), preventing the formation of a functional apoptosome and thus, the activation of caspase-dependent apoptosis. Second, HSP70 is suggested to prevent caspase-independent apoptosis by interacting with apoptosis inducing factor (AIF) (201). Although the specific mechanism remains to be elucidated, HSP70 physically interacts with AIF upon the release of AIF from the mitochondria, and prevents apoptosis. Whether HSPA6 interacts with components of the apoptotic pathway such as Apaf-1 and AIF is not known. *Although the mechanism of action is currently unknown, my experiments show that HSPA6 has a protective role in HTM cells. Thus,*

dysregulation of HSPA6 by mutations in FOXC1, as occurs in ARS patients, is predicted to compromise the ability of TM cells to efficiently respond and adapt to a variety of environmental stresses.

Conclusion

Through multiple mechanisms, FOXC1 mutations are predicted to compromise the ability of TM cells to respond and adapt to stress. The TM cells of ARS patients with FOXC1 mutations may be more vulnerable to environmental stresses including mechanical and oxidative stresses. As a consequence, increased TM cell death may occur, resulting in the dysregulation of aqueous humor drainage, elevation of IOP, and development of glaucoma. TM cell death may occur earlier in ARS patients with FOXC1 mutations, accounting for and/or contributing to the earlier onset of glaucoma in this subset of ARS patients.

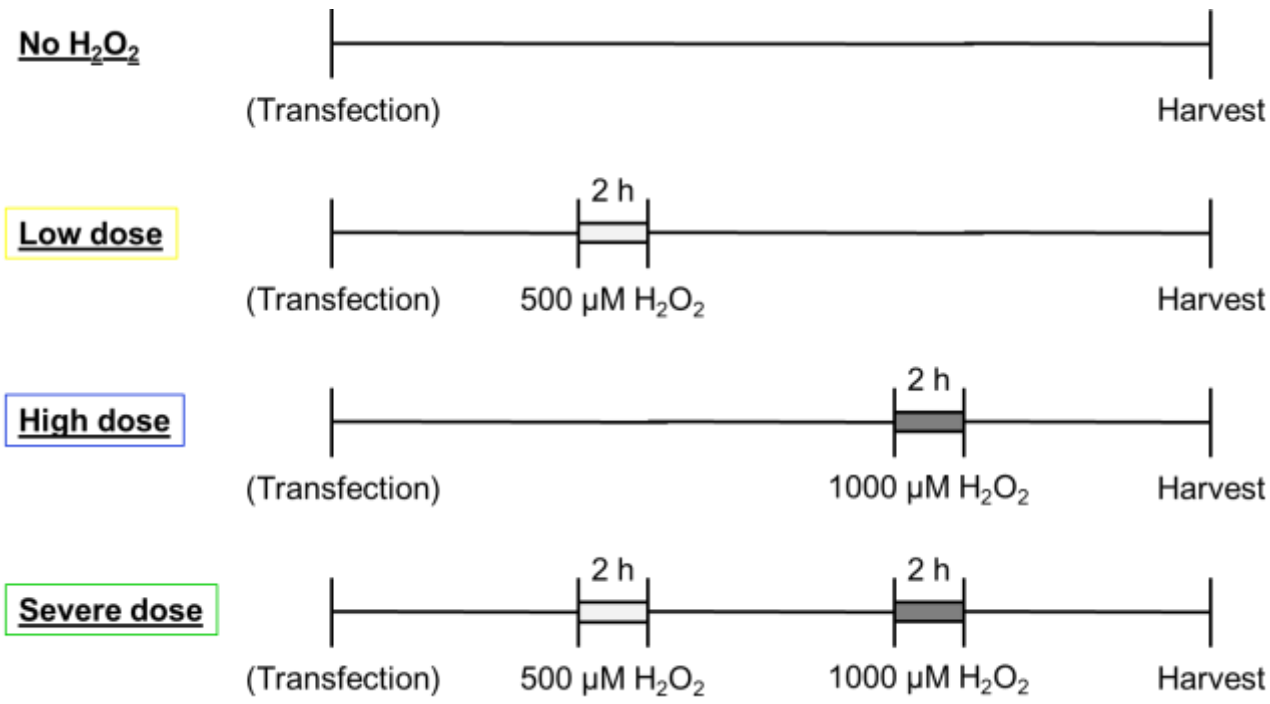
No H_2O_2
(Transfection)
Harvest
Low dose
2 h
(Transfection)
500 μM H_2O_2
Harvest
High dose
2 h
(Transfection)
1000 μM H_2O_2
Harvest
Severe dose
2 h
2 h
(Transfection)
500 μM H_2O_2
1000 μM H_2O_2
Harvest

Figure 1: Outline of two-step hydrogen peroxide (H_2O_2) treatment. For the 'severe dose' stress, HTM cells were treated with a lower dose 500μM H_2O_2 for 2h, then allowed to recover in fresh media for 22h. Subsequently, the HTM cells were treated with a higher dose 1000μM H_2O_2 for 2h. Cells were harvested for analysis after an additional recovery period of ~22h. For each experiment, there was a 'low dose' and 'high dose' control where the HTM cells were exposed to either 500μM or 1000μM H_2O_2 for 2h, respectively. These samples were exposed to H_2O_2 at the same time as the 'severe dose' samples. The 'no H_2O_2' samples were not exposed to H_2O_2.

A

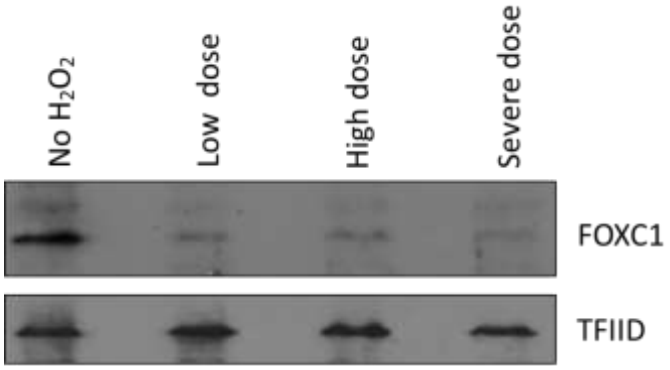
No H_2O_2
Low dose
High dose
Severe dose
FOXC1
TFIID

B

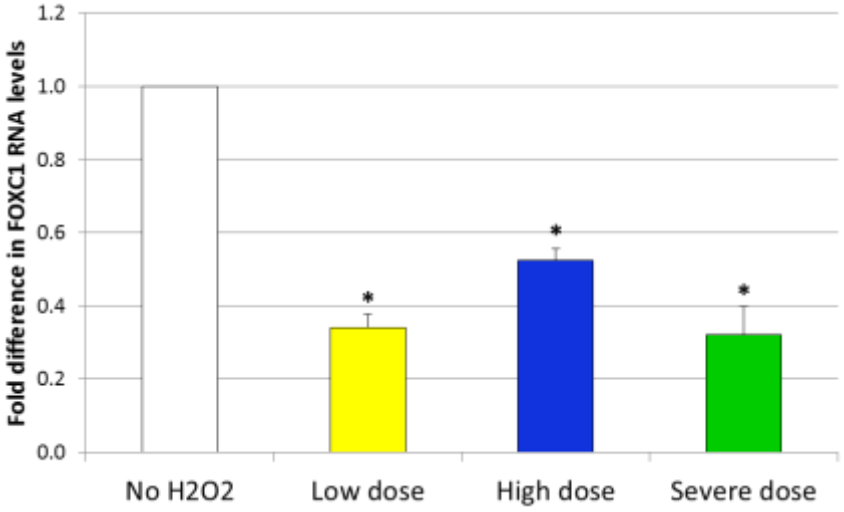
Fold difference in FOXC1 RNA levels
1.2
1.0
0.8
0.6
0.4
0.2
0.0
*
*
*
No H2O2
Low dose
High dose
Severe dose

Figure 2: H_2O_2-induced oxidative stress decreases endogenous FOXC1 levels. HTM cells were exposed to a low dose (500µM), high dose (1000µM), or severe dose (500µM followed by 1000µM) of H_2O_2. A) Nuclear extracts were resolved by 10% SDS-PAGE and immunoblotted using antibodies against endogenous FOXC1 and TFIID. B) Total RNA was extracted and FOXC1 and HPRT1 RNA levels were quantified by qPCR. FOXC1 RNA levels were normalized to HPRT1 RNA levels. The (*) indicates a p-value<0.01 (Student's t-test) relative to 'no H_2O_2' samples.

A

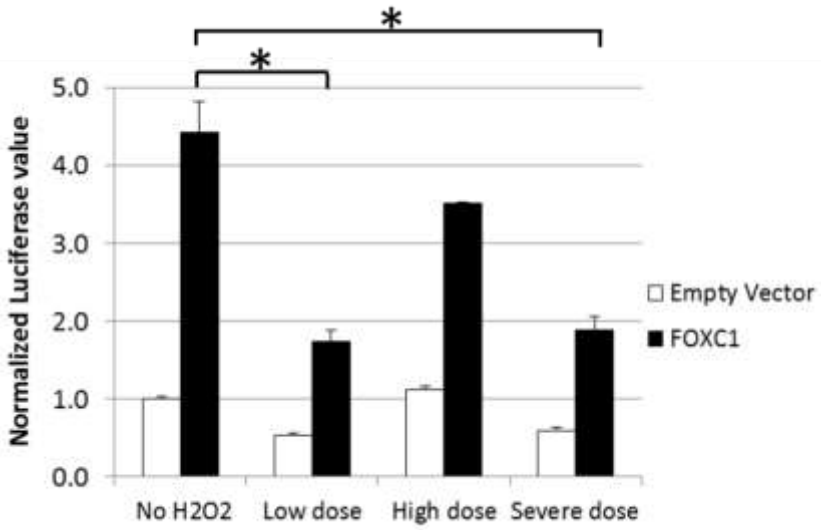
*
*
5.0
4.0
3.0
2.0
1.0
0.0
Normalized Luciferase value
Empty Vector
FOXC1
No H2O2
Low dose
High dose
Severe dose

B

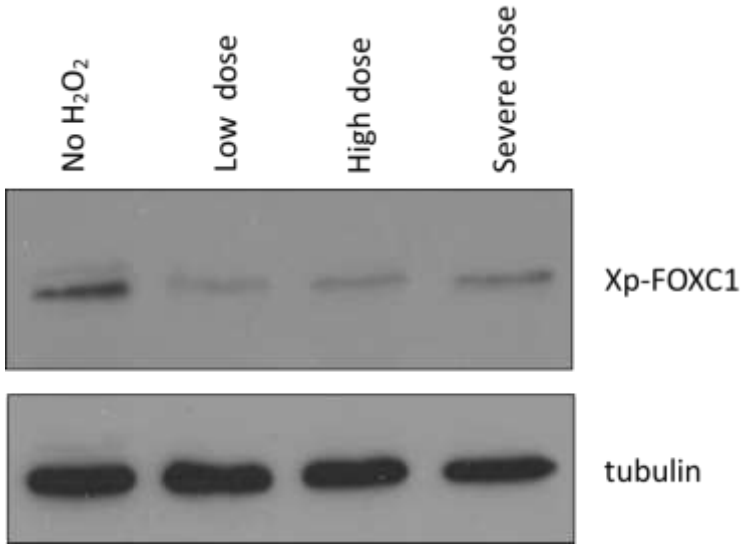
No H_2O_2
Low dose
High dose
Severe dose
Xp-FOXC1
tubulin

Figure 3: H_2O_2-induced oxidative stress decreases ability of FOXC1 to transactivate a luciferase reporter gene. FOXC1 was overexpressed in HeLa cells to examine its ability to transactivate a luciferase reporter gene with a synthetic FOXC1 binding site located upstream of the TK promoter. Transfected HeLa cells were exposed to a low dose (500µM), high dose (1000µM), or severe dose (500µM followed by 1000µM) of H_2O_2. A) FOXC1 was able to transactivate the luciferase reporter gene under 'no H_2O_2' conditions. The transactivation ability of FOXC1 significantly decreased (*) in cells treated with a 'low dose' and 'severe dose' of H_2O_2. B) Immunoblot analysis showed that exogenous FOXC1 protein levels decreased when cells were treated with H_2O_2. Lysates were resolved by 10% SDS-PAGE and immunoblotted using Xpress and tubulin antibodies.

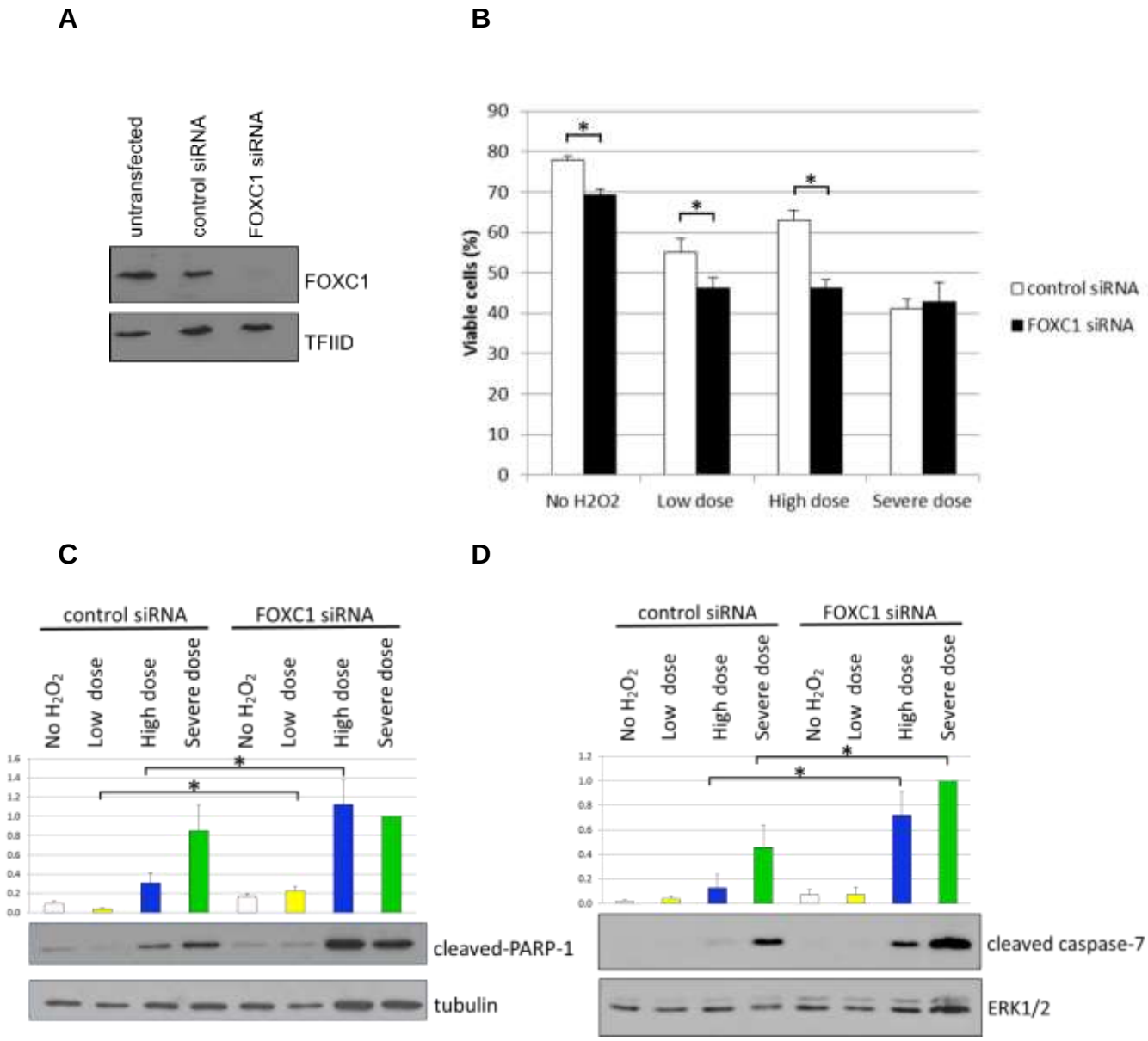
A
untransfected
control siRNA
FOXC1 siRNA
FOXC1
TFIID
B
Viable cells (%)
90
80
70
60
50
40
30
20
10
0
No H2O2
Low dose
High dose
Severe dose
control siRNA
FOXC1 siRNA
C
control siRNA
FOXC1 siRNA
No H2O2
Low dose
High dose
Severe dose
cleaved-PARP-1
tubulin
D
control siRNA
FOXC1 siRNA
No H2O2
Low dose
High dose
Severe dose
cleaved caspase-7
ERK1/2

Figure 4: Knocking down FOXC1 increases apoptotic cell death after exposure of HTM cells to 'low dose' and 'high dose' H_2O_2-induced oxidative stress. A) FOXC1 was knocked down in HTM cells using siRNA. For B) to D), HTM cells were exposed to a low dose (500µM), high dose (1000µM), or severe dose (500µM followed by 1000µM) of H_2O_2. B) Cell viability was quantified by staining with trypan blue. Knocking down FOXC1 significantly decreased (*) cell viability in cells C) and D) Immunoblot analysis showed that (*) decreasing FOXC1 significantly increased the apoptotic markers cleaved PARP-1 and cleaved caspase-7 after cells were exposed to a 'low dose' and/or 'high dose' of H_2O_2.

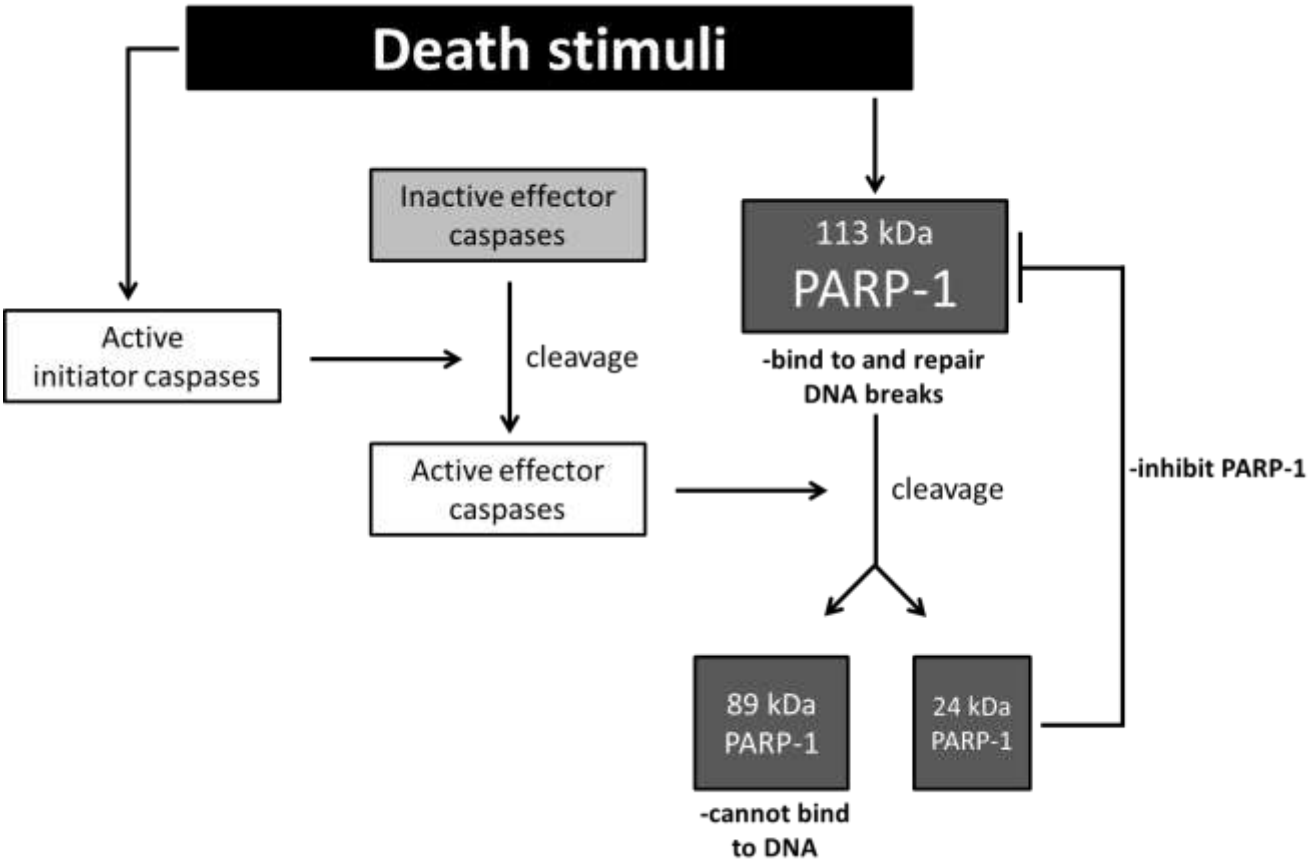
Death stimuli
Inactive effector caspases
113 kDa PARP-1
Active initiator caspases
cleavage
-bind to and repair DNA breaks
Active effector caspases
cleavage
-inhibit PARP-1
89 kDa PARP-1
24 kDa PARP-1
-cannot bind to DNA

Figure 5: Caspase-dependent apoptotic pathway. Death stimuli will result in the activation of initiator caspases, which will then result in cleavage and activation of effector caspases such as caspase-3 and caspase-7. The activated effector caspases will then cleave and activate the nuclear protein, PARP-1. Cleavage of PARP-1 into the 89 kDa and 24 kDa fragments is one hallmark characteristic of caspase-dependent apoptosis. The full length 113 kDa PARP-1 is able to bind to and repair DNA breaks in response to death stimuli. However, overactivation of full length PARP-1 is detrimental to the cell as a switch from apoptotic to necrotic cell death occurs. Cleavage of PARP-1 acts as a regulatory mechanism since the 24 kDa fragments is able to bind and inhibit full length PARP-1.

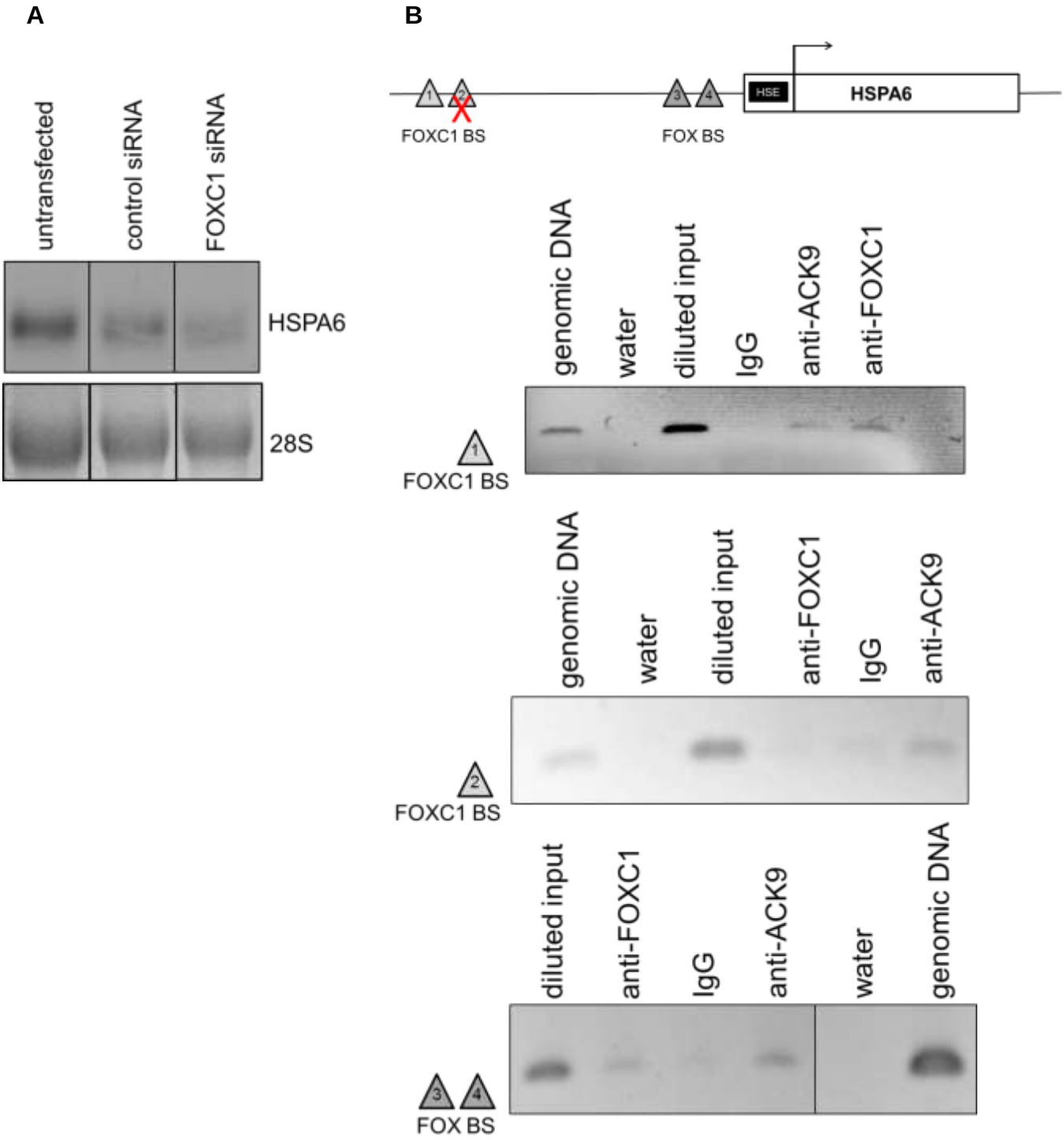
A
untransfected
control siRNA
FOXC1 siRNA
HSPA6
28S
B
HSE
HSPA6
FOXC1 BS
FOX BS
genomic DNA
water
diluted input
IgG
anti-ACK9
anti-FOXC1
FOXC1 BS
genomic DNA
water
diluted input
anti-FOXC1
IgG
anti-ACK9
FOXC1 BS
diluted input
anti-FOXC1
IgG
anti-ACK9
water
genomic DNA
FOX BS

Figure 6: HSPA6 is a direct target gene of FOXC1 in HTM cells. A) HTM cells were transfected with FOXC1 siRNA or control siRNA. After transfection, RNA was harvested and subjected to northern blot analysis. A HSPA6 probe was radiolabeled and hybridized to the blot. Relative to control siRNA, HSPA6 RNA levels significantly decreased when FOXC1 was knocked down ($p=0.01$, $n=4$, Student's t-test). B) Chromatin Immunoprecipitation (ChIP) assay identified BS1, located ~4800bp upstream of the HSPA6 transcription start site, as a *bona fide* FOXC1 binding site. The BS3 region containing two FOX consensus binding sites located ~1300bp upstream of the HSPA6 transcription site was also able to bind FOXC1. HTM cells were crosslinked and immunoprecipitated against FOXC1. Acetylated histone 3 at lysine 9 (Ack9) and IgG were used as positive and negative controls for the ChIP technique, respectively. The immunoprecipitated DNA was amplified by PCR using primers flanking the potential FOXC1 binding site, identified by Possum software. Genomic DNA and water are positive and negative controls, respectively, for the PCR. Primer flanking BS2 did not amplify a product in ChIP products incubated with FOXC1 antibody and thus, BS2 does not bind to FOXC1.

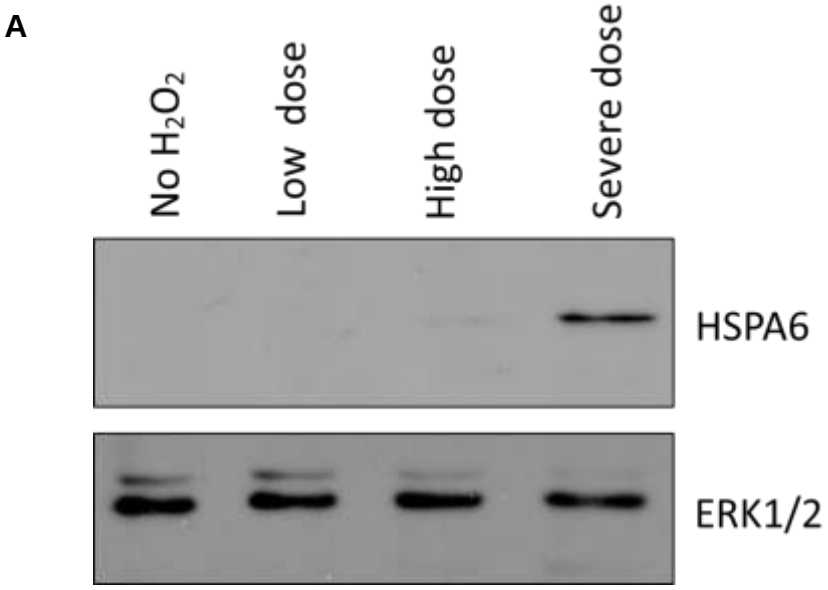
A
No H_2O_2
Low dose
High dose
Severe dose
HSPA6
ERK1/2

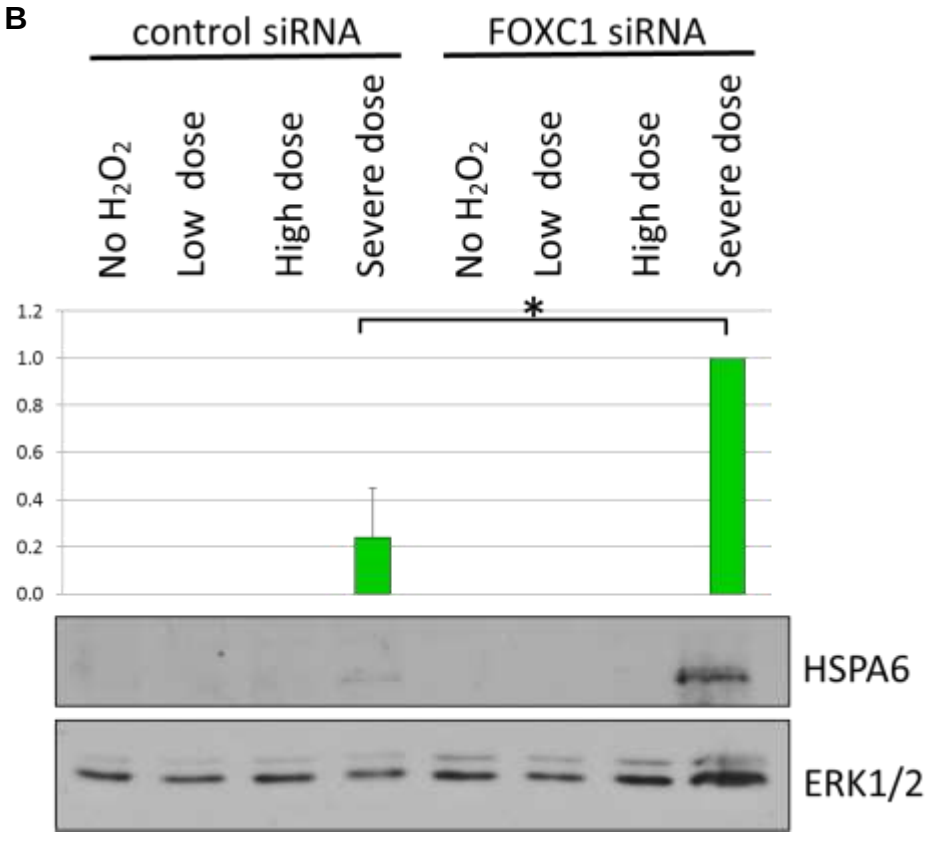
B
control siRNA
FOXC1 siRNA
No H_2O_2
Low dose
High dose
Severe dose
No H_2O_2
Low dose
High dose
Severe dose
*
1.2
1.0
0.8
0.6
0.4
0.2
0.0
HSPA6
ERK1/2

Figure 7: HSPA6 protein is present only after a severe dose of H_2O_2. HTM cells were exposed to a low dose (500µM), high dose (1000µM), or severe dose (500µM followed by 1000µM) of H_2O_2. Protein lysates were resolved on a 10% SDS-PAGE and immunoblotted using antibodies against HSPA6 or ERK1/2. A) Immunoblot analysis shows the presence of HSPA6 protein only in HTM cells exposed to a severe dose of H_2O_2. B) Knocking down FOXC1 in severely oxidatively-stressed cells resulted in a significant increase (*) in HSPA6 protein (p=0.02. Student's t-test).

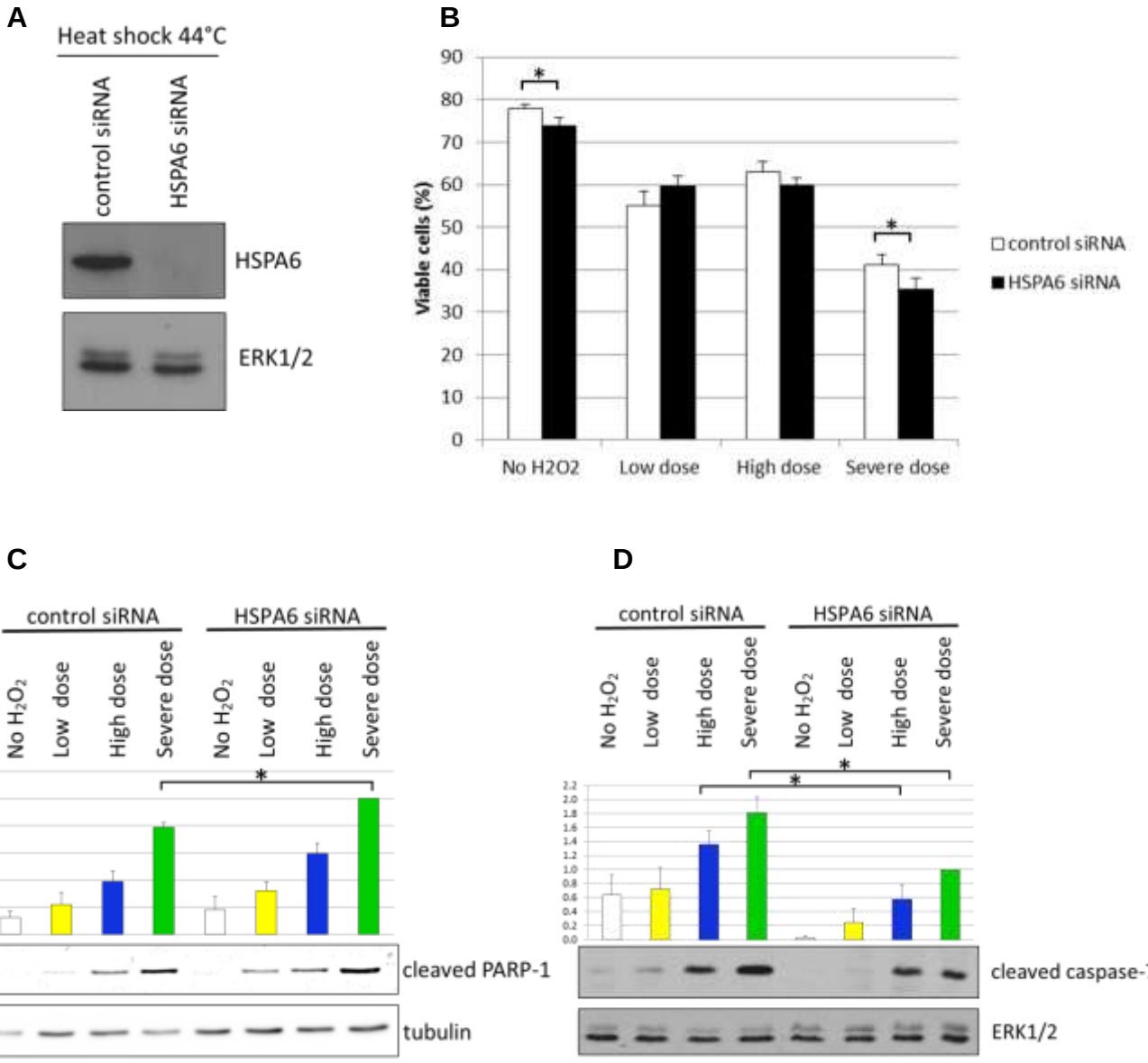
A
Heat shock 44°C
control siRNA
HSPA6 siRNA
HSPA6
ERK1/2
B
Viable cells (%)
90
80
70
60
50
40
30
20
10
0
No H2O2
Low dose
High dose
Severe dose
control siRNA
HSPA6 siRNA
C
control siRNA
HSPA6 siRNA
No H2O2
Low dose
High dose
Severe dose
cleaved PARP-1
tubulin
D
control siRNA
HSPA6 siRNA
No H2O2
Low dose
High dose
Severe dose
cleaved caspase-7
ERK1/2
E
control siRNA
HSPA6 siRNA
37°C
44°C
37°C
44°C
cleaved PARP-1
cleaved caspase-7
tubulin

Figure 8: Knocking down HSPA6 increases apoptotic cell death after exposure of HTM cells to 'severe' H_2O_2-induced oxidative stress. A) HSPA6 was knocked down in HTM cells using siRNA. For B) to D), HTM cells were exposed to a low dose (500µM), high dose (1000µM), or severe dose (500µM followed by 1000µM) of H_2O_2. B) Cell viability was quantified by staining with trypan blue. HSPA6 knockdown resulted in a significant decrease (*) in cell viability in cells exposed to a 'severe dose' of H_2O_2. C) and D) Immunoblot analysis showed that decreasing HSPA6 significantly increased (*) the apoptotic markers cleaved PARP-1 and cleaved caspase-7 after cells were exposed to a 'severe dose' of H_2O_2. E) Approximately 48h post-transfection, HTM cells were heat shocked at 44°C for 2h. After a recovery period of ~22h, the cells were harvested and analyzed by immunoblot.

A

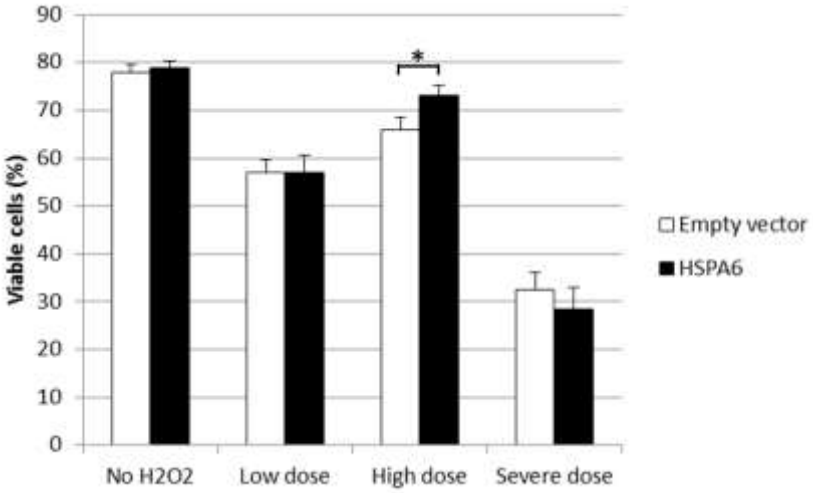
90
80
70
60
50
40
30
20
10
0
Viable cells (%)
*
No H2O2
Low dose
High dose
Severe dose
Empty vector
HSPA6

B

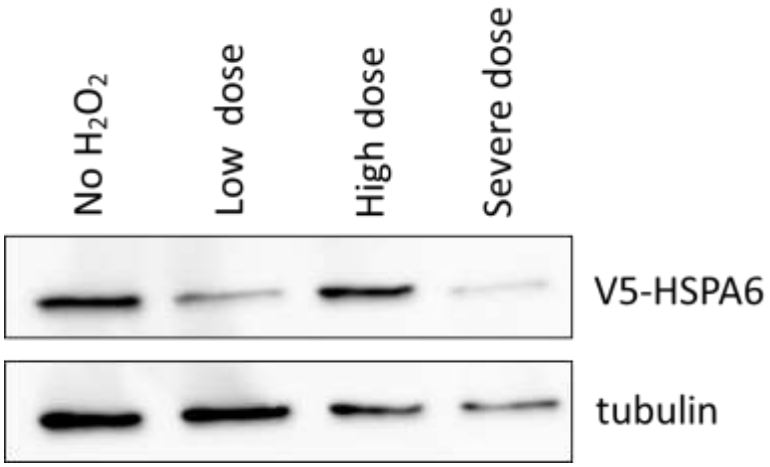
No H_2O_2
Low dose
High dose
Severe dose
V5-HSPA6
tubulin

Figure 9: HSPA6 overexpression increases cell viability after exposure of HTM cells to 'high dose' H_2O_2-induced oxidative stress. HTM cells were exposed to a low dose (500µM), high dose (1000µM), or severe dose (500µM followed by 1000µM) of H_2O_2. A) Cell viability was quantified by staining with trypan blue. HSPA6 overexpression significantly increased (*) cell viability under 'high dose' conditions (p-value = 0.0028, Student's t-test). B) Immunoblot analysis showed that exogenous HSPA6 protein levels decreased when in cells treated with a 'low dose' and 'severe dose' of H_2O_2. Lysates were resolved by 10% SDS-PAGE and immunoblotted using V5 and tubulin antibodies.

A

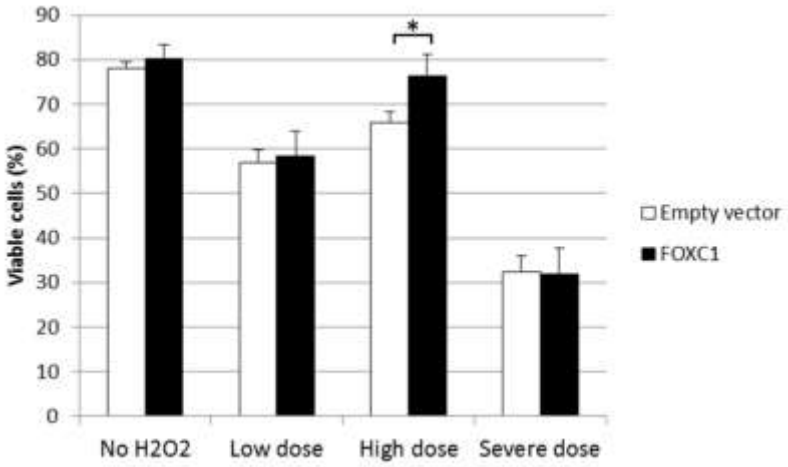
Viable cells (%)
90
80
70
60
50
40
30
20
10
0
No H2O2
Low dose
High dose
Severe dose
*
Empty vector
FOXC1

B

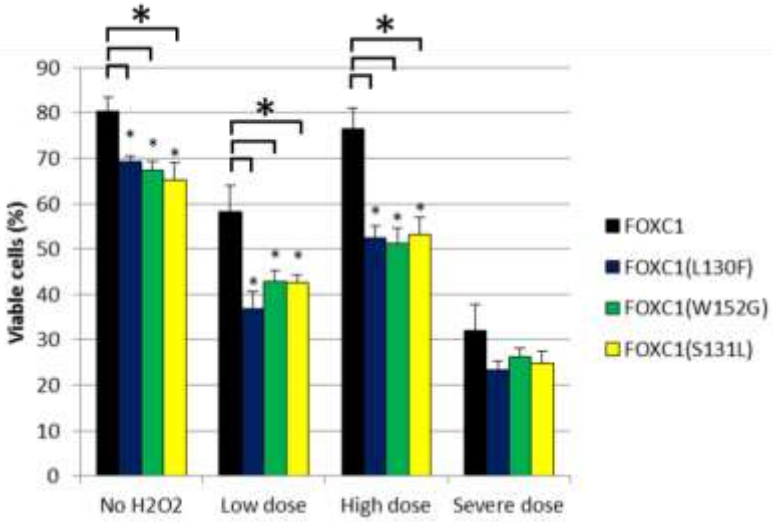
Viable cells (%)
90
80
70
60
50
40
30
20
10
0
No H2O2
Low dose
High dose
Severe dose
*
FOXC1
FOXC1(L130F)
FOXC1(W152G)
FOXC1(S131L)

C

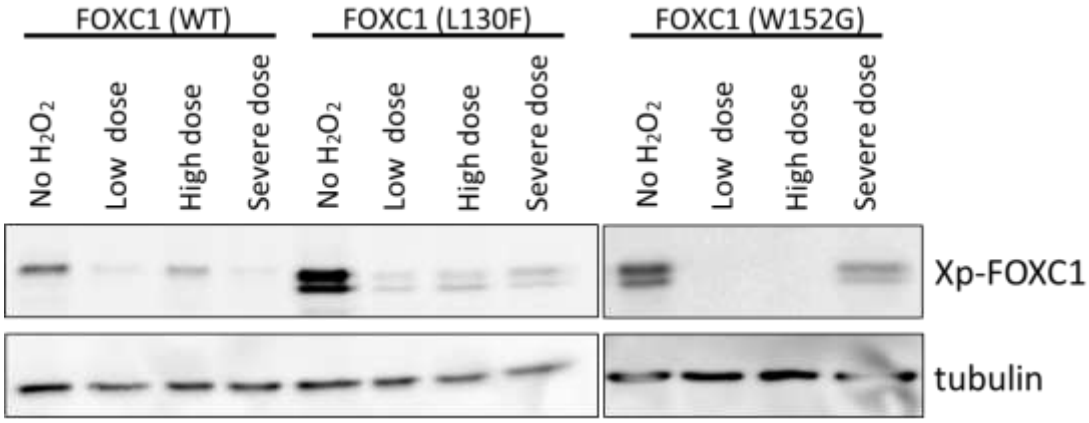
FOXC1 (WT)
FOXC1 (L130F)
FOXC1 (W152G)
No H2O2
Low dose
High dose
Severe dose
Xp-FOXC1
tubulin

Figure 10: Overexpression of wild type and mutant FOXC1s has differential effects on cell viability. HTM cells were transfected with A) wild type FOXC1 or B) three mutant FOXC1s; L130F, W152G, and S131L. Transfected HTM cells were subjected to a low dose (500µM), high dose (1000µM), or severe dose (500µM followed by 1000µM) of H_2O_2. Cell viability was quantified by staining with trypan blue. Wild type FOXC1 overexpression significantly increased (*) viability in cells exposed to a 'high dose' of H_2O_2 ($p < 0.01$, Student's t-test). Mutant FOXC1 overexpression significantly decreased (*) viability in cells under normal conditions or after exposure to either a 'low dose' or 'high dose' of H_2O_2 ($p < 0.01$, Student's t-test). C) Immunoblot analysis showed that FOXC1 protein levels decreased when HTM cells were exposed to H_2O_2-induced oxidative stress.

Table 1: siRNA information

siRNA	Target Sequence	Company
FOXC1	ACAAGAAGAUCACCCUGAA (FHD)	Thermo Scientific (Dharmacon)
HSPA6	GAGGAGAGGACUUCGACAA	Thermo Scientific (Dharmacon)

Table 2: Antibody information

Antibody	Dilution	Company
Anti-V5	1:5000	Sigma-Aldrich
Anti-Xpress	1:5000	Invitrogen
Cleaved Caspase-7 (Asp198)	1:1000	Cell Signaling Technology
FOXC1 (TA302875)	1:1000	ORIGENE
Acetyl-Histone H3 Lys9	N/A	Cell Signaling Technology
HSPA6	1:5000	Assay Designs
p44/42 MAP Kinase (ERK1/2)	1:5000	Cell Signaling Technology
Cleaved PARP (Asp214)	1:5000	Cell Signaling Technology
TFIID (TBP)	1:5000	Santa Cruz Biotechnology
Alpha-Tubulin (DM1A)	1:5000	Santa Cruz Biotechnology

Table 3: ChIP-PCR primer sequences

FOXC1 BS	Approximate distance from transcription start site	Forward primer sequence (5' to 3')	Reverse primer sequence (5' to 3')
BS1	4800bp	gtagggtgagtgcccctctt	gggaaaatagcagtgcagga
BS2	4500bp	ggacacagcatcactgtgc	agcgataaggaactgtgagc
BS 3	1300bp	tcaaggacagtttgattttcca	tggtgttacaatttagcagtgtgtt

Table 4: Molecular characteristics of the FOXC1 L130F, W152G, and S131L mutations

	L130F	W152G	S131L
Protein expression (Immunoblot analysis)	Yes; altered migration pattern	Yes; altered migration pattern	Yes
Localization (Immunofluorescence)	34% nuclear	10% nuclear	72% nuclear
DNA binding (EMSA)	No binding	No binding	No binding
Transactivity (Dual-Luciferase assay)	No transactivation	No transactivation	No transactivation
Aggresome (Immunofluorescence)	Yes	No	Not examined

References

(1) Berry FB, Skarie JM, Mirzayans F, Fortin Y, Hudson TJ, Raymond V, et al. FOXC1 is required for cell viability and resistance to oxidative stress in the eye through the transcriptional regulation of FOXO1A. Hum Mol Genet 2008 Feb 15;17(4):490-505.

(2) Wang WH, McNatt LG, Shepard AR, Jacobson N, Nishimura DY, Stone EM, et al. Optimal procedure for extracting RNA from human ocular tissues and expression profiling of the congenital glaucoma gene FOXC1 using quantitative RT-PCR. Mol Vis 2001 Apr 17;7:89-94.

(3) Ito YA, Footz TK, Murphy TC, Courtens W, Walter MA. Analyses of a novel L130F missense mutation in FOXC1. Arch Ophthalmol 2007 Jan;125(1):128-135.

(4) Ito YA, Footz TK, Berry FB, Mirzayans F, Yu M, Khan AO, et al. Severe molecular defects of a novel FOXC1 W152G mutation result in aniridia. Invest Ophthalmol Vis Sci 2009 Aug;50(8):3573-3579.

(5) Saleem RA, Banerjee-Basu S, Berry FB, Baxevanis AD, Walter MA. Analyses of the effects that disease-causing missense mutations have on the structure and function of the winged-helix protein FOXC1. Am J Hum Genet 2001 Mar;68(3):627-641.

(6) Schwechter BR, Millet LE, Levin LA. Histone deacetylase inhibition-mediated differentiation of RGC-5 cells and interaction with survival. Invest Ophthalmol Vis Sci 2007 Jun;48(6):2845-2857.

(7) Noonan E, Giardina C, Hightower L. Hsp70B' and Hsp72 form a complex in stressed human colon cells and each contributes to cytoprotection. Exp Cell Res 2008 Aug 1;314(13):2468-2476.

(8) Yu H, Liu Z, Zhou H, Dai W, Chen S, Shu Y, et al. JAK-STAT pathway modulates the roles of iNOS and COX-2 in the cytoprotection of early phase of hydrogen peroxide preconditioning against apoptosis induced by oxidative stress. Neurosci Lett 2012 Nov 7;529(2):166-171.

(9) Leung TK, Rajendran MY, Monfries C, Hall C, Lim L. The human heat-shock protein family. Expression of a novel heat-inducible HSP70 (HSP70B') and isolation of its cDNA and genomic DNA. Biochem J 1990 Apr 1;267(1):125-132.

(10) Noonan EJ, Fournier G, Hightower LE. Surface expression of Hsp70B' in response to proteasome inhibition in human colon cells. Cell Stress Chaperones 2008 Spring;13(1):105-110.

(11) Noonan EJ, Place RF, Rasoulpour RJ, Giardina C, Hightower LE. Cell number-dependent regulation of Hsp70B' expression: evidence of an extracellular regulator. J Cell Physiol 2007 Jan;210(1):201-211.

(12) Murphy TC, Saleem RA, Footz T, Ritch R, McGillivray B, Walter MA. The wing 2 region of the FOXC1 forkhead domain is necessary for normal DNA-binding and transactivation functions. Invest Ophthalmol Vis Sci 2004 Aug;45(8):2531-2538.

(13) Saleem RA, Murphy TC, Liebmann JM, Walter MA. Identification and analysis of a novel mutation in the FOXC1 forkhead domain. Invest Ophthalmol Vis Sci 2003 Nov;44(11):4608-4612.

(14) Calnan DR, Brunet A. The FoxO code. Oncogene 2008 Apr 7;27(16):2276-2288.

(15) Berry FB, Mirzayans F, Walter MA. Regulation of FOXC1 stability and transcriptional activity by an epidermal growth factor-activated mitogen-activated protein kinase signaling cascade. J Biol Chem 2006 Apr 14;281(15):10098-10104.

(16) Ray PS, Wang J, Qu Y, Sim MS, Shamonki J, Bagaria SP, et al. FOXC1 is a potential prognostic biomarker with functional significance in basal-like breast cancer. Cancer Res 2010 May 15;70(10):3870-3876.

(17) Kroemer G, Galluzzi L, Vandenabeele P, Abrams J, Alnemri ES, Baehrecke EH, et al. Classification of cell death: recommendations of the Nomenclature Committee on Cell Death 2009. Cell Death Differ 2009 Jan;16(1):3-11.

(18) Kaufmann SH, Desnoyers S, Ottaviano Y, Davidson NE, Poirier GG. Specific proteolytic cleavage of poly(ADP-ribose) polymerase: an early marker of chemotherapy-induced apoptosis. Cancer Res 1993 Sep 1;53(17):3976-3985.

(19) Tewari M, Quan LT, O'Rourke K, Desnoyers S, Zeng Z, Beidler DR, et al. Yama/CPP32 beta, a mammalian homolog of CED-3, is a CrmA-inhibitable protease that cleaves the death substrate poly(ADP-ribose) polymerase. Cell 1995 Jun 2;81(5):801-809.

(20) Lindahl T, Satoh MS, Poirier GG, Klungland A. Post-translational modification of poly(ADP-ribose) polymerase induced by DNA strand breaks. Trends Biochem Sci 1995 Oct;20(10):405-411.

(21) Herceg Z, Wang ZQ. Failure of poly(ADP-ribose) polymerase cleavage by caspases leads to induction of necrosis and enhanced apoptosis. Mol Cell Biol 1999 Jul;19(7):5124-5133.

(22) Lemaire C, Andreau K, Souvannavong V, Adam A. Inhibition of caspase activity induces a switch from apoptosis to necrosis. FEBS Lett 1998 Mar 27;425(2):266-270.

(23) Alvarado J, Murphy C, Polansky J, Juster R. Age-related changes in trabecular meshwork cellularity. Invest Ophthalmol Vis Sci 1981 Nov;21(5):714-727.

(24) Alvarado J, Murphy C, Juster R. Trabecular meshwork cellularity in primary open-angle glaucoma and nonglaucomatous normals. Ophthalmology 1984 Jun;91(6):564-579.

(25) Grierson I, Howes RC. Age-related depletion of the cell population in the human trabecular meshwork. Eye (Lond) 1987;1 (Pt 2)(Pt 2):204-210.

(26) Akerfelt M, Morimoto RI, Sistonen L. Heat shock factors: integrators of cell stress, development and lifespan. Nat Rev Mol Cell Biol 2010 Aug;11(8):545-555.

(27) Brocchieri L, Conway de Macario E, Macario AJ. hsp70 genes in the human genome: Conservation and differentiation patterns predict a wide array of overlapping and specialized functions. BMC Evol Biol 2008 Jan 23;8:19-2148-8-19.

(28) Kampinga HH, Craig EA. The HSP70 chaperone machinery: J proteins as drivers of functional specificity. Nat Rev Mol Cell Biol 2010 Aug;11(8):579-592.

(29) Wisniewska M, Karlberg T, Lehtio L, Johansson I, Kotenyova T, Moche M, et al. Crystal structures of the ATPase domains of four human Hsp70 isoforms: HSPA1L/Hsp70-hom, HSPA2/Hsp70-2, HSPA6/Hsp70B', and HSPA5/BiP/GRP78. PLoS One 2010 Jan 11;5(1):e8625.

(30) Hageman J, van Waarde MA, Zylicz A, Walerych D, Kampinga HH. The diverse members of the mammalian HSP70 machine show distinct chaperone-like activities. Biochem J 2011 Apr 1;435(1):127-142.

(31) Chow AM, Mok P, Xiao D, Khalouei S, Brown IR. Heteromeric complexes of heat shock protein 70 (HSP70) family members, including Hsp70B', in differentiated human neuronal cells. Cell Stress Chaperones 2010 Sep;15(5):545-553.

(32) Saleh A, Srinivasula SM, Balkir L, Robbins PD, Alnemri ES. Negative regulation of the Apaf-1 apoptosome by Hsp70. Nat Cell Biol 2000 Aug;2(8):476-483.

(33) Beere HM, Wolf BB, Cain K, Mosser DD, Mahboubi A, Kuwana T, et al. Heat-shock protein 70 inhibits apoptosis by preventing recruitment of procaspase-9 to the Apaf-1 apoptosome. Nat Cell Biol 2000 Aug;2(8):469-475.

(34) Beere HM, Green DR. Stress management - heat shock protein-70 and the regulation of apoptosis. Trends Cell Biol 2001 Jan;11(1):6-10.

(35) Kim HE, Jiang X, Du F, Wang X. PHAPI, CAS, and Hsp70 promote apoptosome formation by preventing Apaf-1 aggregation and enhancing nucleotide exchange on Apaf-1. Mol Cell 2008 Apr 25;30(2):239-247.

(36) Ravagnan L, Gurbuxani S, Susin SA, Maisse C, Daugas E, Zamzami N, et al. Heat-shock protein 70 antagonizes apoptosis-inducing factor. Nat Cell Biol 2001 Sep;3(9):839-843.

Chapter 5. General Conclusions and Future Direction

This chapter contains work published in:

Ito YA and Walter MA. Genetics and environmental stress factor contributions to anterior segment malformations and glaucoma. In: Rumelt, S, editor. Glaucoma – Basic and Clinical Aspects. InTech; (In Press) (1)

Axenfeld-Rieger Syndrome and glaucoma

Axenfeld-Rieger Syndrome (ARS) is part of the anterior segment dysgenesis spectrum of disorders. Mutations in FOXC1 are associated with ARS. Anterior segment dysgenesis patients are at an increased risk to secondarily develop glaucoma, a progressively blinding condition that results from the death of retinal ganglion cells (RGCs). Approximately 75% of ARS patients with FOXC1 mutations develop glaucoma (67). Glaucoma is an age-related disease as the risk of developing glaucoma significantly increases after age 40 (3,4). Patients with ARS typically have juvenile-onset or early adult-onset glaucoma.

Several factors are predicted to contribute to the earlier-onset glaucoma observed in ARS patients with FOXC1 mutations. First, expression of FOXC1 mutants during development could result in malformation of tissues in the anterior segment of the eye, including the trabecular meshwork (TM). The TM plays a critical role in ensuring proper aqueous humor drainage. Thus, structural maldevelopment of the TM could result in inadequate aqueous humor drainage from the eye, leading to increased IOP, which is a major risk factor for developing glaucoma. In addition to the role of FOXC1 during development, FOXC1 is predicted to function in maintaining homeostasis in the adult eye by mediating the stress response pathway through the regulation of stress-responsive genes (80) (also chapter 4). The TM cells of patients with FOXC1

mutations are thus predicted to have a compromised ability to respond and adapt to stress, which would disrupt the overall functioning of the TM.

Function of FOXC1 during development: proper development of anterior segment structures

Molecular analyses of the mutant FOXC1 proteins have indicated that FOXC1 mutations often result in severe disruptions to the normal abilities of the FOXC1 protein. In chapters 2 and 3, I assessed the molecular consequences of two FOXC1 mutations, L130F and W152G, identified in patients diagnosed with ARS. My results indicate that both mutant proteins have a severely reduced ability to localize to the nucleus, bind DNA, and transactivate a luciferase reporter gene. Mutant FOXC1 proteins are predicted to disrupt the proper regulation of downstream target genes that are essential for the normal development of anterior segment structures. Also, my results indicate that while the L130F mutant protein forms protective aggresomes, the W152G mutant protein just aggregates in the cytoplasm. Thus, the mutant proteins appear to be differently processed within the cell. The molecular disruptions caused by the L130F and W152G FOXC1 mutations are predicted to contribute to the malformation of anterior segment structures found in these patients. However, differences in the molecular characteristics of the mutant proteins, such as the formation of aggregates, may contribute to differences in the severity of the ocular phenotypes in these ARS patients.

Among the FOXC1 mutations previously analyzed, the L130F and W152G mutations cause two of the most severe disruptions to the FOXC1 protein function. Both the L130 and W152 residues are part of a hydrophobic pocket. Mutations that affect residues participating in the hydrophobic pocket appear to have *severe* molecular consequences. I87M is another example of a mutation that affects a residue that interacts in the hydrophobic core (150). No protein product is detected for the I87M, further suggesting that an intact hydrophobic pocket is essential for the normal functioning of the FOXC1 protein. The severe molecular consequences of the L130F and W152G could contribute to the severe congenital glaucoma phenotype observed in these patients. However, one of the patients with the L130F mutation has a mild form of ARS and no glaucoma. Thus, factors other than the FOXC1 mutation, such as environmental and stochastic factors, clearly contribute to the development of the ARS and glaucoma phenotypes.

Function of FOXC1 in adult eye: mediation of stress response

In addition to FOXC1's role during ocular development, the proper expression of FOXC1 is important for maintaining homeostasis in the adult eye. FOXC1 appears to have a protective role in the adult eye by mediating the stress response pathway. FOXC1 continues to be expressed in the adult eye including the TM (98). The TM is located in a highly dynamic environment and is constantly exposed to a variety of stresses including mechanical and oxidative stresses. Similar to other

cells, the cells of the TM have cellular defence mechanisms including the antioxidant system, proteolytic system, and regulation of stress-responsive genes that enable the cell to quickly and efficiently adapt and survive in a dynamic environment.

Under normal conditions, the FOXC1 transcription factor is predicted to regulate a network of genes that involve both survival genes and apoptotic genes. The balanced regulation of these target genes by FOXC1 is likely essential to achieve homeostasis within a system (Figure 1A). In this way, FOXC1 expression in adult ocular structures such as the TM may contribute to maintaining proper aqueous humor flow, which is important in maintaining an appropriate IOP. Interestingly, my results indicate that FOXC1 itself is a stress-responsive gene as exposure of HTM cells to H_2O_2-induced oxidative stress results in a decrease in FOXC1 RNA and protein levels (see chapter 4). When HTM cells are exposed to environmental stresses, the decrease in FOXC1 levels appears to result in initiation of a different signalling program (Figures 1B and 1C). A decrease in FOXC1 results in repression of anti-apoptotic genes, including FOXO1a, and could also induce pro-apoptotic genes that will result in apoptotic cell death. In the event that HTM cells are exposed to severe environmental stresses, the decrease in FOXC1 levels is predicted to mediate a distinct stress-response that involves the induction of the anti-apoptotic gene HSPA6 (Figures 1B and 1C). Under the experimental conditions of this study, I showed that induction of the anti-

apoptotic HSPA6 gene by H_2O_2 treatment did not decrease cell death under severe oxidative stress conditions, most likely because the H_2O_2-induced oxidatively stress completely overwhelmed the cellular defence mechanisms. Nevertheless, the anti-apoptotic nature makes HSPA6 an attractive therapeutic target for preventing TM cell death.

As discussed above, molecular characterization of FOXC1 mutants have shown that the overall consequences of FOXC1 mutations found in ARS patients, including L130F, W152G, and S131L, is decreased capacity to activate downstream target genes. In addition to downstream target genes that function during the development of anterior segment structures, FOXC1 mutations are also predicted to disrupt the regulation of downstream target genes that are involved in executing a rapid and effective stress response during and after development. Furthermore, the FOXC1 mutant protein itself could contribute to proteolytic stress. My results from cell viability experiments showed that even in the absence of stress, overexpression of mutant FOXC1 proteins resulted in a significant decrease in cell viability (see chapter 4). I have also shown that the L130F and W152G mutant proteins are phosphorylated differently compared to the wild type protein, most likely due to misfolding of the protein (see chapters 2 and 3). Misfolded protein would inevitably place additional strain on the proteolytic system even in the absence of environmental stresses. Thus, cells expressing mutant FOXC1 may be more sensitive to environmental stresses because of both dysregulation of stress-

responsive target genes such as HSPA6 and an overwhelmed proteolytic system (Figure 2).

Fluctuation of FOXC1 levels in the adult eye in response to stress may be part of the normal physiology of cells in the TM. However, I have shown that knocking down FOXC1 in HTM cells results in increased cell death most likely through dysregulation of genes involved in the apoptotic pathway. Exposure to chronic oxidative stress, as happens during the aging process, is predicted to result in cell death in part due to an accumulation of ROS and biomaterials combined with less efficient antioxidant and proteolytic systems. In these compromised cells, fluctuations in FOXC1 levels in response to stress may also contribute to the development of a glaucoma phenotype. In ARS patients with FOXC1 mutations, both the copy of FOXC1 from the unaffected allele and the affected allele are predicted to be reduced in response to stress. Thus, the copy of FOXC1 from the unaffected allele is unable to compensate for the mutant allele. I also predict that the stress-responsive nature of FOXC1 contributes to an increase in TM cell death in glaucomatous patients without a FOXC1 mutation. As aging progresses, the cells of the TM are exposed to chronic oxidative stress due to less efficient defence mechanisms that result in the accumulation of toxic biomaterials such as ROS. Thus, in an aging TM, a decrease in FOXC1 levels, which occurs in response to oxidative stress, could further compromise the ability of TM cells to adapt to the dynamic environment. Also, it is possible that

exposure of TM cells to chronic oxidative stress as aging progresses could have long-term effects on the levels of FOXC1, which would be predicted to result in chronic dysregulation of FOXC1 targets that normally act to promote cell survival in response to stress. Maintaining FOXC1 levels by inducing FOXC1 production or increasing FOXC1 protein stability could promote TM cell survival. However, since increased FOXC1 levels and/or overactivation of FOXC1 have also been associated with disease phenotypes (70-72,185), rapid return of FOXC1 protein levels to normal pre-stress levels is likely necessary for TM cell survival. A balance in FOXC1 activity is necessary for proper development of the eye to occur. Both loss-of-function FOXC1 mutations and segmental duplications of the 6p25 region (resulting in additional copies of FOXC1) results in anterior segment dysgenesis (70-72,74). In human basal-like breast cancer (BLBC), high levels of FOXC1 are correlated with poor prognosis due to a more aggressive phenotype such as increased cell proliferation, migration, and invasion (185). In BLBC cells, the elevated levels of FOXC1 activate the NF-κB transcription factor which may contribute to the aggressive phenotype of BLBC tumors (202). Whether FOXC1 regulates the pro-survival NF-κB transcription factor in HTM cells is not known. Nevertheless, these studies show that FOXC1 levels within a cell must be strictly regulated.

Future direction

The regulation of FOXC1 is complex and appears to occur at multiple levels, including the transcriptional and post-translational levels. In ocular cells, p32 and PITX2 have both been shown to physically interact with and repress FOXC1 (90,203,204). PAWR is another regulatory protein that physically interacts with the FOXC1 protein (90). PAWR appears to differentially regulate FOXC1 activity depending on the target gene. While PAWR interaction with FOXC1 increased the transactivity of a luciferase reporter gene with a FGF19 regulatory element, a decrease in transactivity was observed with a FOXO1A regulatory element. The MAPK kinases appear to also regulate FOXC1 activity by phosphorylating specific residues within the FOXC1 inhibitory domain, which promotes FOXC1 stability (82).

The decrease in FOXC1 levels in response to oxidative stress appears to be regulated at the transcript level. The transcription factors that are responsible for repressing FOXC1 transcription specifically in response to oxidative stress have yet to be identified. Knowledge of such regulators of FOXC1 would give insight into how TM cells are able to sense oxidative stress. Cells have stress sensors that are highly specialized for survival in a particular environment. Although the stress sensors specific to oxidative stress are largely unknown, several sensors that detect mechanical stress have been identified. For example, filamin A (FLNA) is a regulator of FOXC1 that is predicted to function as a

mechanostress sensor (166). FLNA inhibits FOXC1 activity in AT melanoma cells. Filamins are structural proteins that anchor actin filaments to transmembrane receptors. Filamins are thought to act as mediators between the extracellular and intracellular environment. Through filamins, signals may be propagated from the extracellular environment where the mechanical stress occurs to the nucleus where the expression of genes such as FOXC1 can be altered (166). Although the role of FLNA regulation of FOXC1 in ocular cells needs to be further examined, identification of regulators of FOXC1 has provided valuable insight into how the extracellular environment can influence FOXC1 activity. This may prove to be especially valuable for identifying oxidative stress sensors since how cells initially sense oxidative stress remains largely unknown (48,205). Also, the duration of time required for FOXC1 levels to recover to pre-stress levels is currently not known. Thus, identifying FOXC1 regulators under stress conditions would give insight into not only the mechanism underlying the initial decrease in FOXC1 in response to stress, but also, the mechanism underlying the subsequent (and presumed) recovery of FOXC1 levels.

Depending on the type and/or magnitude of the stress, different transcription complexes may assemble at the FOXC1 promoter to alter FOXC1 mRNA levels (206,207). Thus, both the assembly of cofactors at the FOXC1 promoter and interaction of FOXC1 with cofactors at a target promoter could be dependent on external stimuli. Differential regulation of

FOXC1 depending on the type and/or magnitude of stress may also result in the activation/repression of a different set of genes. Further identification of FOXC1 targets in response to various stresses is essential in understanding what stress response and cell death pathways FOXC1 is involved in. All components of the complex network of genes that FOXC1 is involved in are potential candidate genes for ARS. Since 60% of ARS patients do not have mutations in either FOXC1 or PITX2, it is likely that there are more causative genes that have yet to be identified.

Since phosphorylation of the FOXC1 protein has functional relevance, further examination of the effect of phosphorylation would be of great interest. In chapters 2 and 3, immunoblot analysis of the L130F and W152G mutant FOXC1 proteins showed an altered migration pattern compared to the wild type protein, possibly due to differences in phosphorylation. Phosphorylation of FOXC1 at the serine 272 residue promotes stability of the FOXC1 protein (82). However, there are most likely other sites other than serine 272 that are phosphorylated within the FOXC1 protein. Methods such as mass spectrometry could be utilized to identify additional phosphorylation sites (208) and to compare the phosphorylation sites between the wild type protein and the mutant proteins such as L130F and W152G. Finally, since phosphorylation/dephosphorylation events at a particular site are context-specific (208), identification of phosphorylation sites would give insight into potential differences in phosphorylation of the FOXC1 protein under

normal and oxidative stress conditions. Thus, differences in phosphorylation could contribute to the post-translational regulation of the FOXC1 protein.

Currently the treatment strategy for glaucoma patients involves lowering IOP by medication or surgery. Close monitoring of individuals is required to ensure that visual field loss has not occurred or progressed. Understanding the molecular mechanisms underlying the ability of TM cells to respond and adapt to stress would potentially lead to preventative care. Components of the FOXC1 network of genes are potential therapeutic targets for preventing or delaying TM cell death. While much more research needs to be carried out, protective genes such as HSPA6 are intriguing therapeutic targets. Targeting HSPA6 may be particularly effective in ARS patients with FOXC1 mutations since FOXC1 mutations are predicted to dysregulate HSPA6.

Finally, since FOXC1 appears to be part of the stress response network in TM cells, FOXC1 may also play a similar role in other ocular structures. FOXC1 continues to be expressed in various adult ocular structures including the ciliary body, cornea, iris, optic nerve head, and choroid/retinal pigment epithelium (98). The anterior segment structures are exposed to similar extracellular stresses as the TM because of their interaction with aqueous humor. The posterior chamber structures are exposed to various stresses including mechanical and oxidative stresses.

Examining the potential role of FOXC1 as a mediator of stress response would further highlight the importance of FOXC1 in the adult eye.

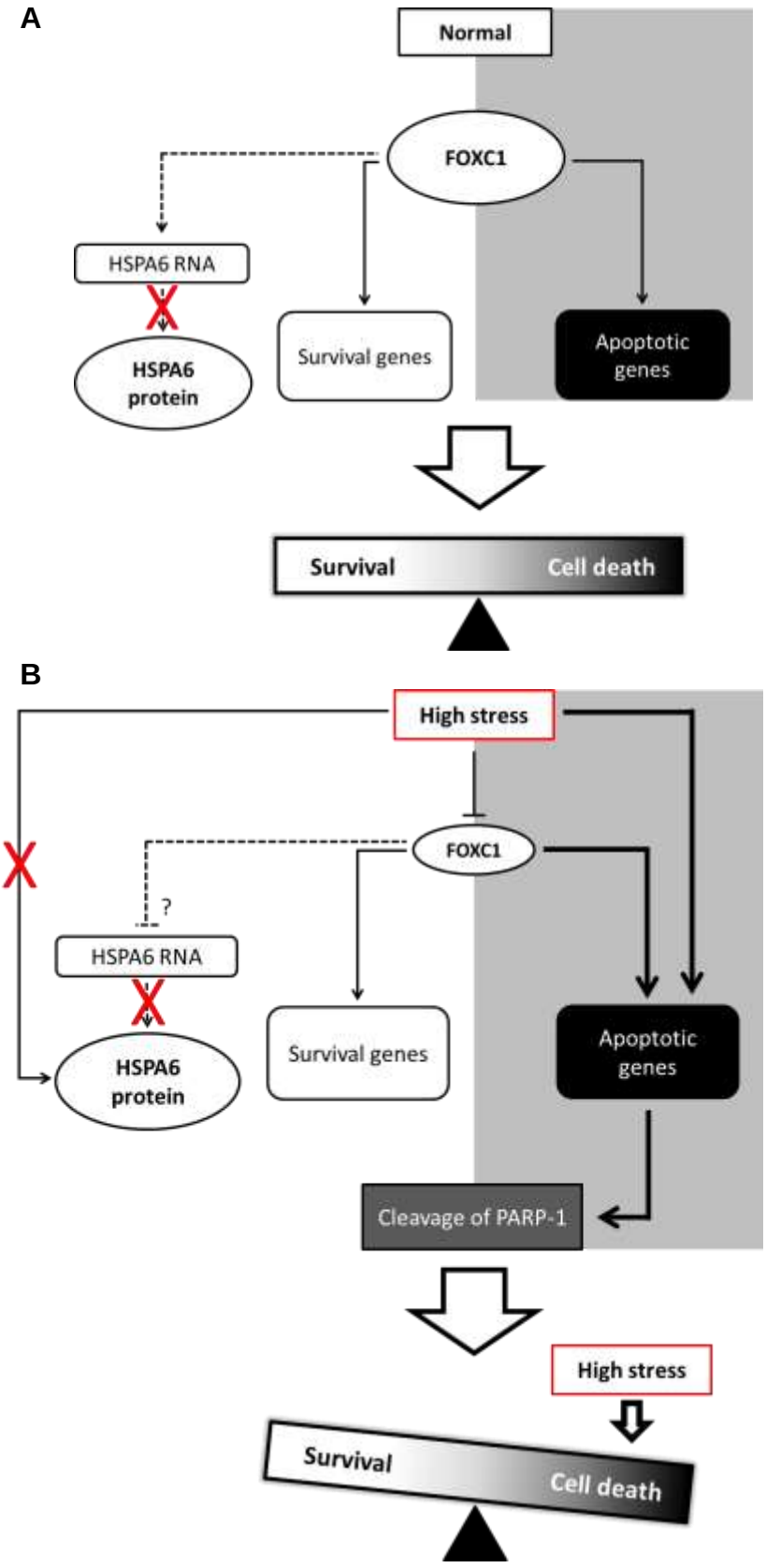
A
Normal
FOXC1
HSPA6 RNA
HSPA6 protein
Survival genes
Apoptotic genes
Survival
Cell death
B
High stress
FOXC1
?
HSPA6 RNA
HSPA6 protein
Survival genes
Apoptotic genes
Cleavage of PARP-1
High stress
Survival
Cell death

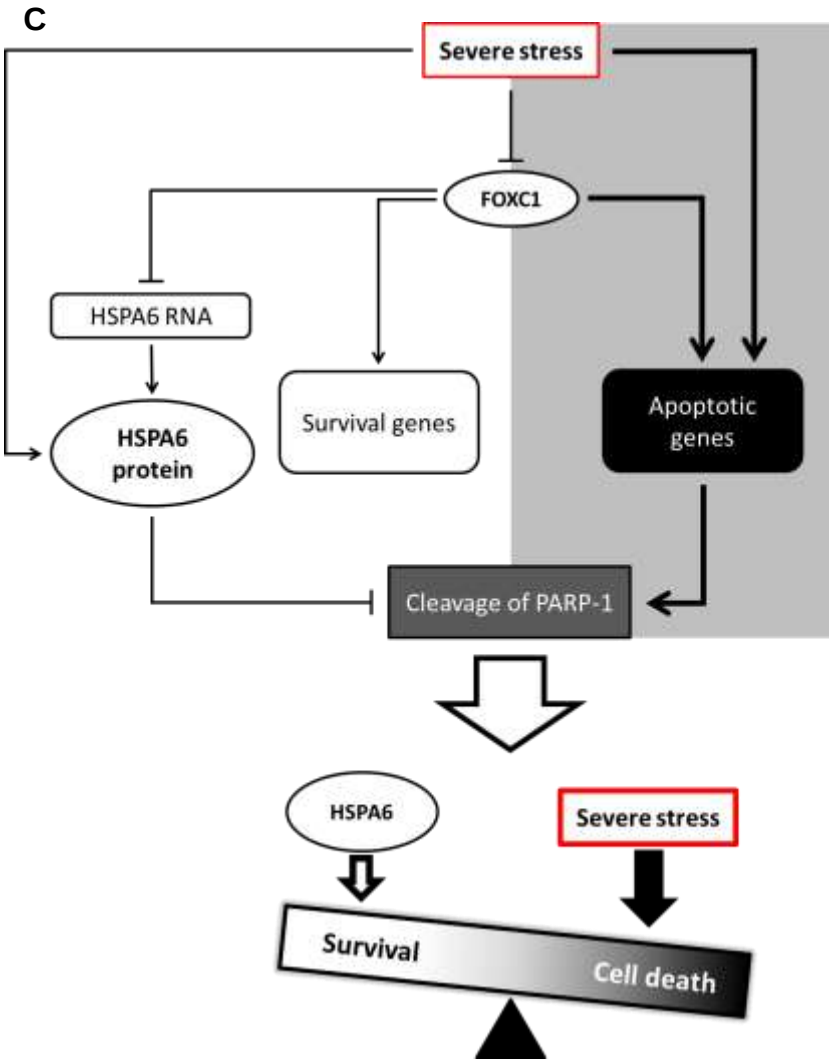
C
Severe stress
FOXC1
HSPA6 RNA
HSPA6 protein
Survival genes
Apoptotic genes
Cleavage of PARP-1
HSPA6
Severe stress
Survival
Cell death

Figure 1: FOXC1 may mediate the stress response pathway by balancing the regulation of survival genes and apoptotic genes. A) Under normal conditions, FOXC1 is predicted to regulate both survival and apoptotic genes in a balanced manner. Thus, the FOXC1 is predicted to be important for maintaining homeostasis. B) Under stress conditions, a decrease in FOXC1 levels is predicted to result in differential regulation of both survival and apoptotic genes compared to normal conditions. Decreased FOXC1 levels may activate apoptotic genes and/or repress survival genes resulting in the cleavage of PARP-1 and thus, apoptotic cell death. C) Under severe stress conditions, a decrease in FOXC1 levels is predicted to result in differential regulation of target genes compared to both normal and non-severe stress conditions. Under severe stress conditions, FOXC1 regulates HSPA6, an anti-apoptotic protein. However, under the experimental conditions examined in this study, cell death continues to occur because the negative consequences of the severe stress outweigh the protective function of HSPA6. Figure from Ito and Walter (1).

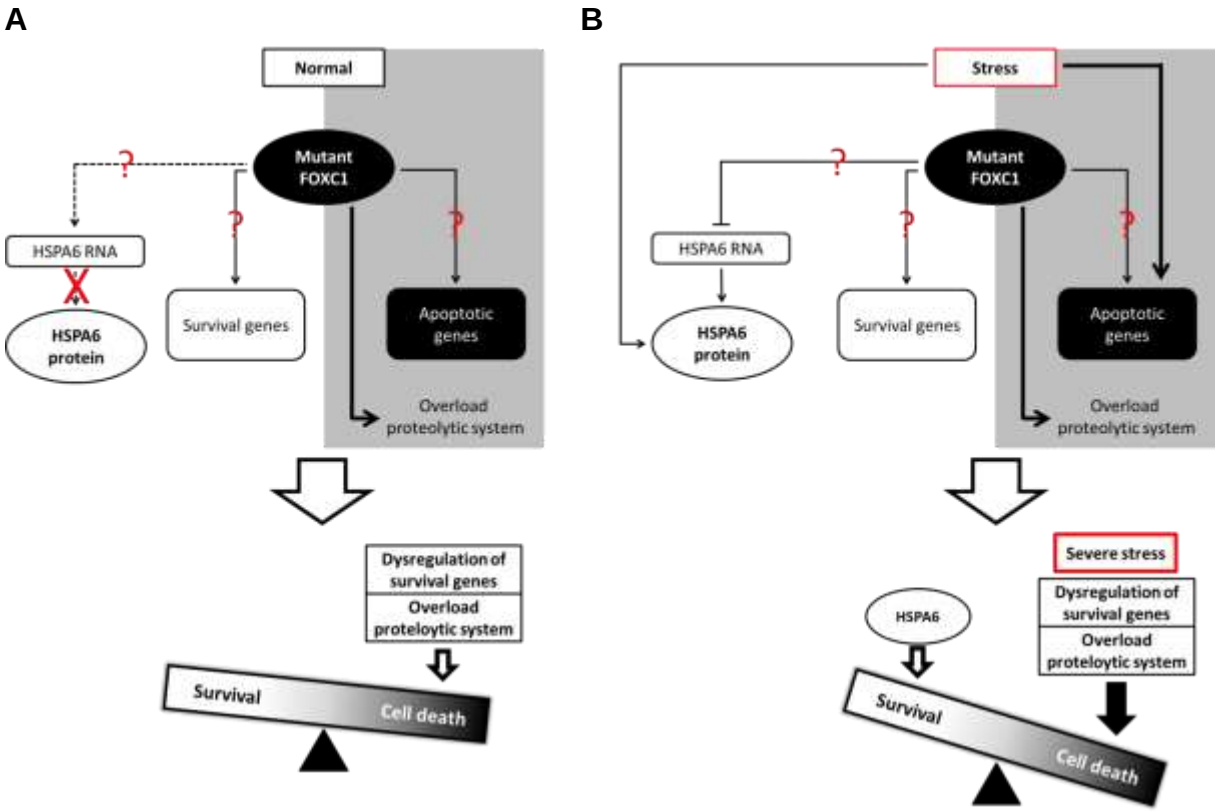
A
Normal
Mutant FOXC1
HSPA6 RNA
HSPA6 protein
Survival genes
Apoptotic genes
Overload proteolytic system
Dysregulation of survival genes
Overload proteloytic system
Survival
Cell death
B
Stress
Mutant FOXC1
HSPA6 RNA
HSPA6 protein
Survival genes
Apoptotic genes
Overload proteolytic system
Severe stress
HSPA6
Dysregulation of survival genes
Overload proteloytic system
Survival
Cell death

Figure 2: FOXC1 mutations may compromise the ability of cells to respond to stress. A) Downstream targets are predicted to be dysregulated by FOXC1 mutant proteins due to disruptions in normal FOXC1 function such as nuclear localization and DNA binding ability. In addition, FOXC1 mutations such as L130F and W152G are predicted to result in misfolded protein, which would place strain on the proteolytic system. B) Cells with FOXC1 mutations are predicted to have a compromised ability to respond to stress, resulting in increased cell death. In the case of TM cells, increased cell death would lead to disruptions in aqueous humor drainage and increased intraocular pressure (IOP), which is a major risk factor for developing glaucoma. Figure from Ito and Walter (1).

References

(1) Ito YA, Walter MA. **Genetics and environmental stress factor contributions to anterior segment malformations and glaucoma**. In: Rumelt S, editor. **Glaucoma – Basic and Clinical Aspects**: InTech; In Press.

(2) Strungaru MH, Dinu I, Walter MA. Genotype-phenotype correlations in Axenfeld-Rieger malformation and glaucoma patients with FOXC1 and PITX2 mutations. Invest Ophthalmol Vis Sci 2007 Jan;48(1):228-237.

(3) Rudnicka AR, Mt-Isa S, Owen CG, Cook DG, Ashby D. Variations in primary open-angle glaucoma prevalence by age, gender, and race: a Bayesian meta-analysis. Invest Ophthalmol Vis Sci 2006 Oct;47(10):4254-4261.

(4) Leske MC. Open-angle glaucoma -- an epidemiologic overview. Ophthalmic Epidemiol 2007 Jul-Aug;14(4):166-172.

(5) Berry FB, Skarie JM, Mirzayans F, Fortin Y, Hudson TJ, Raymond V, et al. FOXC1 is required for cell viability and resistance to oxidative stress in the eye through the transcriptional regulation of FOXO1A. Hum Mol Genet 2008 Feb 15;17(4):490-505.

(6) Saleem RA, Banerjee-Basu S, Berry FB, Baxevanis AD, Walter MA. Analyses of the effects that disease-causing missense mutations have on the structure and function of the winged-helix protein FOXC1. Am J Hum Genet 2001 Mar;68(3):627-641.

(7) Wang WH, McNatt LG, Shepard AR, Jacobson N, Nishimura DY, Stone EM, et al. Optimal procedure for extracting RNA from human ocular tissues and expression profiling of the congenital glaucoma gene FOXC1 using quantitative RT-PCR. Mol Vis 2001 Apr 17;7:89-94.

(8) Lehmann OJ, Ebenezer ND, Jordan T, Fox M, Ocaka L, Payne A, et al. Chromosomal duplication involving the forkhead transcription factor gene FOXC1 causes iris hypoplasia and glaucoma. Am J Hum Genet 2000 Nov;67(5):1129-1135.

(9) Lehmann OJ, Ebenezer ND, Ekong R, Ocaka L, Mungall AJ, Fraser S, et al. Ocular developmental abnormalities and glaucoma associated with interstitial 6p25 duplications and deletions. Invest Ophthalmol Vis Sci 2002 Jun;43(6):1843-1849.

(10) Nishimura DY, Searby CC, Alward WL, Walton D, Craig JE, Mackey DA, et al. A spectrum of FOXC1 mutations suggests gene dosage as a mechanism for developmental defects of the anterior chamber of the eye. Am J Hum Genet 2001 Feb;68(2):364-372.

(11) Ray PS, Wang J, Qu Y, Sim MS, Shamonki J, Bagaria SP, et al. FOXC1 is a potential prognostic biomarker with functional significance in basal-like breast cancer. Cancer Res 2010 May 15;70(10):3870-3876.

(12) Tonoki H, Harada N, Shimokawa O, Yosozumi A, Monzaki K, Satoh K, et al. Axenfeld-Rieger anomaly and Axenfeld-Rieger syndrome: clinical, molecular-cytogenetic, and DNA array analyses of three patients with chromosomal defects at 6p25. Am J Med Genet A 2011 Dec;155A(12):2925-2932.

(13) Wang J, Ray PS, Sim MS, Zhou XZ, Lu KP, Lee AV, et al. FOXC1 regulates the functions of human basal-like breast cancer cells by activating NF-kappaB signaling. Oncogene 2012 Nov 8;31(45):4798-4802.

(14) Huang L, Chi J, Berry FB, Footz TK, Sharp MW, Walter MA. Human p32 is a novel FOXC1-interacting protein that regulates FOXC1 transcriptional activity in ocular cells. Invest Ophthalmol Vis Sci 2008 Dec;49(12):5243-5249.

(15) Acharya M, Huang L, Fleisch VC, Allison WT, Walter MA. A complex regulatory network of transcription factors critical for ocular development and disease. Hum Mol Genet 2011 Apr 15;20(8):1610-1624.

(16) Berry FB, Lines MA, Oas JM, Footz T, Underhill DA, Gage PJ, et al. Functional interactions between FOXC1 and PITX2 underlie the sensitivity to FOXC1 gene dose in Axenfeld-Rieger syndrome and anterior segment dysgenesis. Hum Mol Genet 2006 Mar 15;15(6):905-919.

(17) Berry FB, Mirzayans F, Walter MA. Regulation of FOXC1 stability and transcriptional activity by an epidermal growth factor-activated mitogen-activated protein kinase signaling cascade. J Biol Chem 2006 Apr 14;281(15):10098-10104.

(18) Berry FB, O'Neill MA, Coca-Prados M, Walter MA. FOXC1 transcriptional regulatory activity is impaired by PBX1 in a filamin A-mediated manner. Mol Cell Biol 2005 Feb;25(4):1415-1424.

(19) Llobet A, Gasull X, Gual A. Understanding trabecular meshwork physiology: a key to the control of intraocular pressure? News Physiol Sci 2003 Oct;18:205-209.

(20) Zhou BB, Elledge SJ. The DNA damage response: putting checkpoints in perspective. Nature 2000 Nov 23;408(6811):433-439.

(21) Zhang B, Chambers KJ, Faller DV, Wang S. Reprogramming of the SWI/SNF complex for co-activation or co-repression in prohibitin-mediated estrogen receptor regulation. Oncogene 2007 Nov 1;26(50):7153-7157.

(22) Balciunas D, Galman C, Ronne H, Bjorklund S. The Med1 subunit of the yeast mediator complex is involved in both transcriptional activation and repression. Proc Natl Acad Sci U S A 1999 Jan 19;96(2):376-381.

(23) Mann M, Ong SE, Gronborg M, Steen H, Jensen ON, Pandey A. Analysis of protein phosphorylation using mass spectrometry: deciphering the phosphoproteome. Trends Biotechnol 2002 Jun;20(6):261-268.

Appendix

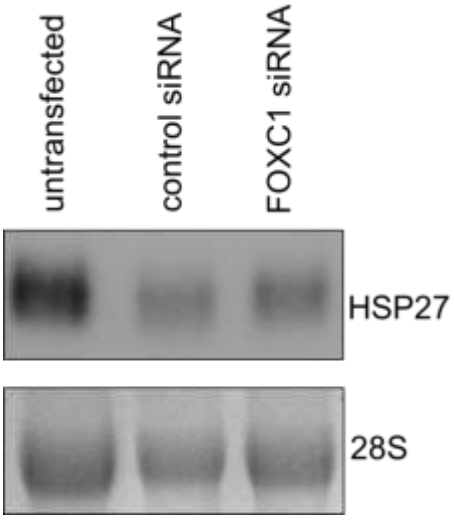

Figure 1: HSP27 is most likely not a target gene of FOXC1 in HTM cells. HTM cells were transfected with FOXC1 siRNA or control siRNA. After transfection, RNA was harvested and subjected to northern blot analysis. A HSP27 probe was radiolabeled and hybridized to the blot. Relative to control siRNA, HSP27 RNA levels were not altered when FOXC1 was knocked down ($p>0.01$, $n=4$, Student's t-test).

cattctgtttacctttcagggctgtattgattggggtgtagactgaactatccggggtctgtttcttttcggtga
tgaaagtcttgagaaggtagtaatggataagatgtgagggagaggagagagggagatttggagtgta
gggtgagtgcccctcttcttagaactgaatactcttcttctaatgaacttgtattcttgtttccatgtcttcttccc
tttccttctatagcaaataaagcattcactttgttttggaacacaagttgtcagaaaggcaaacttcaggtg
aattgtcagtggagactgctgacttcctgcactgctattttcccagtgcagttaccagaaggatgtgaccctt
ctcagagaagtcattccaggcagattagaaacatgacccacagtctccttgatggtttggtgagtgccct
taaagagccttccattttcctgggacacagcatcactgtgcacaattcttgcatttgaaaagtagcagcttt
ctctgttggatagtttacatcgatttttaaggaggctatggagcttccacccaccccttccaaactctatgtatt
agtctgtctctatgtattagtctgttctcacgctgctatgaagaaatacctgagactgggttatttatgaaga
aaagagggttaattggctcacagttccttatcgctggggaggcctcaggaaacttacaatcacagcag
aaggcaaaggagaagcaggcaccttctgcacatgatggcaggacagagtgagtgcaagcaggga
aggtgccagacacttataaaaccctaagctctcgtgagactcactcactattatgagaacagcatggg
gaaaccgtcgccatgacccagttacctccacctggtcccacttttgacagatggggattatgaggatga
caactcaagacgagactttgggtggagacagagccaaaccatatcaccctagacagaggctcctca
aatatgtaaagccttgttaaatcctgcttttacattaaaatgcacccaacaatctgactgcttctcagtattct
actcctaccaccctggtccaagccaccatcatttctcacttggattactccaatagcctcctgactggcct
ccctgcactcacccttgccatcctatagtctattctcaccataacagctattgtgatcttttaaaaatgtgtgt
catatttgtcacttcttttccccaaatcatatactatcttccccttgtggttggagtaaaggctagagcttttcc
aatattctacaggatgctacaggatcttgctcttcactctctctgacctcatctcctactgcttttccttgcttgc
tgttggtcactcttgctcttccttgaacgtgccaattatacttctgcccagagcctatgttatttcctgtttctgg
aatgttctttctcatagacccacattatgcctcattatgtcctttaggtctttactcacatgtcaccttatcagtg
aggtctccttgatcattcggtataacctgtcgccctcccatactcttaatgtccctttccttcttcatttttctccat
tgtgcttattactactgatgtactattaatatatgtttactgtttgttttgtgtctgacttccccactcctctcattag
aatgtgagctccaggagaggtctttgtctgttttgttcactaccacatactcagagcccaggtcagtgtcta
gtgcatagtaaagcgcttaataaatatgtgcggaatgagtaaattctttgacgtttgaaatcagagacttt
aaactggaaagtccttagaaacaatgtagtccaatctcttcattttaaaacggaggaagctgtggccca
gacaggtgaaatgacttgttcaaggacaaacaggtagtggatgtcactgacttttatatatatatagtttg
gattatactacaaattttgttctatagtgaaatggtttggctgtgtccccacccgaatatcatcttgaattccc
acaacacatgggagggacccagtggaaggtaactgaatcatggggcaggtctttcccatgctgttctt
gtgatagtgaataagtctcatgagatctgatggttttaaaaaggggagtttccctgcacaagctctctcttc
tcttgtttgccaccatgtgagacatgactttcacctttgccatgattgtgaggcctcccagccacgtggaa
ctgtaagtccattaaacctctttctttttgtaaattgccccgtctcaggtatgtctttattagcagtgtgagaatg
ggctaacacatacaacttgctttttttttgtactcaatattgagtcgtgagctttgcaccacattagaatgtct
atttaagtcattactttaaggtcggttctatttttaaagctactcaaactaagctactaaacataagtggatat
atttaagtgtatgtataaaatttatactaggccagctgcagtggctcatgcctgtaatcccaaagctgtgg
aaggtagaggtgggactgattgaggccacgagttcaaggctgcagtgagctgtgattgcatcactgta
ctccagcctgagggacagagcaggaaccagaaaaaaataaaataaaaagaaacaaacaaaaa
aacccccaacaaccctacagtggctcttttagaaaaaacaaacaaacaaaaccaaaactgtactgc
atgcataagctcccctatgctatgtttgaaccactctgaagagatcaattaaaaagaagtgagtgatatt
ggaagcatgcctctgtgatgctgtggtaacattcataggctgcgttagggctatgcctgtaactcttggag
atgagtgggtaagtggggttttgaggtggctgggggctggaagagaaggttggaggagcccacaca
agacagcccttaacacgccggggcacagaaccccaggctgggccaacttttccctgctgaggtga
agacccgtctcttgcaggccgttggcaaatgtcttgactctggcatccaggtgtgaccagcttagaccct
gagagtgagtgaatttaaagttgacagcttctttccctttggaattatgaaataggttacttcttttcaagga
cagtttgattttccactgtgtaagtcatatattgcacatttcttaaaacattccctttttttcctgaactgatcacctt
accagtacggctgatcctctcaagcagcaaactctaccagctgtcactggtgctctcggagagacgatt

aaccaaggaacccagcccgggaacagtactgacctctacttctggactcctgcctccctcttaaaaag
tcccttgaacttcctagtgggttctaacctgtcaaaggagaaaatagccatctatggagtaagggttttta
gtttctctttttacaaatggaagtttcctctgaatcaggcaagtaacgttaaataagaagccaacttttaagttt
ctctaacacactgctaaattgtaacaccagactgtaccacatactctccagctgccagctattgcagttg
ccatccttgttactatagtggtgagtatctctgcctgtcatgcgtgagagaggggtcgattccccgacgg
ggaggtcacgggaaattgtgtgaggattttgtcaaccttcagaagtctcagaaatgtctccttgttttggctt
tcagcggaaatccgaacgccagcagatctgaatggaatgttctggattgaagaaagtgggaaatggc
ctcaattcacaaagtcacaacctgataaaaaccagtgtgactttactgcccagtgaacccatctcgtcct
ccagcctttaggaggtaggttggactggagcctgcagtagtttactctccacctgagtcctggtctccag
ctgggaacccacttaggccataaagaaaaacgcacactgtgcctctccaccgggcctctggagacg
aggctcctcggggatacaaacagtggggagaacatgagggacatcccgaccgtactctgcgtcctc
ctttcccaggtgttgcgttctctcttgggctgagtggcgaggtctctcccgagtcccagggccacagtgca
atgtcacatctcctttgtggaaagtgactggtaaaggagagagaacaaaactggaggaatgtaaagt
cttcagccacctggtttaatttattcaagagtgattaatcctagatgagaaaaagaattgaaatggatcg
gaaaaaaatgaaagtgcattggccgggaatcgaacccgggcctcccgcgtggcaggcgagaattct
accactgaaccaccaatgctactgtcagctaaagacctgcagtattgtctcttaaagctcactatctctgg
ccattcactaaggaaccaggcaccgtcttaaatcgcggtttggaaaatattttgttcaagataaaactgtt
ttaagatatacgtgtatatatcttatatatctgtattcgcatggtaacatatcttcggccttcctgagccgctg
ggctctcagcggccctccaaggcagcccgcaggcccctgtgtgcctcagggatccgacctcccaca
gccccggggagaccttgcctctaaagttgctgcttttgcagcctctgccacaaccgcgcgtcctc(end
of 5’ upstream sequence)

FOXC1 BS1 – ctatagcaaataaagc

FOXC1 BS2 – ggatagtttacatcga

FOX BS3 – taaaca

FOX BS 4 – taaata

Figure 2: Sequence upstream of the HSPA6 gene. Highlighted region shows the FOXC1 or FOX binding site examined by Chromatin Immunoprecipitation Assay